ABSTRACT

Title of Document: EFFECTS OF COMPLEXATION WITH THE SIDEROPHORE DESFERRIOXAMINE B ON TRANSITION METAL REMOVAL FROM SEAWATER

Emily A. Christenson, Master of Science, 2013

Directed By: Associate Professor, Johan Schijf, Marine Environmental and Estuarine Science

Complexation of transition metals with strong organic ligands of unknown structure and origin plays an important role in their behavior and distributions in seawater. I present here a series of stability constants for complexes of several transition metals with the trihydroxamate siderophore desferrioxamine B (DFOB), representative of a class of small organic ligands that are exceptionally selective for Fe(III) and found in open ocean surface waters at low-picomolar concentrations. Stability constants for DFOB complexes with divalent metals are similar to conditional constants that have been measured in seawater for highly metal-specific, but unidentified organic ligands. Titration data indicate that free Hg^{2+} forms a very stable complex with DFOB, however the more toxic methylmercury cation does not. A revised scavenging model for yttrium and the rare earth elements suggests that their removal from seawater is dominated by sorption onto Mn oxides, yet not significantly influenced by biogenic silica or calcite.

EFFECTS OF COMPLEXATION WITH THE SIDEROPHORE DESFERRIOXAMINE B ON TRANSITION METAL REMOVAL FROM SEAWATER

By

Emily A. Christenson

Thesis submitted to the Faculty of the Graduate School of the
University of Maryland, College Park, in partial fulfillment
of the requirements for the degree of
Master of Science
2013

Advisory Committee:
Associate Professor Johan Schijf, Chair
Associate Research Professor Andrew Heyes
Assistant Professor Laura Lapham

Acknowledgements

This thesis would not be in existence without the encouragement and assistance of many incredible people. First I would like to thank my major advisor, Dr. Johan Schijf, for his enduring guidance and patience throughout this entire process. Many thanks go out to my other committee members, Drs. Andrew Heyes and Laura Lapham, for your thoughtful insights and support with my work. I am especially grateful to Andrew Heyes for all of his assistance with my mercury work and the anaerobic glove bag.

I could not have done this without my lab bubbies, Alison Zoll, Kathleen Marshall, and Caroline Coulter, thank you for always being there when I needed an extra hand or someone to listen to my nonsense. Finally, many thanks go out to my amazingly wonderful support group. To my fellow students, coworkers, and friends at CBL, thank you for all the encouragement and friendships throughout the last three years, I will always cherish the memories we have created. And of course, to my family and loved ones, I would not be where I am today and the person I am today without your continuing love and assurance.

Table of Contents

List of Tables

List of Figures

Figure 4.5. Modeled YREE surface complexation (M_S/[M]) with free [DFOB] fixed at 10^{-13} M for 46 m and 3936 m depth, and with free [DFOB] fixed at 10^{-14} M for 46 m depth, calculated by subtracting the curves in Figure 4.4 from the curves in Figure 4.3. Modeled surface complexation patterns were vertically shifted to coincide at Gd, for visual comparison.

Figure 4.6. The predicted ${}_iK_s$ behavior at 46 m depth from this work (with free [DFOB] fixed at 10^{-13} M) plotted with recent YREE sorption data for (A) hydrated Mn(IV) oxides, (B) Fe(III) hydroxides, (C) an organic surface, *Ulva lactuca*, (D) coral carbonate, and (E) biogenic silicate. YREE sorption data with hydrated Mn oxides was measured at pH 6.98 in 0.5 M NaCl (Marshall and Schijf, *Chemical Geology*, in prep). YREE sorption data with Fe hydroxides was measured at pH 8.38 in 0.5 M NaCl (Schijf and Marshall, 2011). YREE sorption data with *Ulva* was measured at pH 8.2 in 0.5 M NaCl (Zoll and Schijf, 2012). Distribution patterns of REE in coral carbonate samples are from Frankland Island, off the Great Barrier Reef in Australia (Wyndham et al., 2004). Distribution patterns of REE in laminated diatom mats are from the upper unit (0–286 cm) of core WPD-03 (Xiong et al., 2012). Measured sorption patterns were vertically shifted to coincide at Gd for comparisons with the modeled pattern.

Figure 4.7. Modeled YREE surface complexation (M_S/[M]) with the free [DFOB] concentration fixed at 10^{-13} M at 46 m depth (red dashed line) and 3936 m depth (blue dashed line), compared to the average stability constant for REE complexation with 15 simple monocarboxylic acids (black line) (Byrne and Kim, 1990).

Chapter 1: Introduction

1.1. Marine biogeochemistry of trace metals

Trace metals are of interest both as essential micro-nutrients, and as environmental toxins. Over the past three decades, our knowledge and understanding of the chemical behavior of trace metals in the oceans have grown significantly. Since trace metals occur in the world's oceans at picomolar to nanomolar concentrations (Bruland, 1980), reliable measurements in seawater demand meticulous attention to all sample processing steps, from collection to analysis. With recent advances in analytical methods and instrumentation, trace metal-clean sample collection and handling, and carefully designed protocols, numerous datasets have been produced that contribute to a fundamental understanding of the concentrations and distributions of dissolved trace metals in the major regions of the global ocean. Consequently, consistent oceanic profiles revealing the existence of distinct vertical and horizontal concentration gradients are now available for a number of important trace metals (Sohrin and Bruland, 2011; Biller and Bruland, 2012).

The oceanic distribution and biogeochemical behavior of each trace metal is influenced by complex interactions among inputs, removal, and recycling processes, combined with physical mixing within and between the ocean basins. Trace metal behavior can generally be divided into three categories according to their oceanic profiles: conservative, nutrient-like, and scavenged (Bruland, 1983a; Whitfield and Turner, 1987).

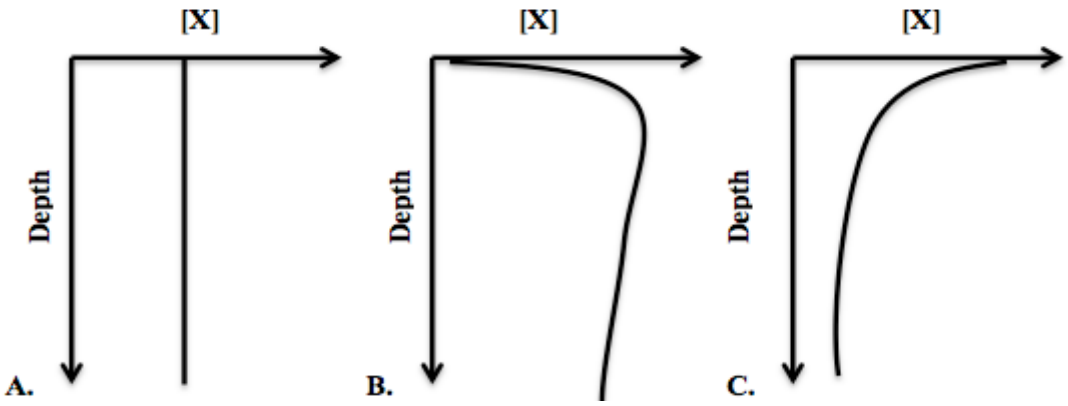

Figure 1.1. Schematic oceanic depth profiles for the three major types of dissolved trace metal distributions, with [X] representing the total dissolved concentration of metal X, normalized to salinity. (A) Conservative profile; (B) Nutrient-like profile; (C) Scavenged profile.

Conservative distributions (Figure 1.1A) are observed for elements whose concentrations are directly proportional to salinity, due to very slow removal from the oceans. These elements have high concentrations in seawater relative to their crustal abundance. Trace metals with nutrient-like vertical distributions (Figure 1.1B) exhibit surface water depletion, due to biological uptake, and increasing concentrations with depth, displaying a strong correlation with the major nutrients nitrate, phosphate, or silicate. The increase of the dissolved concentrations of these trace metals with depth is explained by the gradual decomposition of sinking dead biota and fecal pellets, releasing associated nutrients and metals back into the water column. Scavenged trace metal distributions (Figure 1.1C) primarily reflect their terrestrial and atmospheric sources, with concentrations decreasing away from both the ocean surface and coastal waters, due to rapid removal from the water column by adsorption onto sinking particles (Bruland et al., 1994).

An example of a conservative trace metal is cesium. These trace metals interact weakly with particles and have oceanic residence times much greater than the mixing time of the oceans (~1,000 years). Although metals exhibiting these distributions are involved in biogeochemical cycling, the resulting fluxes are generally negligible relative to their concentrations in seawater.

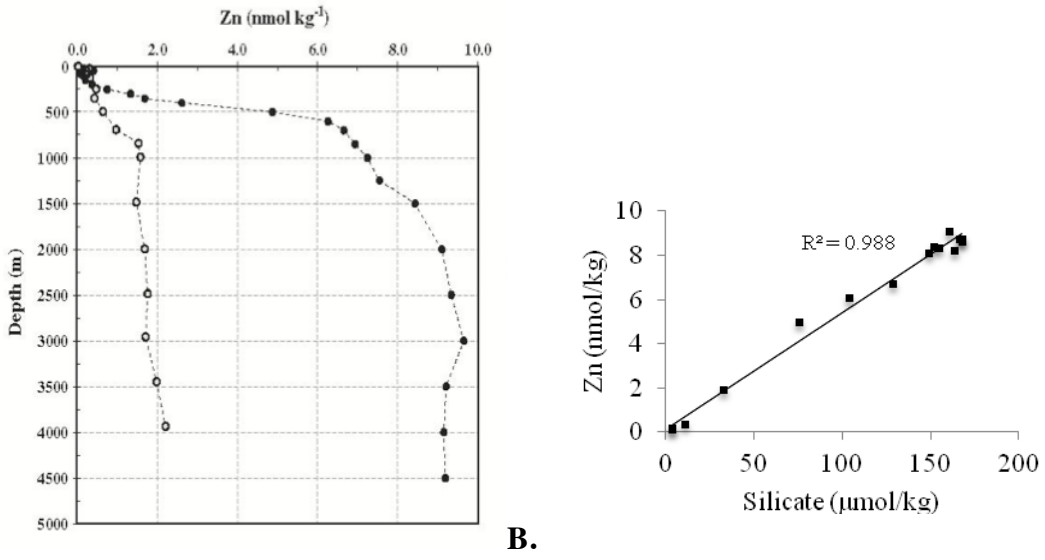

Figure 1.2. (A) Vertical concentration profile of Zn in the Atlantic Ocean (gray circles) and Pacific Ocean (black circles) (Biller and Bruland, 2012); (B) Zinc concentration versus silicate in the North Pacific. Data from H-77 station 17 (32°41.0'N, 144°59.5'W), September 1977 (Bruland, 1980).

Zinc and cadmium are two prominent examples of nutrient-like metals in seawater. Zinc occurs at nanomolar concentrations, lowered at the surface by biological activity and increasing with depth (Figure 1.2A). The vertical distribution of Zn is significantly correlated with that of silicate (Figure 1.2B), suggesting similar mechanisms of biological uptake and regeneration. Dissolved Cd is characterized by a strong gradient from low-picomolar concentrations in surface waters to a mid-depth maximum of around 1 nM (Figure 1.3A). Its vertical distribution is highly correlated with that of dissolved

phosphate (Figure 1.3B), which suggests that Cd is being incorporated into biogenic tissues near the surface and then remineralized with the organic debris at greater depths (Boyle et al., 1976).

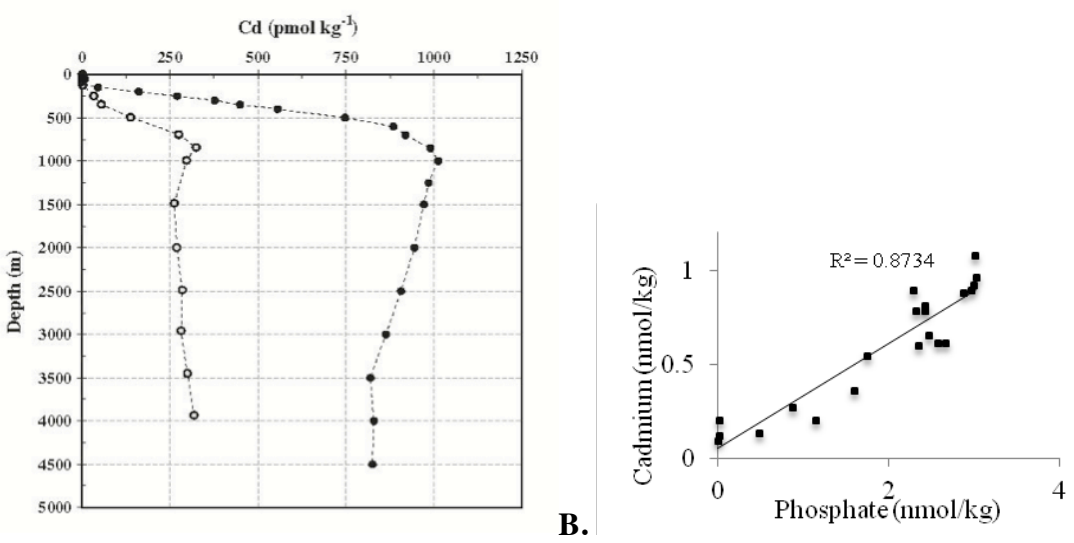

Figure 1.3. (A) Vertical concentration profile of Cd in the Atlantic Ocean (gray circles) and Pacific Ocean (black circles) (Biller and Bruland, 2012); (B) Cadmium concentration versus phosphate in the North Pacific (Boyle et al., 1976).

Lead is representative of trace metals with a scavenged distribution, with concentrations in the open ocean between 5 and 100 pmol/kg. It is a non-essential and potentially toxic metal, and therefore a metal of interest in the environment. Lead concentrations are high in surface waters primarily due to aerosol deposition, specifically atmospheric inputs from alkyl-leaded gasoline, and decrease with depth as dissolved Pb is rapidly removed by adsorption of the ions or ionic complexes onto particle surfaces, such as clay minerals, organic matter, bacteria, fecal pellets etc., sinking to the ocean floor (Santana-Casiano et al., 1995) (Figure 1.4).

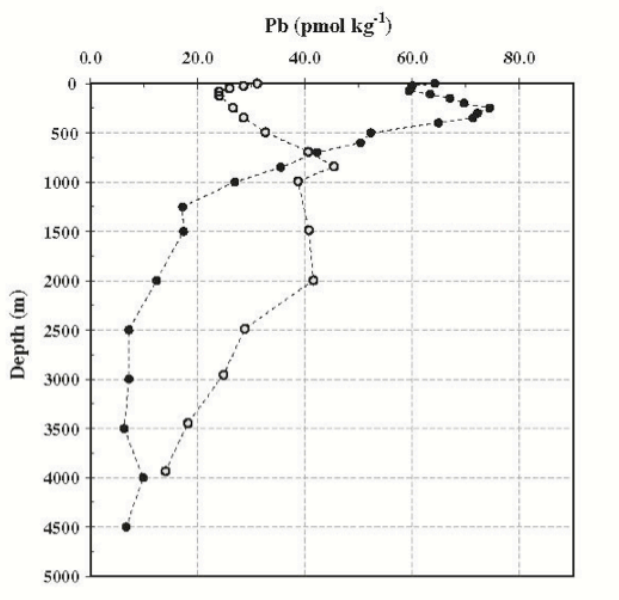

Figure 1.4. Vertical concentration profile of Pb in the Atlantic Ocean (gray circles) and Pacific Ocean (black circles) (Biller and Bruland, 2012).

Because nutrient-like and scavenged trace metals exist at low concentrations in seawater relative to their crustal abundance, they have been classified as "reactive" trace metals (Whitfield and Turner, 1987). Some reactive trace metals play critical roles in ocean productivity and biogeochemistry, and are required for a wide range of enzymatic functions and redox reactions in marine microorganisms. While the distribution patterns of reactive trace metals in the oceans are influenced by biological processes and microorganisms, trace metals in turn clearly affect the productivity and species composition of phytoplankton and bacteria (Sunda, 2012). As a result, a continuous feedback loop exists between the biological systems in the ocean and their chemical environment (Figure 1.5). These complex interactions have shaped both the chemistry and biology of the present ocean, and have had a profound effect on the evolution of marine biology over time (Henderson et al., 2007).

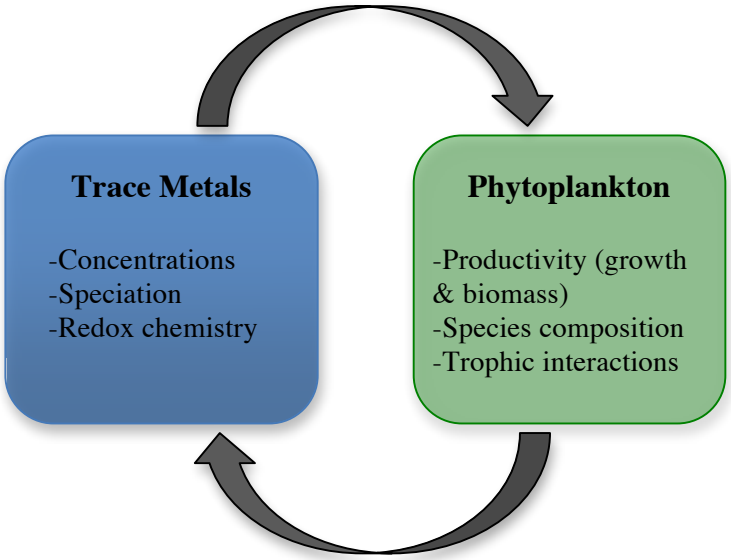

Figure 1.5. Schematic illustration of the continuous feedback loop that exists between trace metals and phytoplankton in the oceans. Trace metal concentrations, speciation, and redox chemistry control the productivity, species composition, and trophic relations of marine phytoplankton. In turn, marine phytoplankton control the distribution, speciation, and cycling of trace metals through uptake and remineralization mechanisms, sorption onto biogenic particles, and production of organic ligands (adapted from Sunda, 2012).

1.2. Trace metal complexation

1.2.1. Key concepts

The mobility, bioavailability, and toxicity of reactive trace metals in the oceans are governed by the competing processes of sorption on solid substrates, which involves complexation with proton-bearing functional groups on the particle surface, and solution complexation with dissolved ligands. Metal complexation with dissolved ligands tends to facilitate bioavailability and uptake of trace metals (Martin, 1967; Maldonado et al., 2005), while sorption onto solid surfaces tends to decrease bioavailability and sequester metals (unless the solid surface is a living cell) (Vraspir and Butler, 2009). Ultimately,

the fate and reactivity of a metal in the environment are determined by the balance that exists between solution complexation and surface sorption.

The most frequently used parameter for quantifying the degree of complexation between metals and ligands is the stability constant (K_n or β_n), which is controlled by the chemical properties of both the ligand and the metal ion. Stability constants are a measure of how strongly a ligand coordinates or complexes with a metal. The larger the value of the stability constant, the more stable the complex, and the greater the proportion of complex formed relative to the free metal ion. In describing the quantitative stability of a complex for the following equilibrium reaction in a constant ionic medium,

$$\mathrm{M} + n\mathrm{L} \leftrightarrow \mathrm{ML}_n ,$$

the stability constant, β_n, is defined:

$$\beta_{\mathrm{n}} = \frac{[\mathrm{ML_n}]}{[\mathrm{M}][\mathrm{L}]^{\mathrm{n}}}, \qquad (1.1)$$

where [M] is the activity of the free metal, [L] is the activity of the free ligand, and [ML_n] is the activity of the metal–ligand complex, with the subscript n denoting the number of moles of ligand L per mole of metal M in the complex.

The environmental impact of trace metals in aquatic systems is determined by their *chemical speciation*, which refers to the distribution of a dissolved ion or molecule among its different chemical forms. In the ocean, dissolved trace metals can exist as the free hydrated ion, or as its complexes with inorganic and organic ligands.

1.2.2. Complexation with inorganic ligands

The complexation of trace metals with inorganic ligands in the ocean, estuaries, and freshwater environments has been generally well characterized through the use of

thermodynamic models that are based on decades worth of measuring the stability constants of metal complexes with specific inorganic ligands in a controlled laboratory setting. Furthermore, seawater has a relatively constant pH and major ion composition, therefore the inorganic speciation of trace metals varies little over most of the open ocean's waters. The inorganic speciation of trace metals in seawater comprises hydroxide, fluoride, chloride, sulfate and carbonate complexes, and has been summarized by Turner et al. (1981) for 58 trace elements using stability constants for more than 500 metal complexes in model seawater (pH 8.2 and 25°C). This model was later updated by Byrne et al. (1988) with new constants and additional complexes, as well as an assessment of the influence of temperature and pH. Although much is understood about inorganic metal complexation, it is relatively unimportant. The inorganic speciation of many divalent metals in seawater only accounts for a small fraction of the total dissolved concentration, with organic complexes making up the major part (van den Berg and Dharmvanij, 1984; Bruland, 1992).

1.2.3. Complexation with strong organic ligands

A similar approach has been attempted to study organic complexation of trace metals, but the most abundant organic ligands in seawater are weak ligands, and therefore are relatively unimportant for trace metal speciation. Although there is an extensive amount of data available from laboratory studies concerning weak organic ligands (*e.g.* acetate, citrate, gluconate, etc.), the less abundant, *strong* organic ligands are the major players when it comes to trace metal organic complexation. Unfortunately, the identities, speciation, and distributions of these strong organic ligands in seawater are unknown. Because most of the required information concerning organic ligands in seawater is still

undetermined, it is impossible to accurately model metal complexation with organic compounds in the oceans.

As a result, a different approach has been used to study trace metal complexation with organic ligands, focused on measuring the speciation of individual metals. Identifying organic molecules capable of complexing metals in seawater has proven to be a challenging analytical task because there are thousands of compounds, and without knowing in advance what one is looking for, it is hard to characterize single ligands. But this situation is quickly changing with the recent development of more precise and chemically selective analytical techniques. In the past, the main method used for characterizing organic ligands in seawater has been adsorptive cathodic stripping voltammetry combined with competitive ligand exchange (CLE-ACSV), which can establish the stability constants and dissolved concentrations of stable metal–organic complexes (Gledhill and van den Berg, 1994; Rue and Bruland, 1995; Ellwood and van den Berg, 2001).

Whereas their identities are unknown, organic ligands in seawater have been characterized mainly by their binding affinity, or stability constant. Depending on the range of stability constants determined for a particular metal, organic trace metal-binding ligands either comprise a single class, usually referred to as L, or as multiple distinct classes, referred to as L_1, L_2, etc., which are most likely different for each metal. These stability constants are typically reported as conditional stability constants (K'), meaning they are appropriate only to the conditions under which they were measured. Unlike the thermodynamic stability constant in Eq. (1), which is defined at zero ionic strength, a

conditional stability constant may depend on the concentration and composition of the medium, as well as other parameters such as temperature or pH.

Using CLE-ACSV, it is well established that complexation with organic compounds of unknown structure and origin dominates the chemical speciation of several trace metals (Bruland, 1989, 1992; Kozelka and Bruland, 1998; Witter and Luther, 1998), thereby regulating their availability to the biota (Bruland et al., 1991). Copper, for example, is highly complexed with strong organic ligands (~99%) throughout the ocean (Moffett and Dupont, 2007). Copper ligands are generally grouped into two distinctive classes based on their stabilities, where L_1 is a smaller pool of ligands with a higher conditional stability constant (log K' = 12–14) restricted to the upper ocean and L_2 has lower conditional stability constants (log K'= 9–12) but is present throughout the water column (Coale and Bruland, 1988; Moffett and Dupont, 2007).

Many experiments have been conducted to assess the toxicity of copper to algae, and it has been shown that its uptake, and therefore its toxicity, depends on the free Cu^{2+} concentration (Sunda and Guillard, 1976; Anderson and Morel, 1978; Brand et al., 1986; Florence and Stauber, 1986). Some phytoplankton can regulate their cellular Cu content independently of the external Cu concentration by releasing compounds that bind to Cu^{2+} (McKnight and Morel, 1979; Moffett and Brand, 1996). Because the free metal is more available and thus more toxic, the high degree of complexation may serve to diminish the overall toxicity, however if organisms are unable to take up the complexed species, it could also cause Cu limitation. A delicate balance exists between the beneficial and harmful effects of Cu, which could be maintained by organic ligands.

Previous work (McKnight and Morel, 1979; Haygood et al., 1993; Martinez et al., 2000; Ozaki et al., 2006) has shown that microorganisms produce a diverse array of low-molecular-weight organic compounds that bind metals with high affinities. These compounds have been found to possess a variety of functional groups, including carboxylic acid, amine, thiol and hydroxy groups (Martinez et al., 2003; Gledhill et al., 2004; Vraspir and Butler, 2009; Butler and Theisen, 2010; Hider and Kong, 2010). These strong organic ligands may be released in seawater by microorganisms either as components of high-affinity uptake systems, or as a byproduct of cell death/lysis. It has been found that a number of planktonic species produce Cu-complexing organic molecules with conditional stability constants similar to the L_2 ligands found in seawater (Croot et al., 2000). Moffett et al. (1990) also observed that the marine cyanobacteria *Synechococcus* spp. produce a chelator with a strong conditional stability constant within the range of the L_1 ligands found in seawater, when grown in culture under elevated Cu levels. In response to increasing Cu concentrations, two novel Cu-binding thiols, arginine-cysteine and glutamine-cysteine, as well as cysteine, were produced in culture by *E. huxleyi* (Dupont et al., 2004). Therefore it was proposed that sulfur-containing compounds of low molecular weight are an important part of the ligand pool that dominates Cu complexation in surface waters. Although a number of different candidates has been suggested, including thiols, the nature of marine Cu-binding ligands or classes of ligand remains unknown.

Whereas much has been learned about Cu using CLE-ACSV, unfortunately this basic technique does not provide the detailed structural information that is necessary to identify these ligands. Geochemists are now focusing on uncovering the connection

between the binding strength of ligands measured in natural marine waters and their structure, by combining liquid chromatography-electrospray ionization-mass spectrometry (LC-ESI-MS) with nuclear magnetic resonance (NMR) (Martinez et al., 2001; 2003; Mawji et al., 2008). This combination of techniques results in key chemical information, however only for one or two compounds at a time. The advent of ultra-high resolution Fourier transform ion cyclotron resonance mass spectrometry (FT-ICR-MS) in the last decade has proved more promising, providing molecular formulas of hundreds of individual molecules from organic mixtures (Koch et al., 2008). However, due to the high resolution of this technique, it can be difficult to determine what is actually present in a seawater sample.

Similar to Cu, a lot of work has been conducted concerning iron in seawater. Iron is the most important of all the essential trace metals and often limits the growth of marine phytoplankton (Raven et al., 1999). Through both iron-enrichment mesocosm bottle experiments, as well as mesoscale iron-addition experiments to patches of surface water, several groups have confirmed that naturally low concentrations of Fe limit primary production and regulate phytoplankton species composition in 30–40% of the oceans, particularly in high nitrate-low chlorophyll (HNLC) regions (Martin et al., 1994; Coale et al., 1996; Boyd et al., 2007). Almost all dissolved Fe(III) in open ocean surface waters (~99%) is complexed with strong organic ligands (Rue and Bruland, 1995). Using stripping voltammetry techniques, these Fe(III)-binding ligands have been detected at several different oceanic locations and have a range of stability constants depending on phytoplankton composition and the ambient microbial community (Table 1.1). Stability constants of several "model" organic ligands have also been established in seawater for a

class of Fe(III)-binding ligands called siderophores (after the Greek words for "iron carriers") (Rue and Bruland, 1995; Witter and Luther, 1998), which have been well studied in soil for many decades. The stability constants determined for Fe(III)–siderophore complexes produced from a culture (log K_{Fe} ~ 21.6–24.0) (Witter et al., 2000) were found to be very similar to the conditional stability constants of Fe(III) complexes isolated from seawater. Similar stability constants and structural characteristics suggest that some marine Fe(III) chelators are siderophores that could make up part of the strong dissolved Fe(III)-binding ligands in seawater previously known as the L_1 and L_2 class of organic ligands (Lewis et al., 1995; Martinez et al., 2003; Gledhill et al., 2004).

Table 1.1. Ligand concentrations and conditional stability constants (determined by cathodic stripping voltammetry) for Fe(III)-binding ligands compiled from the literature.

Location	Ligand concentration (nM)	log $K_{Fe^{3+}\text{-}L}$	Reference
North Atlantic	3.0 ± 0.1 4.8 ± 0.3	18.8 ± 0.1 19.7 ± 0.5	Gledhill and van den Berg (1994)
Northwestern Atlantic Ocean	0.60 ± 0.20	20.6 ± 0.3	Luther and Wu (1997)
Northwestern Atlantic Ocean	1.67 ± 0.27 4.62 ± 1.20	22.2 ± 0.5 22.9 ± 0.3	Witter and Luther (1998)
Central North Pacific	0.44 (L_1) 1.5 (L_2)	23.1 ± 0.6 21.5 ± 0.6	Rue and Bruland (1995)
Equatorial Pacific Ocean	0.31 ± 0.08 (L_1) 0.19 ± 0.90 (L_2)	23.7 22.8	Rue and Bruland (1997)

1.3. Siderophores as marine organic ligands

As an important nutrient, iron plays a crucial role in the metabolism of practically all

organisms. Because Fe(III) is highly insoluble in oxygen-rich environments, its concentrations are very low in ocean waters, making it a scarce nutrient for microbial life (Neilands, 1981). In order to overcome this low iron availability, microorganisms can sequester iron through the production and excretion of siderophores (Winkelmann, 2002). Siderophores, produced mainly by single-celled organisms, are low-molecular-weight organic ligands that have an extremely high affinity for Fe(III) (Anderegg et al., 1963b). In order to compete for the limited amount of bioavailable iron in natural waters, many microorganisms have developed their own distinct siderophore.

The mechanism of siderophore-mediated iron uptake, although mostly hypothetical, is reasonably well defined (Boukhalfa and Crumbliss, 2002). Microorganisms release strong iron-binding siderophores into the surrounding medium under iron-limiting conditions, which solubilize iron by complexation. The iron–siderophore chelates are then brought into the cell by specific membrane transport proteins, after which the iron is reduced from Fe(III) to Fe(II) and released for assimilation via degradation of the siderophore or by complexation with a stronger, Fe(II)-specific ligand (Neilands, 1981).

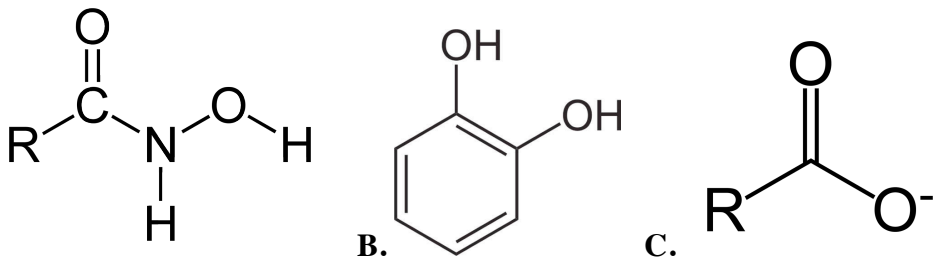

Figure 1.6. The most commonly identified organic functional groups responsible for metal–siderophore complexation. (A) hydroxamate; (B) catecholate; (C) carboxylate.

The majority of siderophores can be divided into three main structural classes based on

the presence of hydroxamate, phenolate-catecholate, and carboxylate functional groups (Figure 1.6). Hydroxamate siderophores include examples such as ferrioxamines and ferrichromes. Siderophores containing catecholate groups include the enterobactins and vibriobactins, while carboxylate and mixed-ligand hydroxamates include pyoverdines, azotobactins and ferribactins (Neilands, 1995). So far, almost 500 terrestrial compounds with a range of structures that incorporate either hydroxamate or catecholate groups have been classified as siderophores. These compounds constitute the most efficient iron-binding ligands found in nature (Vraspir and Butler, 2009).

Although hundreds of different siderophores have been identified, the majority of these ligands are produced by terrestrial and primarily pathogenic microorganisms. Very little is known about siderophores in the ocean, however several unique and prominent structural features have been identified specifically for the marine siderophores that have been discovered to date (Butler and Theisen, 2010). One unique structural feature of marine siderophores is the prevalence of α-hydroxy-carboxylic acid functional groups, either in the form of the amino acid α-hydroxy aspartic acid or citric acid. A second characteristic is the predominance of amphiphilic siderophores that contain an Fe(III)-binding head-group linked to a series of fatty acids (Figure 1.7). The presence of the fatty acid chains on marine siderophores is particularly interesting, as it increases the surface activity of the molecules, giving them the ability to form micelles. As a result, these ligands may stay bound to the cell surface when they are secreted, which ultimately slows the rate of diffusion away from the organism, maintaining a comparatively high local siderophore concentration (Hider and Kong, 2010). The majority of siderophores

found in the marine environment contain both of these distinguishing structural features (Vraspir and Butler, 2009).

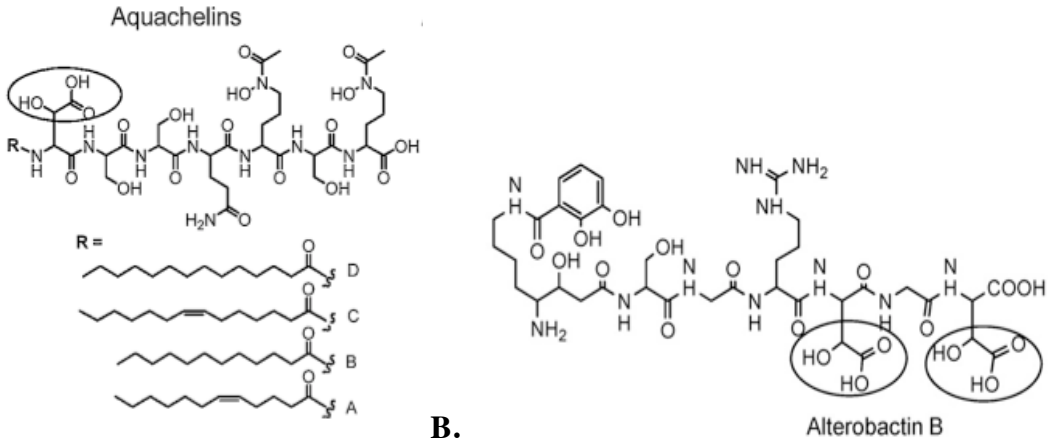

Figure 1.7. Structures of selected marine siderophores with the α-hydroxy-carboxylic acid in each structure circled. (A) Aquachelins, amphiphilic siderophores produced by *Halomonas aquamarina*; (B) Alterobactin B, a hydrophilic marine siderophore produced by *P. luteoviolacea* (Butler and Theisen, 2010).

By combining high-performance liquid chromatography (HPLC) with electrospray ionization-mass spectrometry (ESI-MS), several groups have been able to identify four members of the amphibactin family as well as several of the ferrioxamines in seawater by comparing mass spectral data with previously characterized ferrioxamine and amphibactin siderophores (Martinez et al., 2003; McCormack et al., 2003; Gledhill et al., 2004).

Although siderophores form the most stable complexes with Fe^{3+}, they can also complex with a variety of other elements (Farkas et al., 1997), particularly trivalent and tetravalent metal cations (Yoshida et al., 2004b). Siderophore interactions have the ability to increase the dissolution of common minerals (Liermann et al., 2000; Bi et al., 2010;

Simanova et al., 2010) and affect the reactivity of dissolved metals by modifying their speciation in seawater.

1.4. Research overview

As most of the research thus far has focused on the micronutrients Fe and Cu, little is known about the structure and sources of other essential trace metal-binding ligands in seawater. Analogous to Fe and Cu, greater than 98% of Zn in Pacific surface waters is complexed by strong and unidentified organic ligands exhibiting conditional stability constants of log $K \sim 11.0$ (Bruland, 1989). About 70% of dissolved Cd in surface waters is complexed with organic ligands with a conditional stability constant ranging from log $K \sim 9.8$–10.9 (Ellwood, 2004) to log $K \sim 12.0$ (Bruland, 1992). Both Zn and Cd are more highly complexed in surface waters than at greater depths, signifying that these ligands are produced by microorganisms (Bruland, 1989, 1992). It is possible that a portion of these Zn- and Cd-complexing ligands may be low-molecular-weight molecules, similar to those that form complexes with Cu or Fe. Investigations of marine siderophores with various trace metals can provide insight into the potential configurations, functional groups, and metal-binding affinities of these unknown organic ligands in seawater.

Metal-binding ligands control the bioavailability of trace metals and influence primary productivity and plankton community structure, therefore it is crucial to expand our understanding of their role in marine biogeochemistry. These strong organic ligands are clearly important in seawater, but their true identity remains unknown. My research aims to examine organic complexation of trace metals with a model siderophore, as well as describe the potential effects of siderophores on metal speciation in seawater.

1.4.1. Desferrioxamine B: a representative siderophore

Because the structural identities of strong organic ligands are unknown in natural seawater, I used a structurally characterized siderophore as a model ligand to investigate the organic complexation of trace metals other than Fe. The siderophore selected for this study is the linear trihydroxamate desferrioxamine B (DFOB) (Figure 1.8), the only siderophore that is currently commercially available in macroscopic quantities. Desferrioxamine B is produced as the drug Desferal® to treat iron overload disorders in humans (Bernhardt, 2007). Because this molecule is readily available, the stability of DFOB with Fe(III) has been thoroughly investigated throughout the last several decades, determining stability constants of $\beta_3 \sim 10^{31}$ in a variety of media (Schwarzenbach and Schwarzenbach, 1963; Anderegg et al., 1963a; b; Gould and Langerman, 1982; Evers et al., 1989). DFOB belongs to a group of siderophores called the ferrioxamines, displaying various structural configurations ranging from linear siderophores containing three hydroxamic acid functional groups (*e.g.* desferrioxamine A, B, C, D, F, and G), to cyclic structures (*e.g.* desferrioxamine D2 and E).

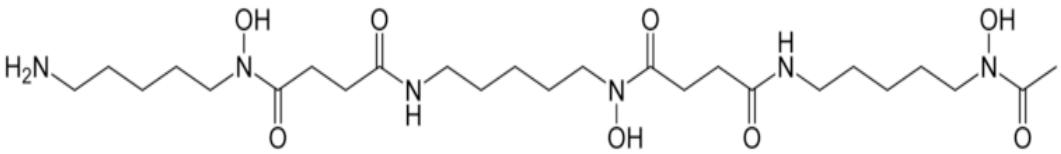

Figure 1.8. Molecular structure of the linear trihydroxamate siderophore, desferrioxamine B.

Thus far, the stabilities of many different metal–DFOB complexes have been measured, resulting in a range of affinities depending on the chemistry of the individual

metal ion (Table 1.2). While the stabilities of other M–DFOB complexes are many orders of magnitude smaller than that of the Fe(III)–DFOB complex (Table 1.2), laboratory measurements of these complexes will help to determine if siderophores fit the observations of L_1/L_2 complexation of divalent metals in seawater. Stability constants for several different M–DFOB complexes have been previously determined, however these measurements were either conducted under different experimental conditions, or an incorrect model was used to derive the stability constants. Due to the fact that most of these studies were performed at an ionic strength of 0.1 M, it may be questionable to use these constants in seawater speciation models, which require stability constants measured at 0.7 M ionic strength. Although there are several theoretical expressions that can be used to extrapolate equilibrium constants to different ionic strength values by means of ion activity models, each is only good for a limited range of ionic strength and few apply directly to seawater. The Davies Equation is an expression that is commonly used in chemical equilibrium computer programs due to its simplicity, and is shown below:

$$\log f = -Az^2 \cdot \left(\frac{\sqrt{I}}{1+\sqrt{I}} - 0.2I \right), \qquad (1.2)$$

where $A = 0.511$ at T = 25°C, z = charge of the ion, and I = ionic strength. However, since the Davies Equation is based on ionic interactions that do not apply to chelates and is only accurate for aqueous systems with $I \leq 0.5$ M, the extrapolation of metal–DFOB stability constants using this equation is not reliable for seawater.

Table 1.2 Stability constants ($\log \beta_1, \log \beta_2, \log \beta_3$) for selected metals with desferrioxamine B (DFOB).

M	$\log \beta_1$	$\log \beta_2$	$\log \beta_3$	Reference
Cd(II)	3.32	5.88	7.88	Anderegg et al. (1963a)[a]
Zn(II)	4.29	7.88	9.55	Hernlem et al. (1996)[b]
Ni(II)	4.36	7.70	10.90	Anderegg et al. (1963a)[a]
Cu(II)	7.66	12.94	13.54	Hernlem et al (1996)[c]
La(III)	4.88	7.70	10.09	Christenson and Schijf (2011)[d]
Lu(III)	6.48	11.25	15.19	Christenson and Schijf (2011)[d]
Co(III)	—	—	36.1 ± 0.4	Duckworth et al. (2009a)[e]
Fe(III)	10.50	21.84	30.60	Gould and Langerman (1982)[f]

[a] Value measured at T = 20°C in 0.1 M $NaNO_3$.
[b] Value measured at T = 25°C in 0.1 M KNO_3.
[c] Value measured at T = 25°C in 0.1 M $NaClO_4$.
[d] Value measured at T = 25°C in 0.7 M $NaClO_4$.
[e] Value measured at T = 25°C in 0.1 M NaCl.
[f] Value measured at T = 25°C in 2.0 M $NaClO_4$.

1.4.2. Research objectives

The goal of my research is to investigate organic complexation of trace metals in seawater by accurately determining stability constants for complexes of several trace metals with my representative siderophore, desferrioxamine B, at seawater ionic strength (0.7 M). These constants can then be compared with those of natural seawater ligands to investigate if the observed class of ligands, L, could be siderophores based on their stability and, furthermore, they can be used to examine the effects of siderophores on trace metal solution speciation in seawater. These measurements create a starting point for guiding the effort to fully understand the connection between biota and trace metal-binding ligands and the extent of organic complexation in the oceans.

Specific research objectives were the following:

1.) To determine if the unidentified organic ligands that strongly complex with Zn, Cd and Pb in seawater might be siderophores, the stability constants of Zn–, Cd–,

and Pb–DFOB complexes were measured at seawater ionic strength (0.7 M) in a non-complexing medium ($NaClO_4$) by potentiometric titrations. Chapter 2 presents values of the stability constant of all M–DFOB complexes at seawater ionic strength derived from non-linear regressions, which are then compared to conditional stability constants measured directly in seawater for unidentified strong organic ligands. The stability constants measured for each metal are also applied to calculations of their solution speciation in seawater.

2.) To determine if siderophores could provide a mechanism for Hg uptake and subsequent methylation within the oceanic water column, the stability constants of Hg– and methyl Hg–DFOB are determined at seawater ionic strength (0.7 M) in a non-complexing medium ($NaClO_4$) by potentiometric titrations through ligand competition experiments. Chapter 3 presents titration data for the Hg– and MeHg–DFOB complexes, albeit stability constants could not be derived from the non-linear regressions.

3.) To estimate the relative affinity of each YREE for natural marine particles, in Chapter 4 the stability constants of yttrium and the rare earth elements (YREE) with DFOB determined from previous work (Christenson and Schijf (2011) are employed in an updated model of YREE solution speciation in seawater, which is then used to determine the nature of marine particles responsible for their removal from the oceanic water column via surface complexation. A comparison is also made between this improved model of YREE–DFOB speciation in seawater and an earlier model of YREE removal by marine particulate organic matter (e.g., Byrne and Kim, 1990), on which it is based.

Chapter 2: Stability of DFOB complexes with Zn(II), Cd(II), and Pb(II)

2.1. Abstract

Results from laboratory studies suggest that complexation of trace metals with strong organic ligands plays an important role in their solution speciation in the surface ocean (Vraspir and Butler, 2009). Previous work has shown that organic complexation can dominate the solution speciation of certain trace metals, such as zinc, cadmium and lead, with ~50–99% of the total dissolved metal in seawater bound to strong organic ligands. However, little is known about the identity and chemical structure of these organic ligands. Known from terrestrial systems, siderophores are Fe(III) chelators excreted by microorganisms to acquire iron, however these organic ligands can also form complexes with a variety of other metals. I present here a series of stability constants for complexes of Zn, Cd, and Pb with the trihydroxamate siderophore desferrioxamine B (DFOB), representative of a class of small organic ligands that have an exceptionally high selectivity for Fe(III) and are present at low-picomolar concentrations in open ocean surface waters (Mawji et al., 2008). Stability constants were measured in a non-complexing medium ($NaClO_4$) at seawater ionic strength (0.7 M) by potentiometric titration of DFOB (pH 3–10) in the presence of the single metal ions. These constants were then compared to conditional stability constants measured directly in seawater for unidentified organic ligands that form stable complexex with Zn, Cd and Pb, in an effort to determine if these strong organic ligands in seawater might be siderophores.

Stability constants for the bidentate (log β_1), tetradentate (log β_2), and hexadentate (log β_3) complexes (Zn^{2+}: 4.81 ± 0.07, 7.99 ± 0.00_3, 9.39 ± 0.03, respectively; Cd^{2+}: 3.43 ± 0.03, 5.78 ± 0.02, 7.21 ± 0.03, respectively; Pb^{2+} (measured in $NaClO_4$): log β_1 = 6.21 ± 0.10, log β_2 = 9.55 ± 0.06; Pb^{2+} (measured in NaCl): log β_1 = 6.37 ± 0.04, log β_2 = 9.28 ± 0.04) were obtained from non-linear regressions of the titration data using FITEQL4.0. Both Zn and Cd were found to form hexadentate complexes with DFOB, whereas the Pb–DFOB complex is tetradentate. Linear free-energy relations (LFERs) of the three stability constants with the first hydrolysis constant ($\log \beta_1^*$) of each metal yield strong linear correlations with regression coefficients, $r^2 > 0.93$. The Zn–DFOB and Pb–DFOB stability constants determined in my study fall within the range of conditional stability constants measured in seawater, which suggests that unidentified organic ligands that form stable complexes with these metals in ocean surface waters may be siderophore-like molecules. Conversely, Cd–DFOB stability constants are substantially lower than conditional stability constants for Cd-specific organic ligands in Antarctic seawater (Ellwood, 2004), suggesting that Cd speciation may be dominated by a different type of organic ligand.

Seawater speciation models, constructed with MINEQL2.0 using the measured stability constants for each of the studied metals, reveal that DFOB exhibits no effect on Zn, Cd, and Pb speciation for realistic open ocean conditions and ligand concentrations. Therefore, for an organic ligand to have an impact on the speciation of these metals, it would have to have either a much higher stability constant or a much higher concentration than DFOB. However, the third and likeliest possibility is that many dozens, if not hundreds of similar compounds contribute to their organic complexation.

These results establish a starting point for assessing the effects of organic complexation comparable to that of DFOB on Zn, Cd, and Pb solution speciation in seawater.

2.2 Introduction

Trace metals play a significant role in the primary productivity of the world's oceans. Some trace metals, such as Zn, are required for the activity of various enzymes and are considered essential for marine biota, while others, like Pb, appear to have no biological function and can be toxic at very low concentrations. However, there are also certain trace metals that exhibit both behaviors. Cadmium, for example, has generally been considered a toxic element to living organisms at all concentrations, yet is now known to also play a more beneficial role through a Cd-dependent carbonic anhydrase found in some species of marine diatoms (Price and Morel, 1990). Comprehensive knowledge of metal and ligand speciation is necessary to understand their behavior. Complexation of Zn, Cd, and Pb with organic ligands may increase or decrease metal uptake, depending on the ligand involved, by making it more or less bioavailable. However, the source and nature of ligands that control the organic speciation of these trace metals need further investigation. In order for a chemical speciation model to be applied to a natural system, appropriate concentrations and stability constants of the metals and ligands present are required. It is crucial to further characterize the underlying chemical, physical, and biological processes controlling these reactive trace metals.

2.2.1. Zinc in seawater

Zinc has been recognized as an essential micronutrient for many marine organisms (mainly plants) for several decades. In aqueous environments, Zn is only present in the

+II oxidation state. Because Zn is intermediate between a soft metal, which strongly prefers soft bases like Cl^- and SH^-, and a hard metal, which prefers hard bases like O and N (i.e. OH^- and CO_3^{2-}) it will form strong bonds with a range of ligand types in aqueous systems and shows a range of affinities. The inorganic speciation of Zn^{2+} has been studied (Stanley and Byrne, 1990) and it is predominantly present in seawater as the free hydrated metal ion (~66%), as well as chloride (~15%) and carbonate complexes (~8%), with minor fractions of both sulfate and hydroxide complexes (~6% each).

Zinc is strongly complexed by organic ligands present in surface waters at nanomolar concentrations, which can account for more than 98% of the total dissolved metal in open ocean waters (Bruland, 1989). Mean conditional stability constants have been measured for Zn-complexing organic ligands, and have reported values ranging from $\log K' \sim 7.4–11$ (van den Berg and Dharmvanij, 1984; Bruland, 1989; Ellwood, 2004). While we have insight into the concentrations and stabilities of these ligands, very little is known about their molecular structure or function (van den Berg and Dharmvanij, 1984). It is hypothesized that some Zn-binding organic ligands may be siderophore-like molecules, allowing certain microorganisms to gain a competitive advantage for this potentially biolimiting element by assimilating the organically complexed Zn (Ellwood, 2004; Xu et al., 2008; Vraspir and Butler, 2009).

As mentioned in Chapter 1, the nutrient-type vertical distribution of Zn is significantly correlated with that of silicate, suggesting similar patterns of biological uptake and regeneration (see Figure 1.2). Due to its role in metabolic processes, Zn is essential to living organisms. It has been found to serve as a cofactor for several enzymes, including carbonic anhydrase, alcohol dehydrogenase and alkaline phosphatase (Plocke et al.,

1962). As a biolimiting micronutrient in certain parts of the ocean, Zn availability may influence distributions of phytoplankton species (Morel et al., 1994). Brand et al. (1983) showed that growth rates of various algae and cyanobacteria are affected differently when cultured in an EDTA-buffered medium over a range of Zn^{2+} activities, with most oceanic species showing maximal reproductive rates and no or slight evidence of Zn limitation, while the reproductive rates of many of the coastal species studied were limited by low Zn^{2+} activities. Crawford et al. (2003) also investigated the potential limitation of Zn to phytoplankton, and found an increase in the reproductive rates of the coccolithophore *Emiliania huxleyi* with the addition of Zn to NE Pacific surface waters compared to a control.

2.2.2 Cadmium in seawater

Cadmium is present in natural waters in the +II oxidation state, which is its only stable redox state in aqueous solution. Because Cd is chemically classified as a soft, B-type metal, it tends to form relatively stable complexes with Cl^- and with sulfur-bearing organic ligands. In seawater, inorganic Cd(II) is dominated by moderately stable chloride complexes, predominantly $CdCl_2^0$ and $CdCl^+$, leaving only ~3% present as the free metal (Byrne et al., 1988).

Although the inorganic speciation of Cd in seawater is for the most part well characterized, less data exist regarding Cd complexation with organic ligands. Bruland (1992) found that ~70% of dissolved Cd in the surface waters of the North Pacific is bound to strong, Cd-specific organic ligands present at low-nanomolar concentrations, with a mean value for the conditional stability constant of log K' = 12. More recently,

Ellwood (2004) found substantially lower conditional stability constants for Cd of log $K' \sim 9.5–10.5$ in the subantarctic waters east of New Zealand. Although the actual composition and structure of these strong, organic ligands remains unknown, it is likely that specific organic ligands play a significant role in altering the speciation of Cd, particularly at the low concentrations present in surface waters.

Similar to Zn, dissolved Cd displays a nutrient-like profile in the open ocean, characterized by a strong gradient from low picomolar concentrations in surface waters to a mid-depth maximum of around 1 nM (see Figure 1.3A). Its vertical distribution is highly correlated with that of dissolved phosphate (see Figure 1.3B), which suggests that Cd and phosphate have similar chemical reactivity near the surface and are remineralized with biogenic debris at greater depths (Boyle et al., 1976). While Cd exhibits nutrient-like behavior, it is also known to be a very toxic element for many marine organisms and has been found to produce negative effects on osmoregulation, larval development, and reproductive behavior (Mason et al., 2000). Considering these opposing roles, it is likely that phytoplankton regulates the toxicity and/or bioavailability of Cd(II) through the production of certain strong organic ligands. Cadmium may be taken up by phytoplankton in Zn-depleted waters and it has been found to substitute for Zn(II) or Co(II) in a functional, although less effective form of carbonic anhydrase, a key enzyme enabling the assimilation of bicarbonate into organic matter (Price and Morel, 1990; Sunda and Huntsman, 1995; Xu et al., 2008). As a result, the once general belief that Cd has no known biological function (Lee et al., 1995) is no longer widely held.

2.2.3. Lead in seawater

Analogous to Zn and Cd, Pb also exists in seawater in the +II oxidation state. Like Zn, Pb is considered intermediate between a soft and hard metal and therefore will bind with a variety of ligands. Chloride complexes ($PbCl_2^0$) and carbonate complexes ($PbCO_3^0$) dominate the inorganic speciation of Pb^{2+} in open ocean surface waters (Byrne, 1981; Easley and Byrne, 2011). In contrast to Zn and Cd, Pb is a toxic, non-essential metal that is not currently known to serve any biological function. Displaying scavenged behavior, Pb concentrations are high in the surface waters due to atmospheric input and decrease with depth as dissolved Pb is rapidly removed by adsorption of the ions or ionic complexes onto sinking particle surfaces, such as clay minerals, organic matter, bacteria, fecal pellets etc. (Santana-Casiano et al., 1995) (see Figure 1.4).

Relatively little is known about the organic complexation of Pb. According to Capodaglio et al. (1990), ~50% of total Pb in surface waters is bound with a Pb-specific class of strong organic ligands observed at subnanomolar concentrations, having a mean conditional stability constant of log K' = 9.7. In Narragansett Bay, Kozelka and Bruland (1998) found two classes of Pb-binding ligands, a strong class with a mean conditional stability constant of log K' ~ 10 and a weaker class with a mean conditional stability constant of log K' ~ 8.8.

2.2.4. Zn, Cd, and Pb complexation with DFOB

As discussed in Chapter 1, siderophores are organic ligands excreted by microorganisms in seawater to facilitate the acquisition of biolimiting iron and are

present in open ocean surface waters (Gledhill and van den Berg, 1994; Martinez et al., 2001; Mawji et al., 2008). Desferrioxamine B (DFOB), is a member of the hydroxamate siderophores and the stability of its complexes with a variety of metals has been examined quite extensively (e.g., Hernlem et al., 1996; Farkas et al., 1997; Duckworth et al., 2009a). DFOB has such a large affinity specifically for iron ($\beta_3 \sim 10^{31}$) (Anderegg et al., 1963b) because the microorganisms evolved to produce molecules that perfectly match the ionic radius and coordination number of Fe^{3+} as it wraps around the metal cation (Figure 2.1). While the stabilities of DFOB complexes with divalent metals are many orders of magnitude lower than that of the Fe(III) complex, they may nonetheless match the stability of the unknown classes (L_1, L_2) of natural organic ligands identified from field measurements.

As shown in Figure 1.8, DFOB is characterized by three hydroxamate groups, with a terminal amine group. The sequential deprotonation of DFOB is shown in the following general reaction:

$$H_pDFOB^{(p-3)+} \leftrightarrow H^+ + H_{p-1}DFOB^{(p-4)+} \quad (p = 4,\ 3,\ 2,\ 1) \tag{2.1}$$

where the corresponding acid dissociation constants are expressed in terms of single deprotonation steps (i.e. K_{a1} describes a single deprotonation of H_4DFOB^+, K_{a2} describes a single deprotonation of H_3DFOB^0, and so on):

$$K_{aj} = \frac{[H^+][H_{p-1}DFOB^{(p-4)+}]}{[H_pDFOB^{(p-3)+}]} \quad (j = 5 - p)\,. \tag{2.2}$$

Complexation of Zn, Cd, or Pb with DFOB is described by the following reactions and their corresponding stability constants (β_i):

$$M^{2+} + H_qDFOB^{(q-3)+} \leftrightarrow MH_qDFOB^{(q-1)+} (q = 3, 2, 1) . \quad (2.3)$$

$$\beta_i = \frac{[MH_qDFOB^{(q-1)+}]}{[M^{2+}][H_qDFOB^{(q-3)+}]} \quad (i = 4 - q) . \quad (2.4)$$

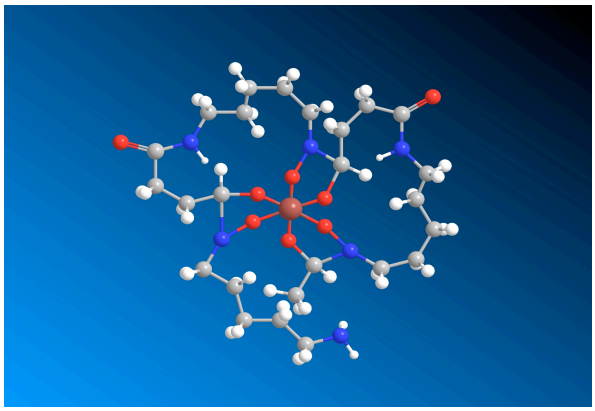

Figure 2.1. Depiction of Fe^{3+} fully complexed with the siderophore, desferrioxamine B, produced with ChemDraw® software. As metals bind to each of the three hydroxamate groups in a step-wise process, the DFOB molecule wraps itself around the central metal cation.

In order to produce an accurate seawater speciation model of these metals that includes my chosen siderophore, stability constants need to be assessed at seawater ionic strength (0.7 M). The only previous report on the stability constant of the Cd(II)–DFOB complex proposes a value of log $\beta_3 \sim 8$ at 0.1 M ionic strength (Anderegg et al., 1963a; b). The stability of the Zn(II)–DFOB complex has been measured at 0.1 M ionic strength in KNO_3 and found to be log $\beta_3(Zn^{2+}) = 9.55$ (Hernlem et al., 1996). Hernlem et al. (1996) also reported stability constants for the Pb(II)–DFOB complex, however their

resulting log β_2 and log β_3 values are very similar (9.25 and 10.00, respectively). These authors overlooked the fact that these nearly identical constants lead to a thermodynamic inconsistency, suggesting that Pb does not form a hexadentate complex with DFOB. Referring back to Eqs. (2.3) and (2.4), which describe the deprotonation reactions and the corresponding stability constants (β_i) for metal complexation with DFOB, it is clear that the values of log β_2 and log β_3 cannot be the same. If $\beta_3 = \beta_2$, then:

$$\frac{[\mathrm{MHDFOB^0}]}{[\mathrm{M^{2+}}][\mathrm{HDFOB^{2-}}]} = \frac{[\mathrm{MH_2DFOB^+}]}{[\mathrm{M^{2+}}][\mathrm{H_2DFOB^-}]}. \tag{2.5}$$

These reaction quotients can be rearranged as follows:

$$\frac{[\mathrm{MHDFOB^0}]}{[\mathrm{MH_2DFOB^+}]} = \frac{[\mathrm{HDFOB^{2-}}]}{[\mathrm{H_2DFOB^-}]} \rightarrow \frac{[\mathrm{H^+}][\mathrm{MHDFOB^0}]}{[\mathrm{MH_2DFOB^+}]} = \frac{[\mathrm{H^+}][\mathrm{HDFOB^{2-}}]}{[\mathrm{H_2DFOB^-}]}.$$

If this were true, then the stability constants of the following two reactions would be equal:

$$\mathrm{M^{2+} + H_2DFOB^+ \leftrightarrow MHDFOB^0 + H^+} \tag{2.6}$$

$$\mathrm{H_2DFOB^+ \leftrightarrow HDFOB^0 + H^+}, \tag{2.7}$$

implying that the deprotonation constant of the third DFOB hydroxamate group is the same whether it is bound to the metal or not. This suggests that the hexadentate complex does not form and that Hernlem et al. (1996) should have removed β_3 from their regression model.

In this chapter I report the first measurements of stability constants of Zn–DFOB, Cd–DFOB, and Pb–DFOB complexes at seawater ionic strength by potentiometric titrations in a non-complexing medium ($NaClO_4$). This is also the first work to report that Pb^{2+} does not fully complex with DFOB, most likely due to its irregular coordination

sphere, which was confirmed by creating three separate speciation models representing different binding mechanisms of Pb–DFOB. In the discussion, the Zn, Cd, and Pb stability constants are interpreted through linear correlations with various metal ion parameters including the first hydrolysis constant, ionic radius and ionic charge. My results suggest that the unidentified organic ligands that strongly complex with Pb and Zn in seawater could be siderophore-like molecules. The data presented here are a starting point for guiding efforts to understanding the character and stability of organic trace metal complexes in the ocean by identifying favorable candidates with the correct combination of properties.

2.3. Materials and methods

2.3.1. Chemical preparation and experimental setup

All standard and experimental solutions were prepared inside a class-100 laminar flow bench with Milli-Q water (18.2 MΩ·cm) from a Millipore Direct-Q 3UV purification system. All solutions were prepared with plastic laboratory materials that had been acid cleaned and thoroughly rinsed with Milli-Q water before use. Large Teflon bottles and non-Teflon items were soaked in cold 4 M HCl for at least one week and small Teflon items were immersed in sub-boiling 8 M HNO_3 for 24 hours.

Potentiometric titrations were conducted with certified carbonate-free sodium hydroxide solution (0.1001 M or 1.0005 M, Brinkmann). The pH standard used for calibrating the glass electrode of the autotitrator was made by dissolving 40.9 g sodium chloride (99.999%, Sigma-Aldrich) in Milli-Q water in a 1-L volumetric flask to obtain a solution of 0.70 M. Its pH was set to 3.000 by addition of certified hydrochloric acid

(HCl, 1.0011 M, Brinkmann). Background electrolyte solution for the titrations was made by dissolving ~100 g sodium perchlorate hydrate (99.99%, Sigma-Aldrich) in Milli-Q water in a 1-L volumetric flask. The density of the $NaClO_4$ solution was determined by weight and its final ionic strength adjusted to 0.700 ± 0.004 M by dilution with Milli-Q water using the empirical relation between density and molar concentration described by Janz et al. (1970). The 0.7 M $NaClO_4$ solution was then set to pH ~3 through the addition of 100 μL of concentrated $HClO_4$. The concentrated perchloric acid (TraceMetal Grade, Fisher Scientific) was manually titrated with 1.0005 M NaOH to the phenol red endpoint and its concentration found to be 11.40 ± 0.02 M (n = 7). An electrode filling solution of 3 M NaCl was made by dissolving sodium chloride in Milli-Q water in a 1-L volumetric flask and was replaced daily prior to titrations.

Desferrioxamine B (DFOB), supplied by Sigma-Aldrich as the methanesulfonate (mesylate) adduct (assay ~95%), was stored at –20°C and used without further purification. When dissolved in acidic solutions, the DFOB molecule is present in the fully protonated form, H_4DFOB^+, in addition to the mesylate ($CH_3SO_3^-$) counter-ion. Stock solutions of ~40 mM DFOB were made daily by dissolving ~263 mg DFOB mesylate in 10 mL of the background electrolyte solution (0.7 M $NaClO_4$). Stock solutions of ~20 mM Cd, and ~40 mM Zn and Pb were prepared separately by dissolving the appropriate amount of metal perchlorate salt in 40 mL (Cd) or 20 mL (Zn and Pb) of the background electrolyte. Cadmium perchlorate hydrate (99.999%) and lead perchlorate hydrate (≥99.995%) were purchased from Sigma-Aldrich, whereas zinc perchlorate hexahydrate (99.997%) was purchased from Alfa Aesar. The exact concentrations of these metal stock solutions were measured by ICP-MS (Agilent 7500cx) after a 10^6-fold

dilution with 1% HNO_3, utilizing a 5-point external calibration line using Ge, In, and Re as internal standards, as described by Schijf and Marshall (2011). For Zn, masses 66 and 68 were measured, which were normalized to ^{72}Ge. For Cd, masses 110, 111, and 112 were measured, which were normalized to ^{115}In. Concentrations resulting from the different isotopes were averaged. For Pb, masses 206, 207, and 208 were measured, normalized to ^{187}Re, and then added together to determine a single Pb concentration.

2.3.2. Potentiometric titrations of Cd+DFOB, Zn+DFOB and Pb+DFOB mixtures

All potentiometric titrations were performed using a Brinkmann Metrohm 809 Titrando autotitrator, running under Tiamo v.1.2.1 software. Automated potentiometric titrations were performed with a custom method written in the Tiamo software using procedures that closely follow those used by Christenson and Schijf (2011). Each titration began by filling the glass reaction vessel with 50.0 mL of the pH standard (0.70 M NaCl, pH 3.000) and sealing the lid. The standard solution was then sparged with N_2 while stirring for 1 min to eliminate any dissolved CO_2 from the system and allow the solution and electrode to equilibrate at the appropriate temperature. Subsequently, the millivolt reading of the electrode was recorded continuously for 1 min, or until it produced a stable reading better than 0.1 mV/min. The final mV reading was used by the Tiamo method to determine a linear equation for converting mV readings to pH (= –log $[H^+]$), assuming a Nernstian slope (–59.16 mV/pH at T = 25°C).

After the electrode was calibrated, stirring was suspended and the pH standard solution was replaced with 50.0 mL of the background electrolyte solution (0.7 M $NaClO_4$), which contained 2 mM DFOB and variable concentrations of single metals to

yield a range of Cd:DFOB, Zn:DFOB, and Pd:DFOB molar ratios. The reaction vessel was resealed and the sample solution stirred and sparged with N_2 for 10 min. Lastly, the sample solution was titrated to pH 10 with certified, carbonate-free NaOH in a dynamic fashion, as the amount of base added per shot was continuously adjusted by the method to produce a relatively constant increase of pH throughout the titration. After every shot of base followed by an equilibration period of at least 1 min, the electrode was monitored for up to 1 min, or until its stability was better than 0.5 mV/min, before recording a mV reading. Final titration data consist of a list of incremental titrant volumes and corresponding mV readings, which is exported in Excel format.

Initial titrations of cadmium at Cd:DFOB molar ratios up to 1.5 showed increasingly poor fits of the titration curves above ratios of 0.9. Towards the end of these high molar ratio titrations, a white precipitate was observed in the experimental solution, which is most likely a $Cd(OH)_2$ precipitate forming due to the excess Cd^{2+} in solution. Therefore, all subsequent titrations of Zn, Cd, and Pb were only conducted at molar ratios of 1:4, 1:2 (in triplicate) and 0.7:1 (M:DFOB) in order to decrease the likelihood of hydroxide precipitates forming throughout the titration. To assess the effect of metal–chloride complexation, one series of lead titrations was conducted in 0.7 M NaCl, also at molar ratios of 0.25, 0.5, and 0.7. A total of 15 titrations of Cd with DFOB were conducted in 0.7 M $NaClO_4$ (one with 1 M NaOH, and 14 with 0.1 M NaOH), 6 titrations of Zn with DFOB in 0.7 M $NaClO_4$ (all with 0.1 M NaOH), and 10 titrations of Pb with DFOB, 5 in 0.7 M $NaClO_4$ and 5 in 0.7 M NaCl (all with 0.1 M NaOH). Since early titrations of Cd–DFOB mixtures revealed that the 1 M NaOH titrant gave inadequate pH resolution, the 0.1 M NaOH titrant was used thereafter.

2.3.3. Determination of Zn–DFOB, Cd–DFOB and Pb–DFOB stability constants

In order to calculate the stability constants of these metal–DFOB complexes, non-linear regressions of the titration data were preformed using the software program FITEQL4.0 (Herbelin and Westall, 1999). The FITEQL program uses a systematic notation that describes the chemical system in algebraic terms, resulting in a matrix of the reactions and mass balance equations, known as a *tableau*. This notation distinguishes the metals and ligands as the "components" of the system, whereas all linear combinations of these components are considered as "species" (Morel and Morgan, 1972). First, separate models for Cd, Zn, and Pb complexation with DFOB were built using the following processes: (i) the deprotonation of water in either 0.7 M $NaClO_4$ or 0.7 M NaCl (for the Pb titrations conducted in NaCl); (ii) the sequential deprotonation of DFOB; (iii) the sequential deprotonation of the three M–DFOB complexes, and (iv) complexation of Cd, Zn, and Pb with other inorganic ligands. These four processes are discussed individually below.

Since FITEQL would use the Davies Equation, which is appropriate only for $I \leq 0.5$ M, to extrapolate equilibrium constants to seawater ionic strength (I = 0.7 M), equilibrium constants for the regression models were applied without extrapolation (Schijf and Ebling, 2010). When setting up the tableau, Na^+ and ClO_4^- (or Cl^-, depending on the background electrolyte) were included as inert ions, with concentrations equal to the ionic strength of the solution (0.7 M). The equilibrium constants determined from the non-linear regressions were calculated at the ionic strength of the experimental solutions

(0.7 M $NaClO_4$ or NaCl), and therefore should be regarded as conditional for the medium in which they were measured.

The deprotonation of water occurs according to the following general reaction:

$$H_2O \leftrightarrow OH^- + H^+ \qquad K_w = [OH^-][H^+] \tag{2.8}$$

The value of K_w, the equilibrium constant for the ionization of water, appropriate for $NaClO_4$ was obtained by refitting data compiled by Turonek et al. (1998). Since a glass electrode was utilized in my study, data obtained by glass electrode were selected for this fit, however for I < 4 M, these data are indistinguishable from data obtained by hydrogen electrode. A fit of the data with an extended Debije-Hückel relation yields $pK_w = 13.740$ at I = 0.7 M in $NaClO_4$ and $pK_w = 13.718$ at I = 0.7 M in NaCl, which is comparable to calculations based on the Specific Interaction Theory (Christenson and Schijf, 2011). These values of K_w were entered in FITEQL and treated as a constant.

Several titrations were conducted without metal or DFOB in 0.7 M $NaClO_4$, serving as blank titrations to check for the presence of carbonate and bicarbonate. These titrations were then fit with a 'blank' model in FITEQL, which confirmed that the only proton exchange occurring was due to the deprotonation of water. This indicates that bubbling with N_2 throughout the titration effectively removed dissolved CO_2 and that no other acid/base pairs were present.

As described in Section 2.2.4, DFOB is a trihydroxamate ligand with a terminal amine group, and thus a tetraprotic acid (it has four exchangeable protons). The ligand can exist in five different forms, $DFOB^{3-}$, $HDFOB^{2-}$, H_2DFOB^-, H_3DFOB^0, and H_4DFOB^+, with the pH-dependent equilibrium between these five species described by four acid

dissociation constants or K_as. Only one of five forms of DFOB can be selected as the component in FITEQL with respect to which the equilibrium reactions with each of the five species are defined. The choice of component species has been evaluated in previous work (Christenson and Schijf, 2011) by constructing five different models, one with each of the five forms of DFOB used as the component. Although the five possible models are theoretically equivalent, no one form is optimal for the full pH range of the titration, therefore each component leads to minor differences in the quality and resulting parameters of the fits. The model that was constructed with H_3DFOB^0 as the component resulted in the best quality-of-fit parameters, or values of WSOS/DF (the weighted sum of squares divided by the degrees of freedom), as well as the lowest RSDs (Christenson and Schijf, 2011). Consequently, H_3DFOB^0 was used as the component in all regressions for my work, with reactions (2.1) and acid dissociation constants (Eq. (2.2)) expressed in terms of this component, as shown below:

$$H_pDFOB^{(p-3)+} \leftrightarrow H_3DFOB^0 + (p-3)H^+ \quad (p = 4,\ 3,\ 2,\ 1,\ 0) \tag{2.9}$$

$$R_j = \frac{[H_3DFOB^0][H^+]^{(p-3)}}{[H_pDFOB^{(p-3)+}]} \quad (j = 5-p). \tag{2.10}$$

The four acid dissociation constants for DFOB have been previously measured in 0.7 M $NaClO_4$ and 0.7 M NaCl through a series of potentiometric titrations with DFOB alone over the pH range 3–11. It was determined that the three hydroxamate protons dissociate in the pH range 8.4–9.7 (pK_{a1}= 8.54, pK_{a2}= 9.06, pK_{a3} = 9.70 in 0.7 M $NaClO_4$ and pK_{a1}= 8.40, pK_{a2}= 8.93, pK_{a3} = 9.58 in 0.7 M NaCl), whereas the terminal amine group deprotonates at a much higher pH (pK_{a4} = 10.89 in 0.7 M $NaClO_4$ and pK_{a4} = 10.74 in

0.7 M NaCl) (Christenson and Schijf, 2011). DFOB acid dissociation constants have also been measured in a variety of different media (KCl, NaCl, and $NaClO_4$), over a range of ionic strengths (0–1 M), and although large errors bars are associated with some of the data, it appears that the pK_{ai} display no clear dependence on either ionic strength or medium composition (Christenson and Schijf, 2011). The four pK_as measured in 0.7 M $NaClO_4$ (or 0.7 M NaCl for 5 of the Pb titrations) were entered in FITEQL and treated as constants in regressions of the Zn–DFOB, Cd–DFOB, and Pb–DFOB titration data.

In order to conform to FITEQL4.0 tableaux and because H_3DFOB^0 was chosen to be the component for the DFOB ligand in all regression models, the complexation reactions (2.3) and their corresponding stability constants (Eq. (2.4)) were rewritten in the following way:

$$M^{2+} + H_3DFOB^0 \leftrightarrow MH_qDFOB^{(q-1)+} + (3-q)H^+ \quad (q = 3, 2, 1) \qquad (2.11)$$

$$Q_i = \frac{[MH_qDFOB^{(q-1)+}][H^+]^{(3-q)}}{[M^{2+}][H_3DFOB^0]} \quad (i = 4-q)\ , \qquad (2.12)$$

so that when Eqs. (2.3) and (2.7) are combined, $Q_1 = \beta_1$, $Q_2 = \beta_2$ x K_{a2}, and $Q_3 = \beta_3$ x K_{a2} x K_{a3} (see Table 2.2). These are the unknown constants of the system that act as adjustable parameters in the model.

The final process included in the model is the complexation of Zn, Cd, and Pb with other ligands. All titrations were performed in a non-complexing medium of $NaClO_4$ (except for the 5 Pb titrations conducted in NaCl) and high-purity perchlorate salts were used in order to minimize chloride competition. Additionally, all titrations were performed under a nitrogen atmosphere in order to eliminate any CO_2 from the system,

which could result in metal–carbonate complexation. The only other ligands in the sample solutions that could form complexes with the individual metals were OH^- and mesylate, the counter-ion of DFOB.

The effect of the mesylate anion on the buffer intensity of the sample solutions has been previously investigated by titrating MSA alone in $NaClO_4$ over the pH range 1.3–11.5. These results were practically identical to blank titrations, indicating that its pK_a likely lies outside this pH window and therefore displays no effect on the buffer intensity of the sample solutions (Christenson and Schijf, 2011). Hernlem et al. (1996) also attempted to measure the pK_a of MSA, which they mistakenly thought was 1.9 due to a sign error in the NIST database (Martell et al., 2004), whereas it is actually –1.9. In previous work, the stability of the Lu–MSA complex was estimated from Lu titrations in the presence of MSA, and was found to likely be no larger than that of the Lu–sulfate complex, which is chemically similar. In order to assess the possibility that the mesylate anion could affect the Zn, Cd, and Pb titrations in this work, a metal–MSA complex was added to the regression model assuming a $\log {}_{MSA}\beta_1$ value equal to the stability of the metal–sulfate complex (*e.g.* $\log {}_{MSA}\beta_1(Pb) = 1.29$; (Byrne et al., 1988). It was concluded that any MSA complexes were minor species during the titrations and did not significantly impact the fitting of my data. Given these results and since accurate values of $\log {}_{MSA}\beta_1$ are not yet available for Zn, Cd and Pb, metal–mesylate complexes were ignored in the model.

Since the titrations ended at pH 10, metal hydrolysis at elevated pH must also be accounted for in the model. This involves the following equilibration reaction and its corresponding formation constant ($\log \beta_1^*$):

$$M^{2+} + H_2O \leftrightarrow MOH^+ + H^+, \quad (2.13)$$

$$\beta_1^* = \frac{[MOH^+][H^+]}{[M^{2+}]} \quad . \quad (2.14)$$

Stability constants of the MOH^+ complexes ($\log \beta_1^*$) were kept fixed in the regressions at values for I = 0.7 M taken from the literature (Table 2.1).

Table 2.1. Stability constants of the MOH^+ complexes ($\log \beta_1^*$) for Zn, Cd, and Pb for I = 0.7 M.

M^{2+}	$\log \beta_1^*$	Reference
Zn	–9.14	Schorsch (1964)
Cd	–10.2	Biedermann and Ciavatta (1962)
Pb	–7.799	Easley and Byrne (2011)

Three separate models were created for Zn, Cd, and Pb describing the complexation with DFOB. For each model, the four processes discussed above must be arranged into a matrix of the reactions and mass balance equations (i.e., a tableau) based on the chemical components and all their species. Table 2.2 shows an example of the tableau created for the metals selected in this study. Once the tableau is set up, data from each individual titration can be read into the FITEQL software, where the equilibrium problem is solved at conditions corresponding to each of the data points provided. Then the individual parameters in the model are iteratively adjusted until the model results fit the data.

Table 2.2. Typical tableau created in FITEQL4.0 for each metal studied (M^{2+} = Zn, Cd, and Pb), which is a representation of all components in the system (first row) and possible species (first column) with their corresponding equilibrium constants. Constants in bold are kept fixed during regressions, whereas β_1, β_2, and β_3 are the adjustable parameters in the model.

	Na^+	ClO_4^-	H_3DFOB^0	M^{3+}	Cl^-	H^+	log K
Na^+	1	0	0	0	0	0	0
ClO_4^-	0	1	0	0	0	0	0
H^+	0	0	0	0	0	1	0
OH^-	0	0	0	0	0	–1	$\mathbf{-pK_W}$
H_4DFOB^+	0	0	1	0	0	1	$\mathbf{-pK_{a1}}$
H_3DFOB^0	0	0	1	0	0	0	0
H_2DFOB^-	0	0	1	0	0	–1	$\mathbf{pK_{a2}}$
$HDFOB^{2-}$	0	0	1	0	0	–2	$\mathbf{pK_{a2} + pK_{a3}}$
$DFOB^{3-}$	0	0	1	0	0	–3	$\mathbf{pK_{a2} + pK_{a3} + pK_{a4}}$
M^{2+}	0	0	0	1	0	0	0
Cl^-	0	0	0	0	1	0	0
$MHDFOB^0$	0	0	1	1	0	–2	$\log \beta_3 + \mathbf{pK_{a2} + pK_{a3}}$
MH_2DFOB^+	0	0	1	1	0	–1	$\log \beta_2 + \mathbf{pK_{a2}}$
MH_3DFOB^{2+}	0	0	1	1	0	0	$\log \beta_1$
MOH^+	0	0	0	1	0	–1	$\mathbf{\log \beta_1^*}$

2.4. Results

Figure 2.2 shows titration data for Zn, Cd and Pb, in addition to data obtained with pure DFOB in the absence of metals (Christenson and Schijf, 2011). The deviation in the metal–DFOB titration curves with respect to the titration curve of DFOB alone (shown in black in Figure 2.2) corresponds to the metal's ability to eject protons from the DFOB molecule. Therefore, the more the pH values are lowered and the further the titration curve deviates from that of DFOB alone, the greater the stability of the metal–DFOB complexes. Parameters derived from non-linear regressions were converted to stability

constants (β_1, β_2, and β_3) of the three corresponding M–DFOB complexes. These metals coordinate only with the hydroxamate groups of the DFOB molecule in bi-, tetra-, and hexadentate configurations, because deprotonation of the terminal amine group was not seen in any of the titrations. Results from each individual regression for Zn, Cd, and Pb are shown in Tables 2.3–2.6. All models fit the data very well, with low WSOS/DF values, which is the quality-of-fit parameter for FITEQL based on the overall variance (Herbelin and Westall, 1999).

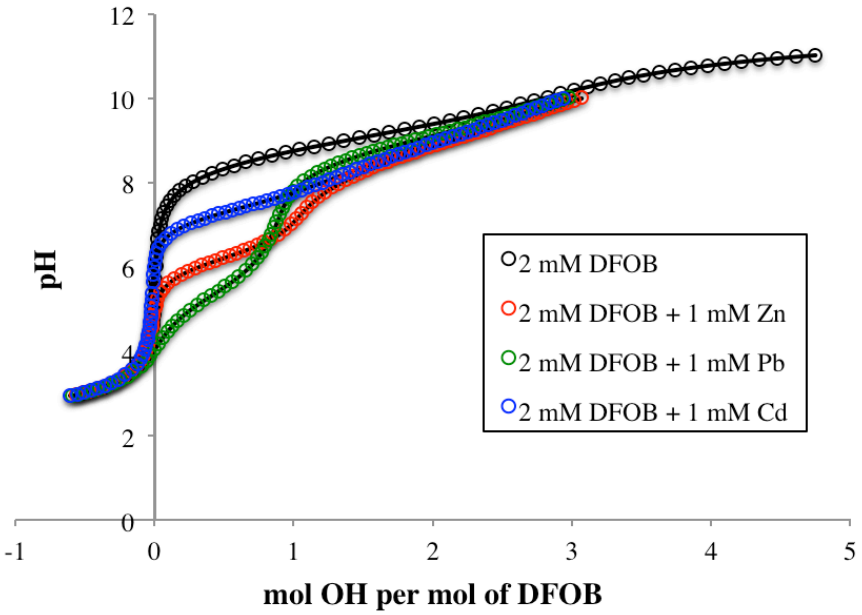

Figure 2.2. Non-linear regressions of potentiometric titrations of DFOB solutions and Zn + DFOB, Cd + DFOB and Pb + DFOB mixtures in 0.7 M $NaClO_4$, where pH (measured with a glass combination electrode) is shown as a function of the amount of base added, or the moles of base (OH^-) per mole of DFOB (computed from titrant volumes). All DFOB solutions contain 2 mM DFOB and each M^{2+} + DFOB mixture also contains 1 mM of a single M^{2+} (Zn, Pb, or Cd). Symbols are actual measurements and solid lines are non-linear regressions performed with FITEQL4.0.

Stability constants were measured in 0.7 M $NaClO_4$ and 0.7 M NaCl for Pb, both

displaying similar trends in the resulting constants. All Pb–DFOB titration data were initially fit with a 3-step, hexadentate coordination model assuming that all three Pb–DFOB complexes are formed, (β_1, β_2, and β_3) (Table 2.5). Using this model, the resulting stability constants (β_2 and β_3) of the tetra- and hexadentate M–DFOB complexes were unrealistically close to one another ($\log \beta_2 \sim 9.60$, and $\log \beta_3 \sim 10.12$), similar to the results of Hernlem et al. (1996). For this reason, all Pb data were refit with a new 2-step, tetradentate coordination model assuming that only the first two complexes are formed (β_1 and β_2), which resulted in better 'quality-of-fit' values and fewer iterations (Table 2.6). Additionally, the β_1 and β_2 values derived from the two-step, tetradentate coordination model were very similar to the β_1 and β_2 values derived from the 3-step, hexadentate coordination model, hence applying the principle of Occam's razor, the simpler, two-parameter model is a better representation of the data. The $\log \beta_2$ determined in this work using the two-step, tetradentate coordination model lies between $\log \beta_2$ and $\log \beta_3$ reported by Hernlem et al. (1996), while my $\log \beta_1$ value agrees closely with their reported value.

Alternatively, I assumed that the final hexadentate complex may actually form via a simultaneous two-proton exchange, rather than two sequential one-proton exchanges, meaning that the second and third bond form simultaneously with the release of two protons. This theory was tested by altering the tableau for Pb so that the second and third reactions occur concurrently. With this new 2-step, hexadentate coordination model (β_1 plus $MH_3DFOB^{2+} = MHDFOB^{0} + 2H^{+}$), FITEQL was unable to converge for any of the titration runs, confirming that with the given data, Pb does not bond with the third hydroxamate group of the DFOB molecule.

Table 2.3. Results from six titrations (pH 3–10) of Zn in 0.70 M $NaClO_4$ solutions containing 2 mM DFOB and using a titrant of 0.1001 M NaOH. Regressions were performed with FITEQL4.0, keeping pK_W = 13.740 and the pK_{ai} of DFOB fixed at values discussed in Section 2.4.1, with $\beta_1, \beta_2, \beta_3$ as adjustable parameters. All regressions converged in 7 iterations (*n*) or less.

Zn:DFOB ratio	$\log \beta_1$	$\log \beta_2$	$\log \beta_3$	[DFOB] (mM)	n [a]	WSOS/DF[b]
0.52	4.83	7.99	9.42	2.04	4	1.44
0.26	4.73	7.99	9.37	2.06	7	0.729
0.72	4.86	7.99	9.38	2.06	4	1.86
0.52	4.84	7.99	9.42	2.06	5	1.33
0.26	4.70	7.99	9.37	2.07	6	0.704
0.72	4.87	7.98	9.37	2.10	5	1.95

[a] Number of iterations for regression to converge.
[b] WSOS/DF (Weighted Sum-Of-Squares divided by the Degrees-of-Freedom) is the quality-of-fit parameter for FITEQL, with values in the range 0.1–20 indicating a good fit (Herbelin and Westall, 1999).

Table 2.4. Results from 15 titrations (pH 3–10) of Cd in 0.70 M $NaClO_4$ solutions containing 2 mM DFOB and using a titrant of 0.1001 M NaOH, except where indicated otherwise. Regressions were performed with FITEQL4.0, keeping pK_W = 13.740 and the pK_{ai} of DFOB fixed at values discussed in section 2.4.1, with $\beta_1, \beta_2, \beta_3$ as adjustable parameters. All regressions converged in 6 iterations (*n*) or less.

Cd:DFOB ratio	$\log \beta_1$	$\log \beta_2$	$\log \beta_3$	[DFOB] (mM)	n [a]	WSOS/DF[b]
0.98[c]	3.37	5.83	7.24	1.97	4	0.870
0.98	3.35	5.81	7.21	1.94	4	0.561
0.97	3.39	5.78	7.18	2.01	3	0.218
0.50	3.49	5.77	7.27	2.05	4	0.359
0.49	3.43	5.76	7.22	2.00	4	0.341
0.49	3.44	5.77	7.23	2.00	4	0.350
0.69	3.54	5.76	7.24	1.99	4	0.348
0.79	3.53	5.77	7.20	1.97	3	0.303
0.89	3.50	5.78	7.19	1.97	3	0.345
0.49	3.43	5.75	7.19	2.02	4	0.304
0.25	3.38	5.80	7.23	2.05	5	0.310
0.59	3.46	5.76	7.20	2.05	4	0.286
0.25	3.34	5.80	7.19	2.07	6	0.324
0.59	3.44	5.75	7.18	2.09	4	0.254
0.40	3.42	5.78	7.21	2.09	5	0.325

[a] Number of iterations for regression to converge.
[b] WSOS/DF (Weighted Sum-Of-Squares divided by the Degrees-of-Freedom) is the quality-of-fit parameter for FITEQL, with values in the range 0.1–20 indicating a good fit (Herbelin and Westall, 1999).
[c] Titrant is 1.0005 M NaOH.

Table 2.5. Results from five titrations each (pH 3–10) of Pb in 0.70 M $NaClO_4$ and NaCl solutions containing 2 mM DFOB and using a titrant of 0.1001 M NaOH. Regressions were performed with FITEQL4.0, keeping pK_W fixed at the appropriate constants (pK_W = 13.740 for $NaClO_4$ titrations and pK_W = 13.718 for NaCl titrations) and the pK_{ai} of DFOB fixed at values discussed in section 2.4.1, with $\beta_1, \beta_2, \beta_3$ as adjustable parameters. All regressions converged in 8 iterations (*n*) or less.

Pb:DFOB ratio	$\log \beta_1$	$\log \beta_2$	$\log \beta_3$	[DFOB] (mM)	*n* [a]	WSOS/DF[b]
0.42	6.23	9.54	10.1	2.02	6	3.48
0.42	6.38	9.66	10.1	2.07	5	0.620
0.42	6.22	9.53	10.1	2.02	6	3.86
0.21	6.11	9.55	9.90	1.94	5	0.818
0.58	6.40	9.72	10.4	1.92	8	7.20
0.42[c]	6.42	9.30	9.8	2.06	6	1.15
0.42[c]	6.42	9.30	9.8	2.05	6	1.16
0.42[c]	6.41	9.29	9.8	1.98	7	1.43
0.21[c]	6.31	9.32	9.7	1.99	7	0.41
0.58[c]	6.52	9.38	10.0	1.98	8	2.06

[a] Number of iterations for regression to converge.
[b] WSOS/DF (Weighted Sum-Of-Squares divided by the Degrees-of-Freedom) is the quality-of-fit parameter for FITEQL, with values in the range 0.1–20 indicating a good fit (Herbelin and Westall, 1999).
[c] Results from titrations measured in 0.7 M NaCl.

Table 2.6. Results from five titrations (pH 3–10) of Pb in 0.70 M $NaClO_4$ and NaCl solutions containing 2 mM DFOB and using a titrant of 0.1001 M NaOH. Regressions were performed with FITEQL4.0, keeping pK_W fixed at the appropriate constants (pK_W = 13.740 for $NaClO_4$ titrations and pK_W = 13.718 for NaCl titrations) and the pK_{ai} of DFOB fixed at values discussed in section 2.4.1, with β_1 and β_2 left as adjustable parameters. All regressions converged in 4 iterations (*n*) or less.

Pb:DFOB ratio	$\log \beta_1$	$\log \beta_2$	[DFOB] (mM)	*n* [a]	WSOS/DF[b]
0.42	6.17	9.51	2.29	4	2.56
0.42	6.33	9.64	2.32	4	0.952
0.42	6.15	9.50	2.29	4	2.79
0.21	6.11	9.58	2.06	4	1.01
0.58	6.29	9.53	2.32	4	6.83
0.42[c]	6.37	9.27	2.31	3	1.26
0.42[c]	6.37	9.28	2.31	3	1.23
0.42[c]	6.36	9.26	2.24	3	1.36
0.21[c]	6.31	9.35	2.11	4	0.77
0.58[c]	6.43	9.25	2.36	3	1.75

[a] Number of iterations for regression to converge.
[b] WSOS/DF (Weighted Sum-Of-Squares divided by the Degrees-of-Freedom) is the quality-of-fit parameter for FITEQL, with values in the range 0.1–20 indicating a good fit (Herbelin and Westall, 1999).
[c] Results from titrations measured in 0.7 M NaCl.

2.5. Discussion

2.5.1. Comparison of Zn–, Cd– and Pb–DFOB stability constants with literature values

The average stability constants (log β_1, log β_2, log β_3) for the Zn–DFOB and Cd–DFOB complex were calculated to be 4.81± 0.07, 7.99 ± 0.00$_3$, 9.39 ± 0.03, and 3.43± 0.03, 5.78 ± 0.02, 7.21 ± 0.03, respectively. However, for the Pb–DFOB complex, there are only two stability constants (log β_1, log β_2), which values of 6.21 ± 0.10 and 9.55 ± 0.06 in 0.7 M $NaClO_4$, and 6.37 ± 0.04 and 9.28 ± 0.04 in 0.7 M NaCl (Table 2.7).

Table 2.7. Average values of the stability constants of the bidentate (log β_1), tetradentate (log β_2), and hexadentate (log β_3) DFOB complexes of divalent Cd, Zn, and Pb determined from FITEQL4.0 regressions of titrations in 0.7 M $NaClO_4$ (and NaCl for Pb) compared with literature values for these three metals plus Fe. Uncertainties are one standard deviation of the mean, based on at least five titrations.

M	log β_1	log β_2	log β_3	References
Cd^{2+}	3.43 ± 0.03	5.78 ± 0.02	7.21 ± 0.03	This work
	3.32	5.58	7.88	Anderegg et al. (1963a; b)[a]
Zn^{2+}	4.81 ± 0.07	7.99 ± 0.003	9.39 ± 0.03	This work
	4.29	7.88	9.55	Hernlem et al. (1996)[b]
Pb^{2+}	6.21 ± 0.10	9.55 ± 0.06	–	This work (0.7 M $NaClO_4$)
	6.37 ± 0.04	9.28 ± 0.04	–	This work (0.7 M NaCl)
	5.92	9.25	10.00	Hernlem et al. (1996)[b]
Fe^{3+}	10.50	21.84	30.60	Gould and Langerman (1982)[c]

[a] Value measured at 0.1 m ionic strength ($NaNO_3$) at T = 20 °C.
[b] Value measured at 0.1 M ionic strength (KNO_3) at T = 25 °C.
[c] Value measured at 2.0 M ionic strength ($NaClO_4$) at T = 25 °C.

Comparisons with other literature values determined at 0.1 M ionic strength are shown in Table 2.7. The average constants determined at 0.7 M ionic strength for this work agree closely for Zn, Cd and Pb constants determined at 0.1 M ionic strength,

indicating that ionic strength does not strongly affect the stability constants of metal–DFOB complexes. This outcome is expected since the Debije-Hückel theory does not apply to (i) polarized, non-spherically symmetric ligands or (ii) multi-dentate complexation (Anderegg et al., 1963b). Consequently, ionic strength dependent models like the Davies Equation should *not* be used to extrapolate equilibrium constants involving DFOB to different ionic strength values.

2.5.2. Zn–, Cd– and Pb–DFOB coordination chemistry

Siderophores are particularly selective for Fe^{3+} because of their ideal molecular dimensions and the ability to bind in its preferred 6-fold coordination. DFOB is a long, linear, somewhat flexible molecule and therefore is able to place its three hydroxamate groups, separated by 9-atom spacers, in the appropriate arrangements by wrapping itself around the metal cation. Its central cavity evolved to perfectly fit Fe^{3+} yet, although other metals can be accommodated, the structural arrangement becomes less than optimal for much larger or much smaller ions, or for ions with a different charge or coordination number (Hernlem et al., 1996; Albrecht-Gary and Crumbliss, 1998; Dhungana et al., 2001; Butler and Theisen, 2010). Winston and Kirchner (1978) investigated the effect of trihydroxamate siderophore structure on the selective chelation of Fe^{3+} in water and found that molecules with 11-atom spacers had a greater affinity for Fe^{3+} than those with 9 or 13 atoms, whereas the molecule with 13-atom spacers had a greater affinity for the smaller Al^{3+} ion.

All of the metals studied here are larger than Fe^{3+}, which has an ionic radius of 0.64 Å (Shannon, 1976). With an ionic radius of 0.74 Å, Zn is much smaller than both Pb and Cd

(1.19 and 0.95 Å, respectively) (Shannon, 1976) and appears to form a stable hexadentate complex. Cd is also able to form the hexadentate complex, yet, because Cd is substantially larger than Zn, the stability constants are much smaller, perhaps because the DFOB molecule is not able to stretch. Lead is even larger than Cd, and may be too large to fit in the central cavity. However, Cu was also found to only complex with two hydroxamate groups of the DFOB molecule (Kailee Potter, unpublished data), despite the fact that the Cu^{2+} ion is small (0.73 Å) (Shannon, 1976), hence it appears that the metal coordination sphere is at least as important as its ionic radius.

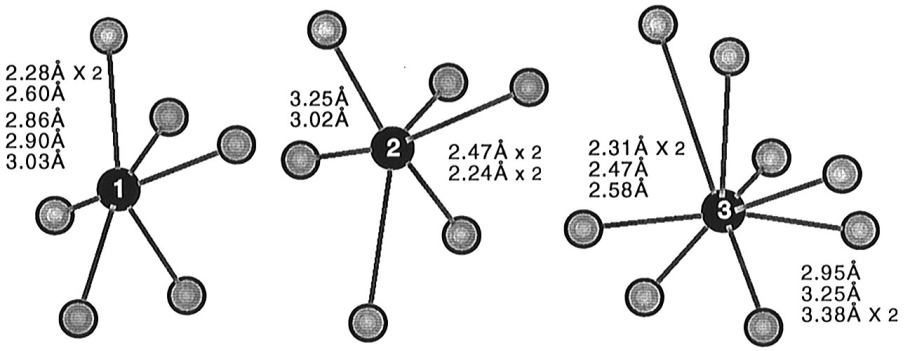

Figure 2.3. Three Pb coordination sites in $PbSiO_3$ depicting the irregularity of the Pb–O distances. Pb(1) and Pb(2) sites can be considered 3- and 4-fold coordinated (if the nearest oxygens are taken into account) or 6-fold coordinated (if the next-nearest oxygens located at ~3 Å are considered to participate in the chemical bond with Pb). The Pb(3) site is less defined with four nearest oxygens at 2.31–2.58 Å and four others at 2.95–3.38 Å (Manceau et al., 1996).

Compared to the other metals studied, Pb(II) possesses irregular coordination with a wide range of bond lengths, as shown in Figure 2.3 (Manceau et al., 1996). Considering this irregular distribution of bonds, it is possible that the separation of the O-atoms in the hydroxamate group, sometimes referred to as the 'bite', is not right for accommodating the Pb cation. In spite of this, Pb exhibits the largest stability constants for bidentate and

tetradentate complexes of all the metals studied. This may be explained by the fact that the Pb^{2+} ion has a higher affinity for O-bearing ligands than Zn and especially Cd. This observation will be illustrated in more detail in the next section.

2.5.3. Correlations of DFOB−metal stability constants with various metal ion parameters: hydrolysis constants and z/r

Prior studies have demonstrated with data for several DFOB complexes that correlations exist between their stability constants and chemical properties of the metal cation (Hernlem et al., 1999; Duckworth et al., 2009b). These correlations are typically referred to as linear free-energy relations, or LFERs. In order to better understand which metal parameters are controlling the selectivity of ligands for various metals, the affinity or complexation constants of these ligands can be plotted against a variety of metal ion properties. Hernlem et al. (1999) have previously examined the correlations between metal–DFOB complexation constants and various metal parameters, including the ionic charge to ionic radius ratio (z/r), the ionic charge to metal–ligand interatomic separation ratio (z/d), and the first hydrolysis constant of the metal ion ($\log \beta_1^*$). They determined that the first hydrolysis constant results in a better correlation with DFOB stability constants, compared to both *z/r* and *z/d*, and that metal hydrolysis is a good representation of the affinity of the metal ion for negatively charged O-donor groups, such as the hydroxamate groups in the DFOB molecule.

The resulting DFOB stability constants for Zn, Cd and Pb fall directly on an LFER between $\log \beta_i$ and the first hydrolysis constant, only for the bottom plot of $\log \beta_1^*$ vs $\log \beta_1$ (Figure 2.4). Because there is no $\log \beta_3$ for Pb and Cu, they are not included in the top plot. As seen in Figure 2.4, each relation results in a good regression coefficient

($r^2 > 0.87$), with increasing slopes of ~1, 2, 3 for the three different constants (log β_1, log β_2, and log β_3). This high correlation suggests that DFOB, like OH^-, is an intermediate ligand (i.e., neither firmly A-type nor B-type) in terms of its bonding and coordination characteristics. One can see several trends emerging from these results, most significantly the trend that metals in the +III oxidation state (Y, La, and Lu) seem to produce more stable complexes with DFOB compared to those metals with the +II oxidation state. It is expected that metal ions with high charge densities will more readily displace protons from surrounding water molecules and therefore more readily displace protons from the ligand, which is illustrated in the LFER shown in Figure 2.4. However, one can also see that both Pb and Cu deviate from this trend (see middle plot in Figure 2.4), which is most likely due to their irregular coordination chemistries. Similar to Pb, Cu displays a distorted coordination sphere, with four short equatorial bonds and two long bonds (Manceau and Matynia, 2010) and therefore was also found to not form a hexadentate complex with DFOB (Kailee Potter, unpublished data).

A comparison was also made between the three M–DFOB stability constants, (log β_1, log β_2, and log β_3), and the parameter z/r, the ionic charge to ionic radius ratio (Figure 2.5). As before, because there is no log β_3 for both Pb and Cu, they are not included in the top plot. This LFER shows a strong correlation for these metals (Pb and Cu were not included in the regression), displaying good regression coefficients ($r^2 \sim 0.9$). Similar to the LFER in Figure 2.4, for these LFERs both Pb and Cu deviate significantly from the trend and are obviously behaving differently compared to the other metals. Even though Pb and Cu produce more stable complexes with DFOB compared to the other divalent metals, they do not fit inside the DFOB molecule.

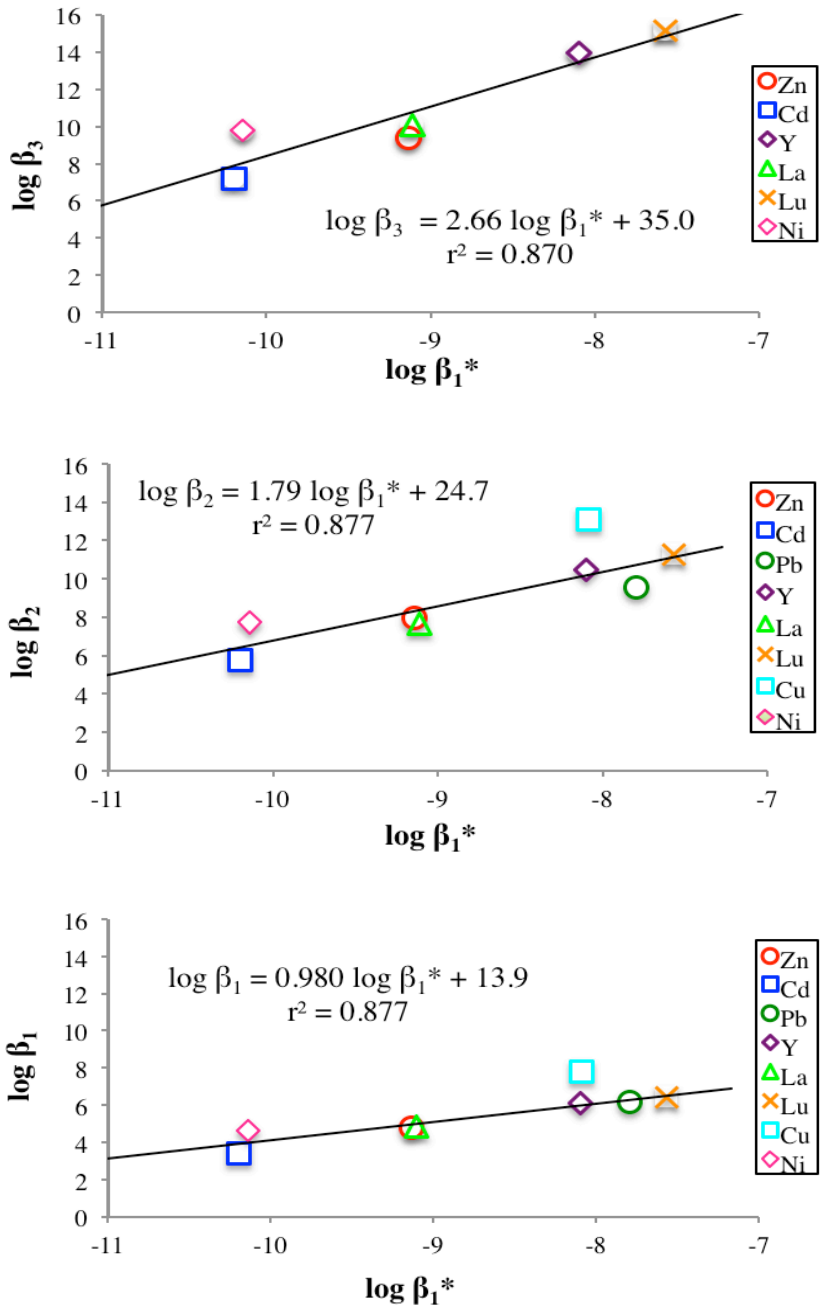

Figure 2.4. Linear free-energy relations between the three M–DFOB stability constants, (log β_i) from this work, and the first hydrolysis constants (log β_1^*) for Zn (Schorsch, 1964), Cd (Biedermann and Ciavatta, 1962), and Pb (Easley and Byrne, 2011), in addition to constants for copper (Cu) and nickel (Ni) (Kailee Potter, unpublished data), as well as yttrium (Y), lanthanum (La), and lutetium (Lu) determined from previous work (Christenson and Schijf, 2011). Each colored symbol represents a single element.

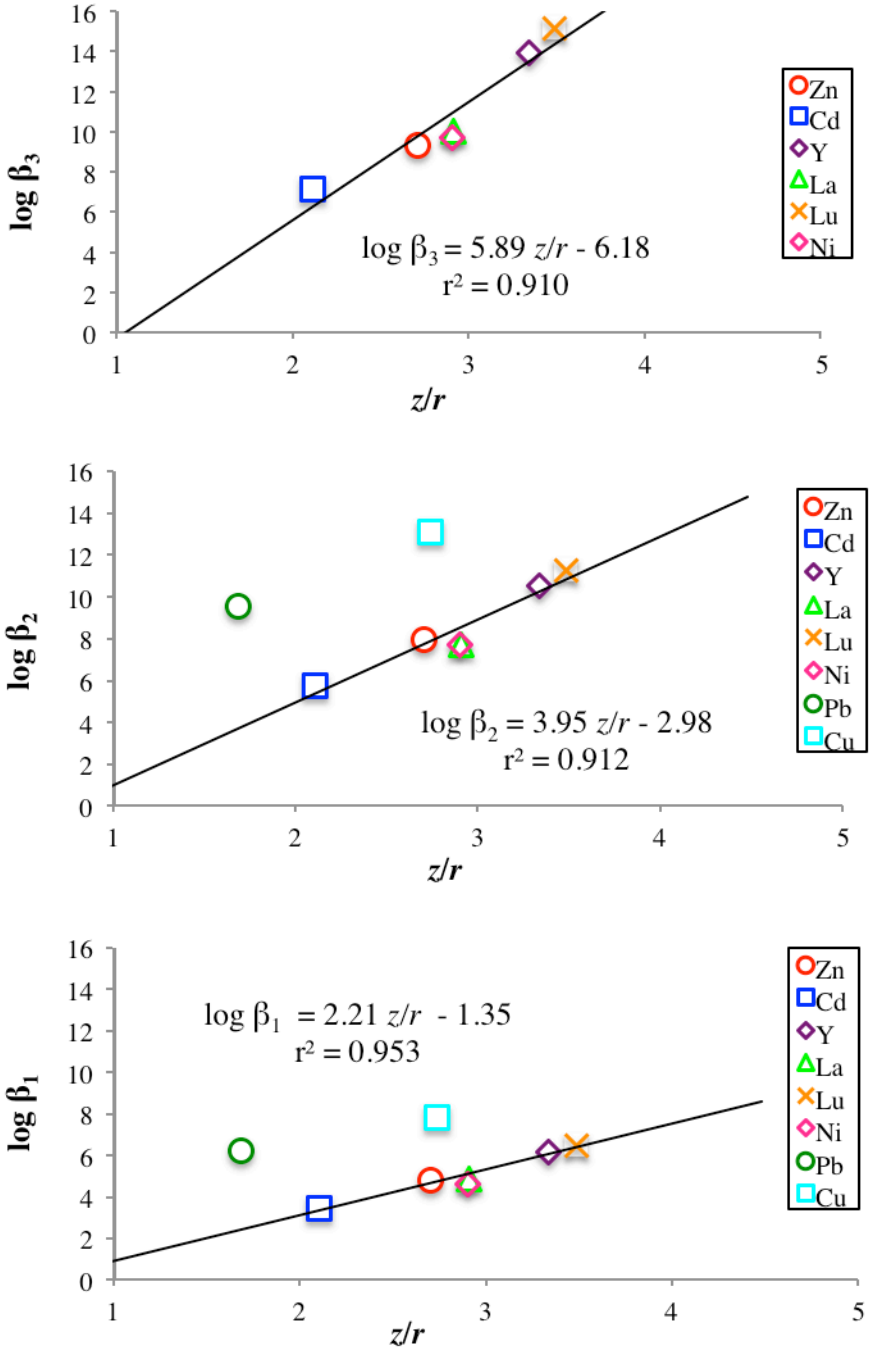

Figure 2.5. Linear free-energy relations between the three M–DFOB stability constants, (log β_i) from this work, and the ionic charge to ionic radius ratio (z/r) for Zn, Cd, and Pb, in addition to constants for copper (Cu) and nickel (Ni) (Kailee Potter, unpublished data), as well as yttrium (Y), lanthanum (La), and lutetium (Lu) determined from previous work (Christenson and Schijf, 2011). Ionic radius data are from Shannon (1976). Each colored symbol represents a single element.

2.5.4. Comparison of Zn–, Cd– and Pb–DFOB stability constants with conditional stability constants for metal-specific organic ligands in seawater

The Zn–DFOB (log β_3) and Pb–DFOB (log $\beta_2 = 9.55 \pm 0.06$) stability constants measured in this study are similar to conditional stability constants that have been measured in seawater for classes of organic ligands that are Pb- and Zn-specific. Capodaglio et al. (1990) reported a mean value of log $K' = 9.7$ for the conditional stability constant of a Pb-specific class of organic ligands in the surface waters of the eastern North Pacific. More recently Kozelka and Bruland (1998) found two classes of Pb-binding ligands in Narragansett Bay, with conditional stability constants ranging from log $K' \sim 8.8–10$. The two Pb–DFOB stability constants (log $\beta_2 = 9.55 \pm 0.06$ in $NaClO_4$ and 9.28 ± 0.04 in NaCl) reported here are in the middle of this range and are very similar to the value reported by Capodaglio et al. (1990).

Conditional stability constants have also been reported for Zn-complexing organic ligands in several different locations. Van den Berg and Dharmvanij (1984) reported a constant of log $K' \sim 7.4–9.3$ in the Gulf of Thailand, however Bruland (1989) measured Zn-specific organic ligands in the NE Pacific and found a higher conditional stability constant of log $K' \sim 11$, and more recently Ellwood (2004) found a conditional stability constant ranging from log $K' \sim 9.75–10.28$ in the Southern Ocean. Although the conditional stability constants reported for Zn-complexing organic ligands in seawater are variable, the Zn–DFOB constants (log $\beta_3 = 9.39 \pm 0.03$) measured here fall near the middle of that range (log $K' \sim 7.4–11$). This suggests that the unidentified organic ligands that complex strongly with Pb and Zn in ocean surface waters may be siderophore-like

molecules.

As with the other metals, a range of conditional stability constants has been measured for a group of Cd-specific ligands in seawater, with measurements on the order of log K' ~ 9.5–12 (Bruland, 1992; Ellwood, 2004). Although it is clear that these metal binding ligands exhibit variable stabilities depending on where they were measured, these are all substantially higher than the Cd–DFOB stability constants (log $\beta_3 = 7.21 \pm 0.03$) measured here. It is possible that hydroxamate siderophores play a role in Cd speciation in seawater, however it is more likely that Cd speciation is dominated by a different kind of organic ligand. Based on its strong affinity for sulfur-bearing ligands, thiol-containing compounds, like cysteine or glutamine (Laglera and van den Berg, 2003), may be an important part of the ligand pool that binds a large fraction Cd in surface seawater.

2.5.5. Potential effect of desferrioxamine B on Zn, Cd, and Pb speciation in seawater

The stability constants of the M–DFOB complexes measured in 0.7 M $NaClO_4$ in Table 2.7 can be applied to predict whether Zn, Cd, and Pb complexation with siderophores and strong organic ligands in general, could have a significant effect on their speciation in open ocean surface waters. In order to assess the potential impact of DFOB on Zn, Cd, and Pb speciation, model calculations were performed with MINEQL2.0 (Westall et al., 1976). Unlike FITEQL, which determines unknown constants from a given speciation, MINEQL determines metal speciation from known constants and the composition of a given system. First, a seawater (SW) model was created with pH fixed at 8.2 and containing the four major cations (Na, K, Mg, Ca), two major anions (chloride, sulfate) plus carbonate and borate, and their respective concentrations and ion pairing constants (Schijf et al., 1995). MINEQL extrapolates all

equilibrium constants to the calculated ionic strength using the Davies Equation, which is not valid for seawater (I = 0.7 M). In order to avoid improper extrapolation of the equilibrium constants, the THRM.DAT database was updated with constants appropriate for I = 0.7 M, entering them as if they were thermodynamic equilibrium association constants, and the model ionic strength of the initial solution was set to zero (I = 0), regardless of its true ionic strength. This basic seawater model was used to create three individual models for the three metals studied. Each metal was initially added into their respective models at fixed total concentrations, using realistic values in order to ensure that the speciation of the solution is not altered. In addition, the best known stability constants for all relevant inorganic Zn, Cd, and Pb complexes in seawater at I = 0.7 M were also added to each model. The total Cd concentration was set at 0.1 nM (Bruland, 1980) and relevant Cd solution species are $CdCl_n$ (n = 1–4), $CdOH^+$, $CdCO_3^0$, $CdSO_4^0$ (Turner et al., 1981), and three Cd–DFOB complexes. The total Zn concentration was set at 5 nM (Bruland, 1980) and the relevant Zn solution species are $ZnCl^+$, $ZnOH^+$, $ZnCO_3^0$, $ZnSO_4^0$ (Byrne et al., 1988; Stanley and Byrne, 1990), and three Zn–DFOB complexes. The total Pb concentration was set at 20 pM (Schaule and Patterson, 1981) and the relevant Pb solution species are $PbCl_n$ (n = 1–3), $PbOH^+$, $Pb(CO_3)_n$ (n = 1–2), $Pb(CO_3)Cl^-$ (Easley and Byrne, 2011), and two Pb–DFOB complexes (measured in 0.7 M $NaClO_4$). The results of the three speciation models of Zn, Cd, and Pb in seawater prior to the addition of DFOB into the system are shown in the pie charts on the left in Figure 2.6.

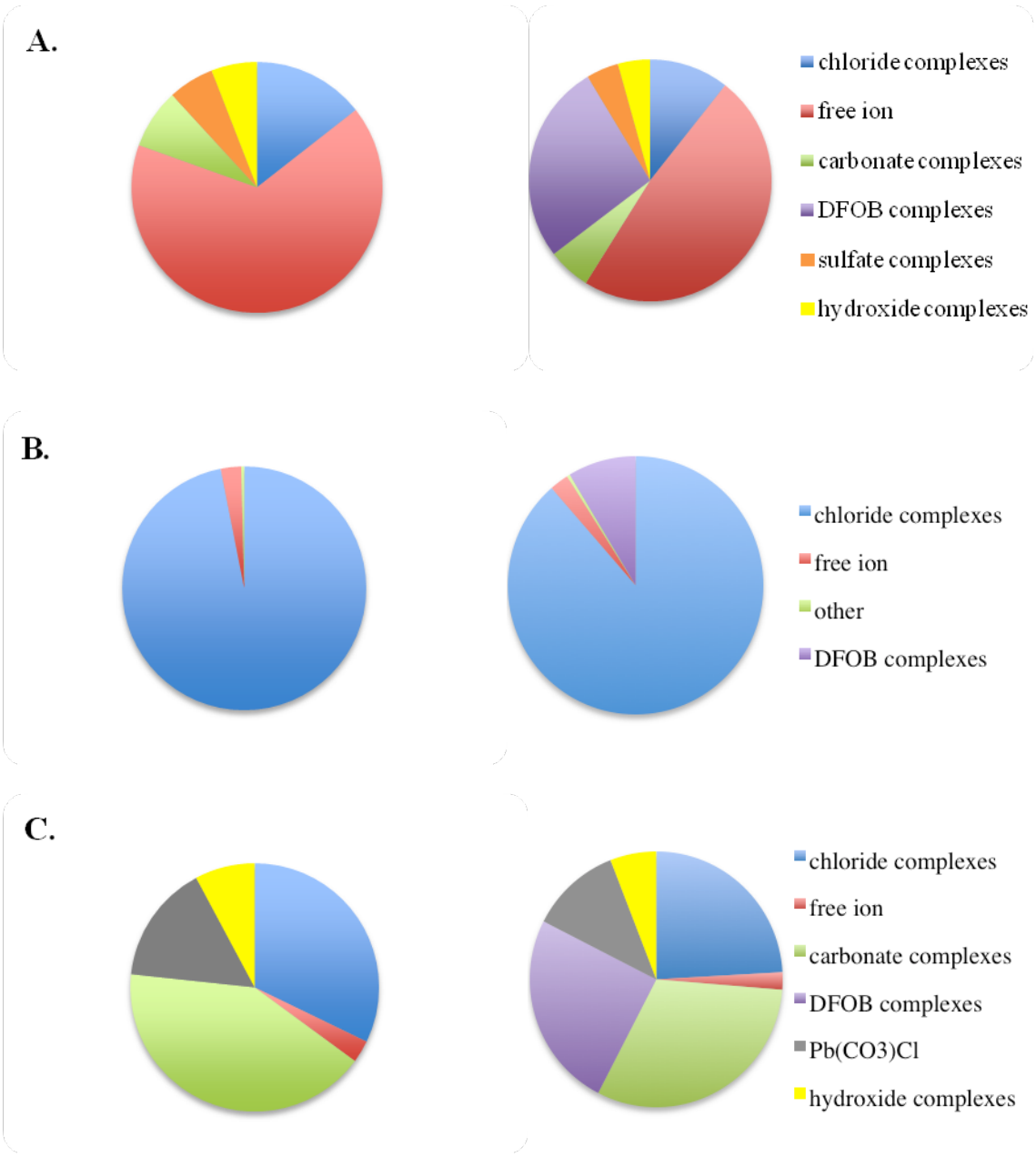

Figure 2.6. Solution speciation models of the three M–DFOB combinations in standard seawater (S = 35, pH = 8.2), calculated with MINEQL (Westall et al., 1976). (A) left: 5 nM total Zn before the addition of DFOB into the model; right: 5 nM total Zn + 10^{-10} M *free* $HDFOB^{2-}$ (fixed); (B) left: 0.1 nM total Cd before the addition of DFOB into the model; right: 0.1 nM total Cd + 10^{-7} M *free* $HDFOB^{2-}$ (fixed); (C) left: 20 pM total Pb before the addition of DFOB into the model; right: 20 pM total Pb + 10^{-10} M *free* $HDFOB^{2-}$ (fixed). Pie wedges represent contributions of the corresponding species as percentages of the total M concentration.

Lastly, DFOB was added to each speciation model as fixed *free* concentrations, together with the acid dissociation constants of DFOB previously measured in $NaClO_4$ (see Section 2.3.3) and the stability constants of the three M–DFOB complexes determined in 0.7 M $NaClO_4$ from this study (Table 2.7). Although DFOB has been identified in seawater, it has yet to be quantified (McCormack et al., 2003). Gledhill et al. (2004) were able to detect both desferrioxamine B and G in cultured water samples from the English Channel, but were unable to measure their concentrations. A few years later Mawji et al. (2008) found and measured desferrioxamine E and G (but not DFOB) at individual concentrations of up to 12 ± 1 pM in surface waters of the North and South Atlantic Ocean. More recently Mawji et al. (2011) identified a total of 23 different siderophore type chelates in surface waters of the Atlantic Ocean, including the linear hydroxamates, desferrioxamine B and G, as well as two cyclic hydroxamates, desferrioxamine D and E.

To make the model more generally applicable, rather than total concentrations, free DFOB concentrations (entered as the component species $HDFOB^{2-}$) were fixed in MINEQL. Since the relative abundance of a complex depends on the free ligand concentration, these model results are applicable for any seawater sample with equivalent free DFOB concentrations, regardless of its composition. Because a large fraction of DFOB in the surface waters is complexed with Fe, its free concentration is reduced (Mawji et al. 2008). My seawater speciation model was initially fixed at a *free* DFOB concentration of 10^{-14} M, which would constitute only ~0.1% of total measured concentrations of individual ferrioxamine siderophores in the Atlantic (Mawji et al. 2008). From previous work, it was determined that at this concentration of *free* DFOB

yttrium and the rare earth elements (YREEs) began to complex with DFOB in a standard seawater model (Christenson and Schijf, 2011), therefore this was used as a starting concentration for this model. However, when DFOB was added to each of the three speciation models fixed at a *free* concentration of 10^{-14} M, no change was seen in the Zn, Cd, and Pb speciation, indicating that it does not affect their speciation at these concentrations. Therefore, *free* DFOB concentrations were increased an order of magnitude and rerun until complexation of DFOB was observed for each metal. For both Zn and Pb, this did not occur until the *free* DFOB concentration was raised to 10^{-12} M, however the DFOB complexes for each only constituted ~0.5% of the total metal in seawater. When the concentration was increased to 10^{-11} M, ~2% of Zn and Pb were found to complexed with DFOB, but the free DFOB concentration had to be increased to 10^{-10} M in order to see a significant proportion of each metal complexed with DFOB (~25%), which can be seen in the pie charts on the right in Figure 2.6. Cadmium, on the other hand, did not significantly complex with DFOB until its free concentration was fixed at 10^{-7} M where ~10% of the total Cd was calculated to complex with DFOB.

When the *free* DFOB concentrations remain fixed in the model, its total concentration is calculated by MINEQL. For the case where the *free* DFOB concentrations was fixed to 10^{-12} M, MINEQL calculates a total DFOB concentration of ~780 pM, which is well beyond the natural range of concentrations of desferrioxamine siderophores (~10 pM) found by Mawji et al. (2008). Even under these unrealistic concentrations, DFOB complexation has no effect on Zn, Pb, and Cd speciation in seawater. For an organic ligand to have an effect on the speciation of these metals, it would either have to possess a much higher stability constant or be present in much higher concentrations. It should be

noted that the study of Mawji et al. (2008) focused on a few members of two similar classes of siderophore (amphibactin and ferrioxamine), and considering that all of their samples were collected in the months of May/June, their results only represent a snapshot in time. Because the productivity of microbes varies in annual cycles, periodic blooms can occur which raise the demand for iron, in turn stimulating siderophore release to levels quickly exceeding ambient Fe concentrations (Gledhill et al., 2004). Additionally, a review (Butler and Theisen, 2010) suggests that the hydroxamate compounds measured by Mawji et al. (2008) may represent only a minute fraction of all siderophores in seawater. Some siderophores have been reported to have much higher affinities for Fe^{3+} than DFOB (Boukhalfa and Crumbliss, 2002), and thus possibly for other trace metals as well. At the very least, the overall effect of siderophores on trace metal speciation should be cumulative, so if a concentration of 10 pM is typical for single siderophore compounds, the collective total siderophore abundance may be much higher.

2.6. Conclusions and implications

A delicate balance exists between the beneficial and harmful effects of trace metals to marine microorganisms, which is most likely mediated by organic ligands. It has been repeatedly proposed that organic ligands may well be controlling the behavior and distributions of trace metals in the oceans, however little is known about the interactions between trace metals and these ligands in seawater. In this work, Pb and Zn were found to be more strongly complexed with DFOB than Cd, however Zn and Cd readily expel the last proton from the DFOB molecule, whereas Pb does not. This free hydroxamate group may affect the ultimate fate and bioavailability of the Pb–DFOB complex. One

possible outcome is that this free group could then complex with other dissolved metals, creating a polynuclear complex. These complexes may in turn not be recognized by the cell receptors and therefore not be transported into the cell, or could potentially lead to the uptake of unwanted metals. Another possibility is that this free hydroxamate group could complex with metals bound to particles, which can be supported by recent mineral dissolution research that suggests that just one hydroxamate group in the siderophore is coordinating with reactive Fe at the mineral surface (Cocozza et al., 2002). Since siderophore excretion and recovery requires an extensive amount of energy, this could lead to a costly loss of the ligand as complexation with particles will render the complex unavailable for uptake by biota

For metals such as Zn, Cd and Pb that have been shown to be largely organically complexed, speciation seems to be dominated by one or two strong, relatively element-specific, yet unknown classes of ligands. The DFOB stability constants determined for Pb and Zn in this study suggest that hydroxamate siderophores may be among the unidentified organic ligands that complex strongly with these metals in the surface waters of the ocean. The Cd–DFOB stability constants are substantially lower than conditional stability constants for Cd-specific organic ligands in seawater, therefore these ligands are most likely not hydroxamate siderophores. These data are beneficial by highlighting the extreme specificity of these observed organic ligands and may direct the search towards other classes of ligands with similar chemical properties.

Laboratory experiments have demonstrated that the growth and productivity of marine phytoplankton are not only limited by the availability of the major nutrients nitrogen and phosphorus, but are also regulated by various trace metals (Sunda, 2012). These are

required for photosynthesis, respiration, and nitrogen fixation, and therefore play important roles in controlling the biological cycles of carbon and nitrogen in the ocean. Before the onset of oxygenic photosynthesis, the world's oceans experienced very reducing conditions due to the lack of O_2 in the system (Raven et al., 1999). As oxygen concentrations increased over the last ~2 billion years, the oceans have became more oxidizing, which has altered the stable oxidation states of trace metals in seawater. Some of the essential trace metals, such as Fe, Co, and Mn, have stable oxidation states that are mostly insoluble under these aerobic conditions, resulting in low total dissolved concentrations in seawater. Marine organisms therefore had to adopt mechanisms to acquire essential trace metals to sustain growth, but also prevent toxic effects from high metal concentrations (Sunda, 2012).

As discussed in Chapter 1, iron obviously plays a major role in controlling the carbon and nitrogen cycles in the oceans due to its limitation of carbon and nitrogen fixation. As a result, it also regulates the biological carbon pump that transports carbon (CO_2) from the atmosphere into the oceans, which ultimately controls the balance of CO_2 between the ocean/atmosphere and CO_2-linked greenhouse warming (Martin, 1990; Sigman and Boyle, 2000). It has been proposed that variations in the input of iron-rich continental dust to the ocean have played a major role in controlling glacial-interglacial climate cycles by influencing the intensity of the biological CO_2 pump (Martin, 1990; Falkowski, 1997). Other trace metals have also been shown to promote phytoplankton growth in bottle incubation experiments. Zinc is present in a number of essential proteins that are necessary for cell growth and replication, including carbonic anhydrase (CA) and alkaline phosphatase, and has been found to increase reproductive rates of coccolithophores when

added to natural waters. Because *E. huxleyi* and other coccolithophores are responsible for a major fraction of calcium carbonate formation, which in turn regulates ocean water alkalinity, they also influence the air-sea exchange of CO_2 (Dymond and Lyle, 1985). Therefore, similar to Fe, Zn could also indirectly affect atmospheric CO_2 and global climate by regulating the growth of coccolithophores.

While metals can affect CO_2 concentrations and climate change, climate change and ocean acidification caused by increased levels of CO_2, will also impact trace metals in the ocean. Marine phytoplankton may experience increased nutrient limitation in the surface waters due to intensified stratification in a warming ocean. At the same time, ocean acidification may affect trace metals and assimilation both directly by altering ion channels, as well as indirectly by changing the chemical speciation. The inorganic speciation of Fe, for example, is expected to result in an increase in the free ionic form due to a decrease in Fe-hydroxide and Fe-carbonate complexes. This shift in speciation may thus cause an decrease in the solubility of Fe(III) with decreasing pH. On the other hand, ocean acidification could have beneficial effects on primary productivity by increasing the concentrations of bioavailable iron. However, since the speciation of the trace metals studied here are dominated by organic complexation in seawater, the effects of changes in their inorganic speciation will be minor.

The effect of ocean acidification on Fe becomes more intricate when organic Fe complexation is considered, which is also affected by pH. Given that the predominant functional groups associated with dissolved organic material in seawater are the carboxylic and phenolic O-moieties, trace metal complexation with dissolved organic ligands is a function of pH. In the case of siderophores, a decrease in pH would result in

increased protonation of the binding sites, inhibiting the complexation of Fe and ultimately lowering the amount of bioavailable dissolved Fe. However, if free Fe increases with decreasing pH as predicted, then large portions of the ocean currently limited by Fe availability may experience higher primary productivity, which could potentially lead to changes in Fe requirements of marine phytoplankton, as well as shifts in community structure. Millero et al. (2009) used conditional stability constants, ligand and metal concentrations, and ligand dissociation constants (pK_as) measured from waters off the coast of France (Louis et al., 2009) to assess the effect of pH on the speciation of Cu. They found that decreasing pH from 8.1 to 7.4 resulted in a decrease in the interaction between organic ligands and Cu(II), which caused the free Cu concentrations to rise to levels that may be toxic to certain organisms. The overall impact of ocean acidification on marine trace metal biogeochemistry is difficult to predict. Understanding the bioavailability of trace metals may add clarity to the reactivity and transport of these metals in the ocean, and further guide research to help assess the potential consequences of future climate change.

Chapter 3: Stability of DFOB complexes with Hg(II) and methyl–Hg(II)

3.1. Abstract

Many studies have shown that mercury (Hg) methylation occurs readily in estuarine and coastal sediments, mediated by anaerobic sulfate-reducing bacteria (SRB). Although methylation of inorganic Hg by SRB requires anaerobic conditions, recent evidence suggests that Hg methylation also occurs in oxygen minimum zones in the water column, and is therefore not strictly confined to oxygen-free environments. This may be an indicator that different mechanisms and bacteria are responsible for Hg methylation in the sediments versus the water column. Due to the complex nature of Hg cycling, many questions remain concerning the biogeochemical processes controlling Hg methylation in the open ocean. Mercury uptake and methylation have been suggested to result from passive diffusion of neutral mercury complexes into bacterial cells, however facilitated uptake and methylation are also reported, especially when Hg^{2+} is complexed with small-molecular-weight thiol compounds. Mercury complexation with other organic ligands in seawater is likely to be important, and is expected to affect the bioavailability of mercury and its microbial uptake, leading to the formation of methylmercury.

Mercury uptake and subsequent methylation in the water column could potentially be facilitated by Hg complexation with siderophore-like molecules. Hernlem et al. (1996) made an attempt to measure the stability constants of Hg–DFOB complexes, however they failed due to extensive hydrolysis and precipitation throughout their titrations. In this

work, a series of potentiometric titrations was performed at seawater ionic strength (0.7 M) in a ligand-competition experiment, to determine the stability constants of Hg and possible methyl–Hg complexes with my model organic ligand, desferrioxamine B (DFOB). I discuss titration data for the Hg– DFOB and MeHg–DFOB complexes, albeit stability constants could not be derived from non-linear regressions.

It appears that Hg forms stable complexes with DFOB, as previously predicted from stability-structure relations (Hernlem et al., 1999). On the other hand, I could not detect the presence of any MeHg–DFOB complexes, which was to be expected, since the bulky methyl group attached to the Hg^{2+} ion is likely to sterically hinder their formation. In addition, the presence of the methyl group significantly alters the coordination sphere of the Hg^{2+} ion, leaving fewer bonds available for a multidentate complex.

3.2. Introduction

Mercury is one of the most toxic metals known and thus a hazardous contaminant in aquatic systems. Once Hg is released into the environment, microorganisms may transform inorganic mercury to methylmercury (MeHg), which is both more toxic and more bioavailable to fish than inorganic mercury (Clarkson and Magos, 2006). The process by which inorganic mercury is methylated in the environment has consequently been an area of intensive research over the past several decades. Nonetheless, the environmental factors that determine Hg availability to methylating bacteria remain poorly understood (Morel et al., 1998).

Mercury is emitted to the environment through a number of both natural and anthropogenic activities. Natural emissions of Hg from geological sources, such as

volcanoes, are small compared to current anthropogenic emissions of Hg, most notably the combustion of fossil fuels (Selin, 2009). Mercury released into the atmosphere takes the form of elemental mercury vapor (Hg^0). Elemental mercury is photo-oxidized to inorganic divalent mercury (Hg^{2+}), which combines with water vapor that eventually becomes rain, depositing Hg in soil and water. Inorganic mercury may then be taken up by microorganisms and undergo processes that convert it to the organometallic cation CH_3Hg^+ (methylmercury, MeHg). Methylmercury is effluxed from bacterial cells into the water, where it can be taken up by other organisms and accumulate up the food chain (Figure 3.1).

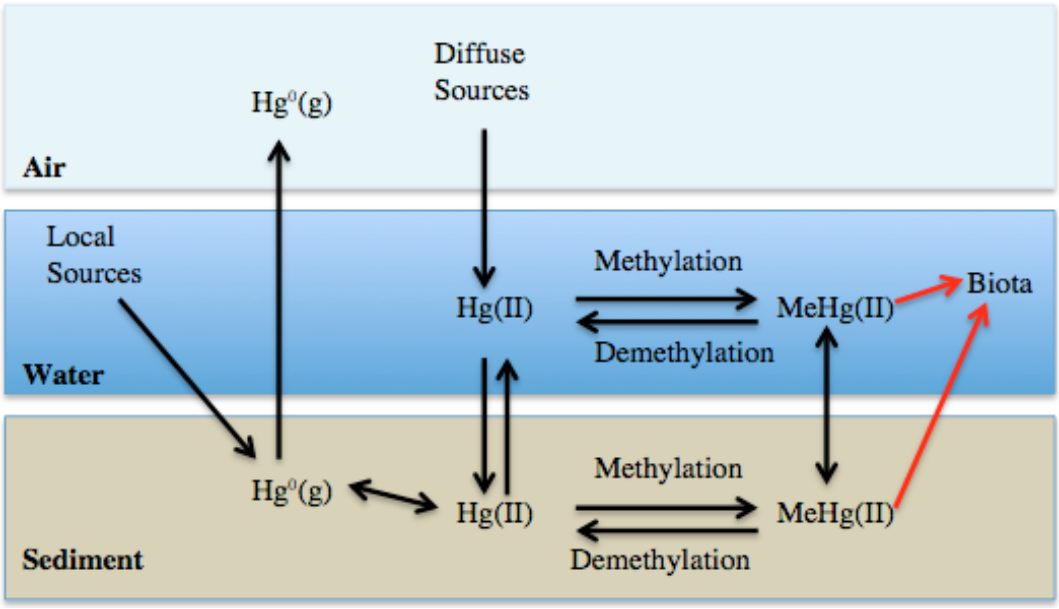

Figure 3.1. Schematic depiction of the cycling and transformation of mercury in the environment as it is transported from the atmosphere into the water column and sediments, where it may be methylated by microbes. This MeHg can be taken up by biota and subsequently biomagnified in higher trophic levels of the aquatic food web.

The uptake of mercury by microorganisms is the first major step in the methylation process, and has consequently been the focus of many recent studies. It is essential to

understand the whole methylation process to accurately predict the magnitude of methylmercury accumulation in the aquatic food chain. Mercury uptake and methylation have been most widely studied in sediments, however they also occur in the water column. Yet the methylation that occurs in seawater appears to be different from that in sediments, which are more likely to be anoxic whereas the open ocean is generally well oxygenated (Malcolm et al., 2010). Although it is known that sulfate-reducing bacteria (SRB) (King et al., 2001) and iron-reducing bacteria (FeRB) (Fleming et al., 2006) have the ability to methylate Hg in sediments, the same bacteria are probably not present in the water column. This suggests that different mechanisms may be responsible for MeHg formation in these two environments.

Mercury concentrations have been measured in several ocean basins, with averages ranging from ~1–3 pM (Laurier et al., 2004). Until recently, concentrations of methylated Hg species have been difficult to measure in seawater due to analytical detection limits, however new advances have allowed these measurements to be performed in several oceanic regions. Figure 3.2 shows vertical profiles of Hg and methylated Hg in the North Pacific, which show a MeHg maximum between 200 and 400 m (Sunderland et al., 2009). This suggests that Hg is acquired and methylated by microbes below the euphotic zone. Sunderland et al. (2009) hypothesized that settling POC not only provides a source of inorganic Hg(II) to microbially active subsurface waters, but also supplies a substrate to facilitate microbial methylation in the water column. Although these findings show that MeHg is being actively produced in the water column, the substrates or complexes responsible for promoting this biological transformation in seawater remain unknown.

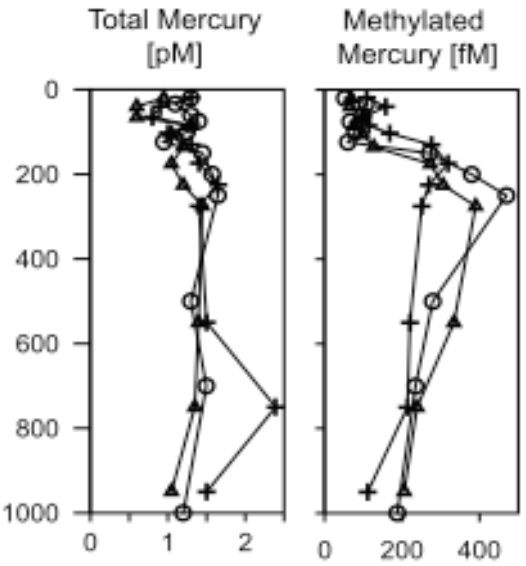

Figure 3.2. Vertical profiles of total Hg and total methylated Hg (MeHg + Me_2Hg) from three different stations in the North Pacific on the P16N cruise in March 2006 (Sunderland et al., 2009).

There are several factors that ultimately control the transfer of Hg and MeHg to microorganisms. These include the total mercury content of the system, the composition of the microbial community, and ambient environmental conditions. Microbes have a major influence on transformations between soluble and insoluble phases of trace metals through a variety of different mechanisms, including the production of siderophores, which makes metals more mobile and bioavailable. Some researchers consider mercury transport and uptake into microbes to be caused by passive diffusion of neutrally charged Hg–sulfide and Hg–chloride complexes (Mason et al., 1996; Benoit et al., 1999). However, others argue that uptake of mercury occurs via facilitated transport. Schaefer and Morel (2009) proposed that microorganisms may take up Hg through active transport of stable mercury complexes, rather than by diffusion of neutral species through cellular membranes. They found that cysteine enhances Hg methylation by facilitating uptake of Hg^{2+} and promoting enzymatic formation of monomethylmercury, and concluded that the

uptake and methylation of Hg are controlled more tightly by biological mechanisms than previously thought.

The speciation of Hg in aquatic systems is complicated and extremely dynamic. In the ocean, Hg can exist as Hg(0), Hg(II), methylmercury, dimethylmercury, and particulate and colloidal mercury (Mason and Fitzgerald, 1993; Morel et al., 1998). Both Hg^{2+} and $MeHg^{+}$ ions have a high tendency to form stable complexes with soft ligands that contain sulfur (Haitzer et al., 2003). In the absence of sulfide, the inorganic speciation of Hg and MeHg in oxic seawater is dominated by chloride complexes, with $HgCl_4^{2-}$ and $HgCl_3^{-}$ being the dominant complexes for Hg^{2+}, and CH_3HgCl^0 for $MeHg^{+}$ (Ullrich et al., 2001). Significant complexation of Hg^{2+} with natural dissolved organic matter (DOM) in surface waters is also suggested by the positive correlation between Hg and DOM (Benoit et al., 2001), however stability constants for Hg complexes with dissolved organic matter in seawater are largely unknown.

Mercury uptake and subsequent methylation could potentially be facilitated by Hg complexation with a siderophore-like ligand. Therefore, the purpose of this research is to investigate the complexation of Hg and MeHg with desferrioxamine B (DFOB) at seawater ionic strength. Measuring the stability of Hg–DFOB complexes was attempted by Hernlem et al. (1996), however they failed due to extensive hydrolysis and precipitation throughout their titrations. They concluded that some interaction was occurring between Hg and DFOB, however their simplest complexation models did not properly fit the data. Hernlem et al. (1999) later predicted that the stability constant $\beta_3 \sim 10^{26}$ based on chemical characteristics of Hg, including its charge and ionic radius, as well as its affinity for hydroxide ions (i.e. the hydrolysis constant). This value is

extremely high compared to other divalent metals and, if accurate, suggests that Hg may form complexes with the class of siderophores of which DFOB is a representative, thereby potentially aiding Hg uptake and methylation within the water column.

The existence of a MeHg–DFOB complex has never been proposed, but given that both MeHg and Hg can form stable complexes with α-substituted carboxylic acids like thioglycolic acid ($\log \beta_1(\text{MeHg}) \sim 17$, Martell et al., 2004), I speculated that MeHg may also bind to DFOB. The stability constants reported for organic MeHg complexes are generally smaller than those for Hg, as the methyl group creates a destabilizing force that decreases the affinity of the Hg ion for additional ligands (Amirbahman et al., 2002). Therefore, MeHg will likely show a lower affinity for DFOB than Hg. Complexation of MeHg with organic ligands such as DFOB may further increase the bioavailability of this toxic ion to phytoplankton, while suggesting a novel pathway for entry into the marine food chain.

In order to accurately measure the stability constants of Hg–DFOB and MeHg–DFOB complexes, hydrolysis must be prevented, which means that dissolved Hg^{2+} and $MeHg^{+}$ must remain fully complexed throughout the titration. Therefore, a different approach is required instead of the normal potentiometric titrations described in Chapter 2. In this study, a competitive ligand-exchange method was used to investigate the interactions of Hg and MeHg with DFOB, using thioglycolic acid, a compound that forms very stable complexes with both Hg^{2+} and $MeHg^{+}$, as the competing ligand.

3.3. Materials and methods

3.3.1. Ligand competition: Theory behind the experimental setup

Hernlem et al. (1996) could not determine the stability of the Hg–DFOB complex because of two challenging problems. First, the Hg^{2+} ion has a strong tendency to hydrolyze when in solution, and second, the Hg–DFOB complex appears to be so stable that it forms instantly when the metal and ligand are combined in solution at pH ~ 2. Therefore, it was not feasible to determine stability constants of the Hg–DFOB complex with the titration procedure used in Chapter 2. I devised an experiment based on ligand competition between DFOB and thioglycolic acid (TGA), a carboxylic acid containing a thiol or mercaptan group (Figure 3.3). Being a soft metal, Hg forms very stable bonds with thiols and sulfides in general, as is evident from the Hg–TGA stability constant ($\log \beta_2$(Hg–TGA) ~ 43.8) (Stricks et al., 1954) defined by the following reaction:

$$Hg^{2+} + 2TGA^{2-} \leftrightarrow Hg(TGA)_2^{2-} \quad ; \qquad {}_{TGA}\beta_2 = \frac{\left[Hg(TGA)_2^{2-}\right]}{[Hg^{2+}][TGA^{2-}]^2} \qquad (3.1)$$

where two TGA molecules bind with Hg^{2+} to form the complex. On the other hand, only one DFOB molecule should bind with Hg^{2+}, so the two ligands will effectively compete for Hg^{2+} if the concentrations of the two complexes can be made equal at some pH within the titration window (i.e., ${}_{DFOB}\beta_n\,[DFOB] \sim {}_{TGA}\beta_2\,[TGA]^2$). In other words, because DFOB and TGA have very different pK_as, their relative affinity for Hg or MeHg will shift as the titration proceeds, causing the DFOB complex to dissociate at some pH in favor of the TGA complex.

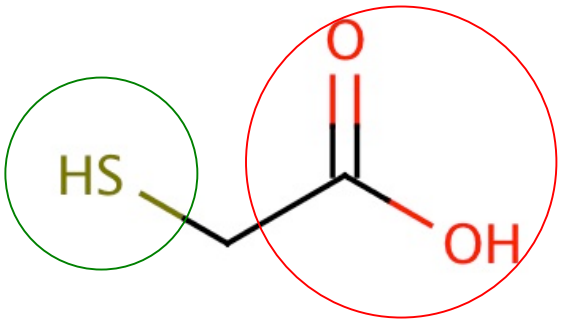

Figure 3.3. Chemical structure of TGA, with the thiol or mercaptan group circled in green and the carboxyl group circled in red.

Thioglycolic acid is not only diprotic, but amphoteric, as the thiol group can act as an acid as well as a base (it can donate, as well as receive a proton). Since the two functional groups behave differently and the Hg complex contains two TGA molecules, it has multiple conceivable structures and the complexation reactions could be written several different ways. For example, upon deprotonation of the carboxyl group, H^+ may be released into the solution or it might be donated to the protonated thiol group to form a zwitterion, as happens in amino acids (see Stricks et al., 1954 for further detail concerning this). This uncertainty makes it difficult to construct a proton balance for the titration and to choose the correct structure for the Hg–TGA complex.

In order to ensure that this ligand competition experiment was feasible, a simple model was created using MINEQL to verify the behavior of Hg+DFOB mixtures without the competing ligand (i.e. Model DFOB: titrated with HCl) and Hg+DFOB mixtures with the competing ligand (i.e. Model TGA+DFOB: titrated with TGA). Figure 3.4 shows the modeled behavior for an experimental solution with a Hg:DFOB molar ratio of 1:2 with and without TGA, where the difference between the two regression curves represents the dissociation of Hg from DFOB and the formation of a Hg–TGA complex as the solution is titrated from high pH to low pH.

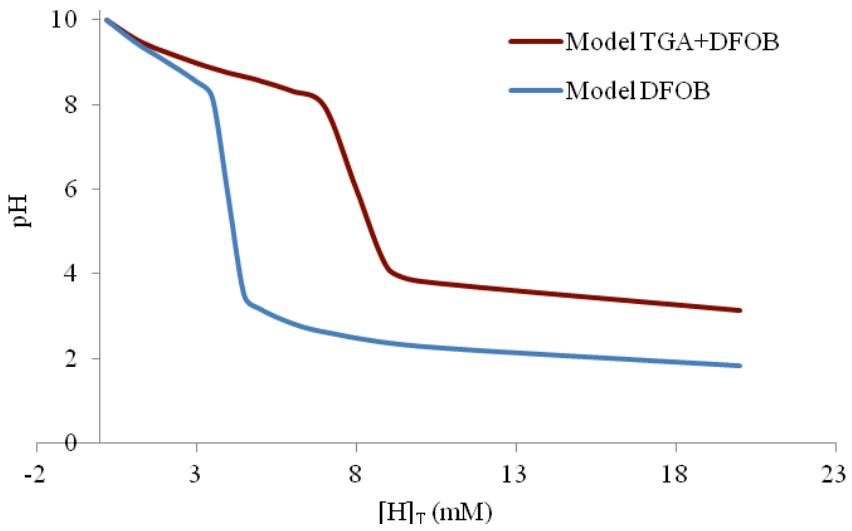

Figure 3.4. Theoretical behavior, modeled with MINEQL, of Hg + DFOB mixtures in 0.7 M $NaClO_4$ titrated with HCl (blue line) and titrated with TGA (red line), where pH is shown as a function of $[H^+]_T$. Model calculations were performed with $[DFOB]_T$ = 2 mM and $[Hg]_T$ = 1 mM.

3.3.2. Potentiometric titrations of Hg+DFOB and MeHg+DFOB mixtures

The chemical preparation and experimental setup closely followed those used in Chapter 2 (see Section 2.3.1). Stock solutions of ~40 mM DFOB and background electrolyte solution were prepared as before. A stock solution of ~40 mM Hg was prepared by dissolving the appropriate amount of metal perchlorate salt in 20 mL of the background electrolyte (0.7 M $NaClO_4$) that was adjusted to pH 1 by addition of perchloric acid. A stock solution of ~4 mM MeHg was prepared by dissolving the appropriate amount of MeHg chloride salt in 100 mL of the background electrolyte (0.7 M $NaClO_4$) at pH 3. Mercury(II) perchlorate hydrate (99.998%) and methylmercury(II) chloride (Cl ~13 %) were purchased from Sigma-Aldrich. The exact

total Hg concentration of the stock solutions was measured by ICP-MS (Agilent 7500cx) after a 10^6-fold dilution (10^5-fold for MeHg solution) in 1% HCl, utilizing a 5-point external calibration line with Re as the internal standard. The exact MeHg content of the MeHg stock solution was determined separately by distillation and ethylation using sodium tetraethylborate and purge-and-trap (Tenax) cold vapor atomic fluorescence detection (CVAF, Tekran Model 2500), following the method of Heyes et al. (2006).

Thioglycolic acid (98%) was purchased from Fischer Scientific and was diluted and stored inside an anaerobic chamber because it is readily oxidized in air. All manual titrations involving TGA, as well the preparation of the TGA solutions were also conducted inside the anaerobic chamber, which was filled with an N_2/H_2 gas mixture. The presence of O_2 was tested every day with oxygen indicator strips. All supplies and plastic-ware used during this preparation were placed inside the anaerobic chamber for five days prior to use, in order to remove oxygen. The TGA was manually titrated inside the glove bag with 1.0005 M NaOH to the phenol red endpoint and its concentration found to be 13.20 ± 0.05 M (n = 6). The concentrated TGA solution was then diluted with Milli-Q water in a 1-L polymethylpentene (PMP) volumetric flask in order to obtain a 0.7 M TGA solution that does not alter the ionic strength of the experimental solution (0.7 M $NaClO_4$). This 0.7 M TGA solution was also manually titrated inside the glove bag with 1.0005 M NaOH to the phenol red endpoint and its concentration found to be 0.690 ± 0.001 M (n = 6). The two deprotonation constants of TGA were determined by titrating 0.7 M TGA alone with 1.0005 M NaOH up to pH 11 using the Brinkmann Metrohm 809 Titrando autotitrator.

Two different sets of automated potentiometric titrations were performed for various

molar ratios of Hg:DFOB and MeHg:DFOB in the mixtures; one series with the competing ligand (TGA), and one series without. Since TGA is an acid, the sample solution must be titrated to high pH before it can be titrated back down with the ligand, causing Hg and MeHg to dissociate from DFOB and form the Hg–TGA, respectively the MeHg–TGA complex. Therefore, in order to compare the two series, they both need to proceed from high pH to low pH. The initial setup for the Hg and MeHg potentiometric titrations followed the procedures used in Chapter 2, however for these titrations, the sample solution was stirred and sparged with N_2 for a longer period of time before the addition of Hg or MeHg and DFOB. In the first series, various molar ratios of Hg:DFOB or MeHg:DFOB were established in an acidic solution where Hg is fully complexed with DFOB. Sodium hydroxide was added to raise the pH and the solution was then titrated down to pH 2 with 1 M hydrochloric acid. In the second series, the same molar ratios of Hg:DFOB or MeHg:DFOB were used. Sodium hydroxide was added to raise the pH to 10 and the solution was then titrated to pH 2 with 0.7 M TGA.

A total of nine titrations was preformed with TGA alone, six were conducted at a TGA concentration of 8 mM (three with 1 M NaOH and three with 0.1 M NaOH) and three were conducted at a TGA concentration of 12 mM (all with 1 M NaOH). For both Hg and MeHg, three series of titrations were conducted with a M:DFOB molar ratio of 1:2 and three series of titrations were conducted with a M:DFOB molar ratio of 1:4.

3.3.3. Determination of Hg–DFOB and MeHg–DFOB stability constants

As discussed in Chapter 2, in order to fit the Hg and MeHg titration data, a comprehensive model (tableau) of all solution reactions in the system is required.

However, for these titrations the model is more complicated than for the other divalent metals studied due to the presence of the competing ligand (TGA) in the system. The following processes were entered into FITEQL in tableau form: (i) the deprotonation of water in sodium perchlorate at seawater ionic strength, which was taken from the literature ($pK_w = 13.740$); (ii) the sequential deprotonation of DFOB in 0.7 M $NaClO_4$, which was determined in previous experiments by titrating DFOB alone in the absence of metal (Christenson and Schijf, 2011) as described in detail in Chapter 2; (iii) the sequential deprotonation of the competing ligand, TGA, which was similarly determined by titrating TGA in the absence of metal; (iv) the sequential deprotonation of Hg–DFOB or MeHg–DFOB complexes, these are the three reactions shown earlier in Chapter 2 with stability constants β_1, β_2, and β_3. Since Hg^{2+} exhibits a square planar geometry it is expected to form at most the tetradentate complex (β_2), whereas MeHg is presumed to form only the bidentate complex (β_1) due to its partially filled coordination sphere, which is reflected in their individual models; and (v) the stability constant of the Hg–TGA complex, which was obtained from Stricks et al. (1954). The unknown parameters in the model are the M–DFOB stability constants, while the other four components are the known parameters. Essentially, the only difference between the two series of titrations is the presence or absence of TGA, therefore the divergence of the two represents the competition between DFOB and TGA for the Hg^{2+} ion. If the model is properly describing the experimental system and all of the known constants entered into the FITEQL model are accurate for the experimental conditions, then the Hg–DFOB and MeHg–DFOB stability constants may be determined from the titration data.

3.4. Results and discussion

Calculating stability constants of Hg and MeHg complexes with DFOB depends on accurate values of the acid dissociation constants, pK_{ai}, in the proper media for the two competing ligands in this study. The four pK_as of DFOB in 0.7 M $NaClO_4$ were determined in a previous study (Christenson and Schijf, 2011). The competing ligand, TGA, presumably has two exchangeable protons, one for the carboxyl group (pK_1) and one for the thiol group (pK_2). While the carboxyl proton dissociates in the pH range 3–4, the thiol group (–SH) remains predominantly protonated below pH 10 (Table 3.1).

Table 3.1 Results from nine titrations (pH 3–11) of TGA in 0.70 M $NaClO_4$ solutions containing either 8 mM or 12 mM TGA and using a titrant of either 1.0005 M NaOH or 0.1001 M NaOH. Regressions were performed with FITEQL4.0, keeping pK_W = 13.740 and pK_{a1} and pK_{a2} as adjustable parameters. All regressions converged in 5 iterations (*n*) or less.

[TGA]	pK_1	pK_2	NaOH	*n* [a]	WSOS/DF
8 mM	3.51	9.75	1 M	5	4.13
8 mM	3.51	9.75	1 M	5	3.98
8 mM	3.51	9.75	1 M	5	4.06
8 mM	3.54	9.78	0.1 M	4	2.47
8 mM	3.54	9.79	0.1 M	4	2.01
8 mM	3.54	9.77	0.1 M	4	2.47
12 mM	3.55	9.74	1 M	4	3.50
12 mM	3.55	9.75	1 M	4	3.60
12 mM	3.56	9.74	1 M	4	4.14

[a] Number of iterations for regression to converge.
[b] WSOS/DF (Weighted Sum-Of-Squares divided by the Degrees-of-Freedom) is the quality-of-fit parameter for FITEQL, with values in the range 0.1–20 indicating a good fit (Herbelin and Westall, 1999).

All nine of the potentiometric titrations of TGA used to determine the acid dissociation constants are plotted in Figure 3.5, and are in excellent agreement with one another for both TGA concentrations and titrants used as all curves are virtually

indistinguishable. The TGA regression model fits all nine titration curves relatively well (WSOS/DF < 5) and none of the pK_{ai} values deviate significantly from the mean (pK_1 = 3.54 ± 0.02 and pK_2 = 9.76 ± 0.02). Although these WSOS/ DF values are considered "good", they are higher than the quality-of-fit values that were found for the regressions of the DFOB titrations (Christenson and Schijf, 2011). As previously mentioned, since the thiol group of TGA is amphoteric, there may actually be three exchangeable protons in this system, whereas these TGA model regressions were only fit assuming two pK_as. As a result, the goodness-of-fit values may be somewhat elevated.

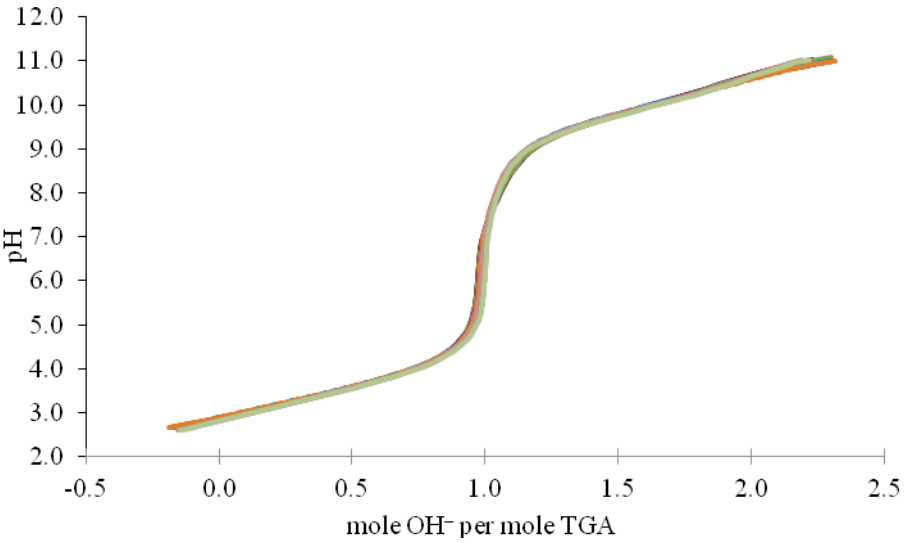

Figure 3.5. Potentiometric titrations of TGA solutions in 0.7 M $NaClO_4$ using either 1.0 M or 0.1 M NaOH as titrant, where pH (measured with a glass combination electrode) is plotted as a function of the moles of base (OH^-) added per mole of TGA (calculated from titrant volumes). All nine TGA titrations are plotted: 3 titrations with 8mM TGA and 1.0 M NaOH, 3 titrations with 8 mM TGA and 0.1 M NaOH, and 3 titrations with 12 mM TGA and 1.0 M NaOH.

Acid dissociation constants of TGA have been previously reported (e.g. Stricks et al., 1954), however many of these publications date back to the 1940s or they do not fully describe the methods and conditions used. Pitman and Morris (1979) report values for the

pK_as of TGA determined at 25°C at I = 0.1 M with pK_{a1} = 3.68, which is very similar to the values determined in this study, and pK_{a2} = 10.71, which is somewhat high compared to the values reported here, however the increased ionic strength used in this study (0.7 M) may account for the lower pK_{a2} value derived from my regressions.

Figure 3.6 shows data for a set of titrations conducted at a Hg:DFOB molar ratio of 1:2 in symbols, with the modeled behavior of the experimental system in solid lines. The deviation of the two titrations suggests that DFOB (blue circles) and TGA (red circles) are competing for the Hg^{2+} ion. The titration data appears to follow the model curves, however there is an offset in proton balance, which may be because the simple model does not accurately account for all protons in the system. Alternatively, the observed discrepancy between the modeled Hg behavior and the titration data may be due to poor resolution of the model, which, compared to the actual titration curves that contains ~80 data points, contains only ~10 data points and therefore may not capture the titration in sufficient detail. Additionally, the stability constants used in the MINEQL model, which were derived from an LFER, could be highly inaccurate resulting in further disagreement between modeled behavior and the actual titration data.

Non-linear regressions of the titration data for Hg+DFOB mixtures were attempted in FITEQL using the processes discussed above in order to determine the stability constants (β_1, β_2, and β_3) of the three M–DFOB complexes. The regressions did not converge and stability constants could not be determined from the data. It appears that the experimental system is not described with sufficient accuracy, or the fits may be under-constrained, most likely due to the intricate behavior of both Hg and TGA in solution.

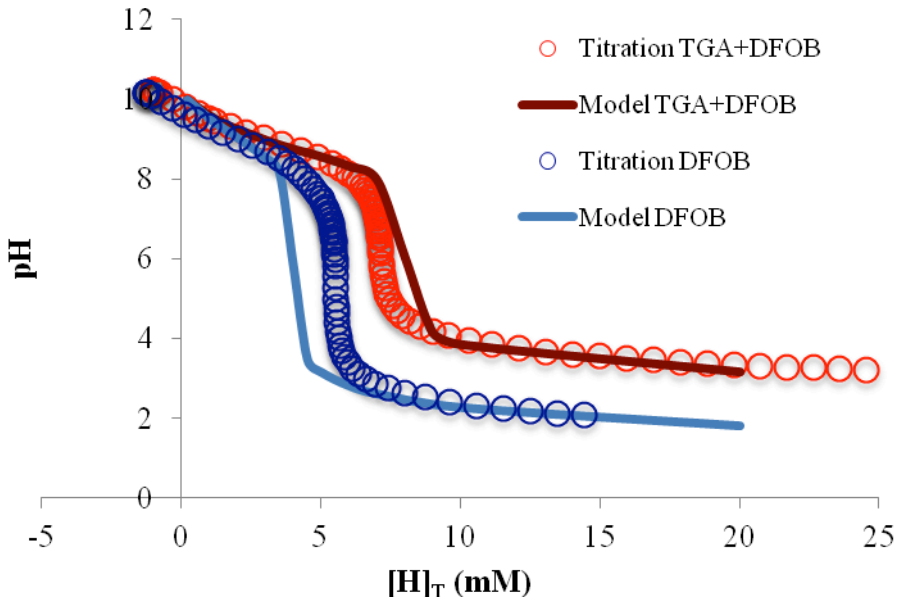

Figure 3.6. Example of potentiometric titrations of Hg + DFOB mixtures in 0.7 M $NaClO_4$ titrated with HCl (blue line) and Hg + DFOB mixtures in 0.7 M $NaClO_4$ titrated with TGA (red line), where pH (measured with a glass combination electrode) is shown as a function of $[H^+]_T$. All Hg + DFOB solutions contain 2 mM DFOB and 1 mM of Hg. Symbols are actual measurements and solid lines are modeled regressions performed with MINEQL.

As stated previously, the interactions of Hg^{2+} and $MeHg^+$ with the two ligands are poorly known and may need to be expressed differently in the model. As already mentioned, the Hg–DFOB stability constants used in the FITEQL model, although acting merely as starting estimates for the regression, are based on an LFER and could be inaccurate as well. It is possible that Hg does not form the full hexadentate complex, as was found for Pb, which would explain why the regressions are not converging and why Hernlem et al. (1999) predicted such a large value. In the future, this possibility will be tested by fitting the Hg data with FITEQL model similar to the one used for Pb (see Chapter 2).

Figure 3.7 shows titration data for a 1:2 molar ratio of MeHg:DFOB, in addition to data obtained with pure DFOB in the absence of metals (Christenson and Schijf, 2011). As discussed in Chapter 2, the deviation in the titration curve with respect to the titration curve of DFOB alone (shown here in orange in Figure 3.7) corresponds to the metal's ability to eject protons from the DFOB molecule. Since these two curves are very similar, this is an indication that MeHg does not bind with DFOB. A slight offset is observed at high pH, where it appears that MeHgOH may be forming, causing the titrations curves to diverge. Although MeHg forms very stable complexes with sulfide ligands, the bulky methyl group attached to the Hg^{2+} ion must be causing some steric hindrance, preventing the complexation of MeHg with DFOB. Under these experimental conditions, it appears that DFOB has no great affinity for MeHg, likely forming no more than a bidentate complex of low stability.

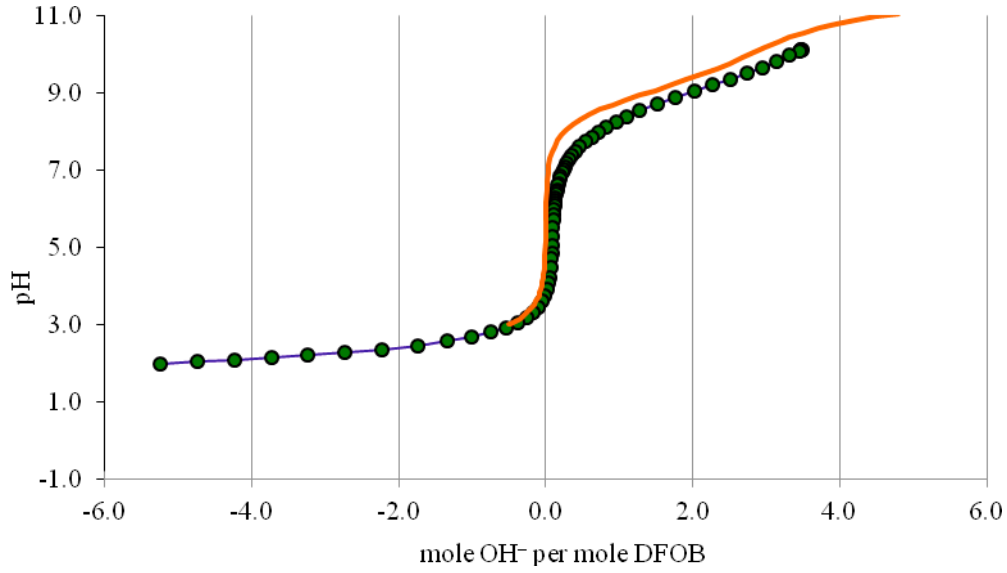

Figure 3.7. Example of potentiometric titration data for a 1:2 MeHg:DFOB molar ratio in 0.7 M $NaClO_4$ (green circles), compared with a non-linear regression obtained with pure DFOB in the absence of metals, also in 0.7 M $NaClO_4$ (orange line) (Christenson and Schijf, 2011).

3.5. Summary and implications

Although the ligand competition approach used in this study appears to prevent the problems with Hg hydrolysis that Hernlem et al. (1996) encountered during their titrations, Hg–DFOB stability constants could not be determined, most likely due to an inaccurate chemical description of the system. It may still be feasible to determine the stability constants from my titration data, however more work is needed at this time to determine all reactions occurring throughout the titration. Once stability constants are determined, seawater speciation modeling can be conducted with MINEQL, in order to investigate if siderophores like DFOB are a major ligand for Hg in seawater.

Nevertheless, the results from this study shed some light on the interactions of TGA and DFOB with Hg and MeHg. Through non-linear regressions of potentiometric titrations of TGA, pK_as were determined for TGA at seawater ionic strength (0.7 M), which are in good agreement with existing literature data. Even though Hg–DFOB stability constants could not be resolved, the titration data indicate that Hg does form a very stable complex with DFOB, and may thus aid the acquisition of Hg by methylating microorganisms in the marine environment. Contrary to Hg, these titration data suggest that MeHg does not form a complex with DFOB, most likely due to its partially occupied coordination sphere.

While numerous studies have demonstrated that Hg forms complexes with natural organic ligands in aquatic environments (Lamborg et al., 2004), the identity and role of these organic ligands in Hg methylation in seawater is not well understood. The predicted stability constant (β_3) of about 10^{26} (Hernlem et al., 1999), implies that complexation with

siderophore-like molecules may be a viable mechanism for transporting dissolved Hg^{2+} from seawater across the cell membrane, as it appears to be for many other transition metals. If this is found to be true, it may provide an alternative to the dominant view that Hg uptake occurs via passive diffusion of neutral Hg complexes. Elucidating the processes that facilitate Hg uptake will provide new insights into the mobility and methylation of mercury in the open ocean.

Chapter 4: Scavenging of yttrium and the rare earth elements in seawater: modeling their partitioning between solution and particles

4.1. Abstract

The relative behavior of yttrium and the rare earth elements (YREE) in seawater is controlled by the competing processes of complexation with dissolved ligands and sorption on the surface of marine particles. Organic complexation of YREE is generally believed to be significant, but is an understudied aspect of YREE solution speciation in the open ocean. Using stability constants for YREE complexes (except Ce and Pm) with the trihydroxamate siderophore desferrioxamine B (DFOB), measured at seawater ionic strength, I created a solution complexation model that includes a model organic ligand in addition to the relevant inorganic ligands in seawater. Combined with recently measured shale-normalized YREE concentrations in seawater, the resulting solution complexation model enables the estimation of the relative affinity of each YREE for marine particles. My modeled surface complexation is compared with laboratory data for YREE sorption on various pure organic and mineral surfaces.

In general, the stability of both YREE solution and surface complexes increases with atomic number. The model results show that YREE sorption characteristics derived for natural marine particles are remarkably similar to those of hydrated Mn oxides, while the HREE (heavy rare earth elements; Ho–Lu) pattern also resembles the macroalga *Ulva lactuca,* representing a typical marine organic surface, and Fe hydroxides. In contrast, the

LREE (light rare earth elements; La–Nd) pattern does not resemble any of the remaining YREE sorption patterns I considered, hence their scavenging in the surface ocean may be controlled by yet another type of particle, possibly authigenic clays.

4.2. Introduction

The Rare Earth Elements (REE) are a series of trace metals that comprises the fifteen elements from lanthanum to lutetium. Since the REE generally occur in nature together with yttrium (Y), and given that yttrium exhibits chemical characteristics similar to those of the REE, it is often included in REE complexation studies. Promethium (Pm) is almost never included in REE geochemical studies because it has no stable isotopes.

Yttrium and the rare earth elements (YREE) are ideal for studying trace metal complexation in seawater because of their chemical properties, which are largely the same but show systematic changes across the series. In solution, YREE always form trivalent cations, however due to the progressive filling of the inner 4*f* electron shell, ionic radii decrease gradually with increasing atomic number (Figure 4.1), a feature referred to as the "lanthanide contraction". When analyzed as a group, plots of stability constants and distribution coefficients display distinctive patterns, allowing the YREE to be used as a sensitive probe of geochemical processes that influence the global cycling of trace metals in seawater (Byrne and Sholkovitz, 1996).

Due to the increased natural occurrence of elements with even atomic numbers, YREE concentrations in natural samples display a saw-tooth abundance pattern. To remove this jaggedness, YREE concentrations are typically normalized to a geological reference, such as the Post-Archaean Australian Shale (PAAS). Mean shale represents the YREE

signature of average crustal rocks, therefore normalization to PAAS allows one to visualize fractionation of YREE abundances in geochemical samples with respect to the average crustal source.

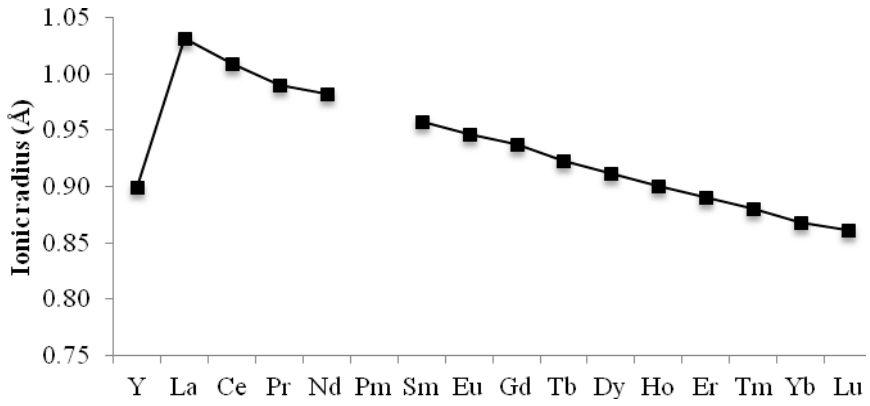

Figure 4.1. Visual depiction of the lanthanide contraction. The trivalent ionic radius (for coordination number 6) decreases with increasing atomic number throughout the rare earth element series (Shannon, 1976).

The oceanic vertical profiles of YREE (except for cerium) are characterized by low concentrations in the surface waters due to removal/uptake from solution, and increasing concentrations with depth as the metals are released during settling and decomposition of particulate matter (Figure 4.2). As discussed in Chapter 1 (see Figure 1.1), such distributions are classified as 'nutrient-like' (Bruland, 1983b). The scavenging of YREE in seawater reflects a delicate interplay between (i) complexation with a mixture of dissolved ligands and (ii) sorption, or surface complexation, on biogenic and mineral particles.

Cerium (Ce) is the only REE that can be oxidized to the +IV oxidation state in natural waters, resulting in increased reactivity and anomalous distributions compared to the other, strictly trivalent YREE. In aquatic environments, oxidation of Ce after sorption onto particles lowers the concentration of surface-bound Ce(III), which promotes

increased Ce removal from solution. Therefore, negative Ce anomalies are a prominent characteristic of seawater (e.g., Elderfield and Greaves, 1982). In contrast, varying positive Ce anomalies in REE patterns have been reported for oceanic ferromanganese nodules and encrustations due to oxidation and increased sorption (e.g., Aplin, 1984).

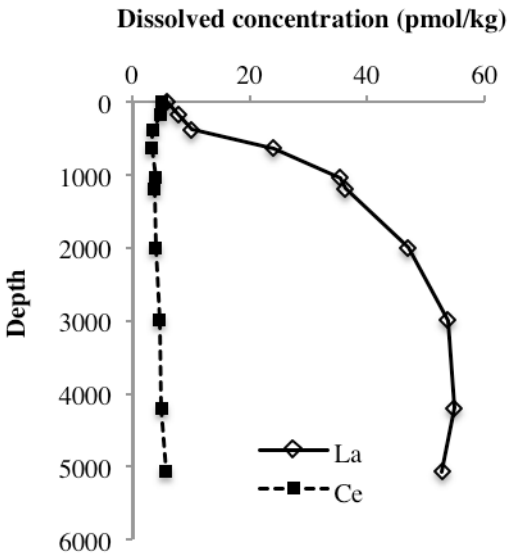

Figure 4.2. Typical profiles of dissolved La and Ce at station TPS 24 271–1 in the western Pacific Ocean (Piepgras and Jacobsen, 1992). Cerium displays a 'scavenged' profile due to enhanced particle-reactivity caused by its unique redox chemistry. Lanthanum, representing the strictly trivalent YREE, displays a 'nutrient-like' profile.

The distribution of YREE in seawater is reflective of the balance between oceanic inputs and outputs, and has been previously expressed (Byrne and Kim, 1990) in terms of solution and surface complexation using the following equation that was derived from a single-box residence time model:

$$\log\left\{\frac{A_{\mathrm{M}}}{\mathrm{d}A_{\mathrm{M}}/\mathrm{d}t}\right\} = \log\left\{\frac{M_T/[M]}{M_s/[M]}\right\} + \text{constant}, \qquad (4.1)$$

where A_{M} is the total amount of metal M in seawater and $\mathrm{d}A_{\mathrm{M}}/\mathrm{d}t$ is the metal's oceanic input flux at steady state. The ratio of $A_{\mathrm{M}}/(\mathrm{d}A_{\mathrm{M}}/\mathrm{d}t)$ on the left-hand side of Eq. (4.1)

represents shale-normalized YREE concentrations in seawater, or a metal's oceanic residence time with respect to its total oceanic input/output. It should be noted that the equation contains a constant that encompasses several unknown quantities related to the properties of marine particles, such as surface site characteristics and densities, and particle residence times and concentrations, which are all independent of the metal M (Byrne and Kim, 1990).

The numerator on the right-hand side of Eq. (4.1) represents the extent of solution complexation, where M_T is the total dissolved concentration of a given metal in seawater and [M] represents a metal's free dissolved concentration. The solution complexation term, (M_T/[M]), can be expressed as a summation over all YREE solution complexes in seawater, shown below:

$$M_T/[M] = \sum_{nj}\left(1 + {}_j\beta_n[L_j]^n\right) \tag{4.2}$$

where ${}_j\beta_n$ are the stability constants of the *n*th complex of metal M with dissolved ligand L_j, as shown below:

$$\mathrm{M}^{3+} + nL_j \xleftrightarrow{{}_j\beta_n} M(L_j)_n; \qquad {}_j\beta_n = \frac{[M(L_j)_n]}{[\mathrm{M}^{3+}][L_j]^n}. \tag{4.3}$$

The denominator on the right-hand side of Eq. (4.1) represents the extent of surface complexation, where M_S is the concentration of metal bound to particles in seawater. The surface complexation term, (M_S/[M]), can be written as a summation over all YREE surface complexes in seawater, shown below:

$$M_S/[M] = \sum_i\left({}_iK_s \times [S_i]\right) \tag{4.4}$$

where ${}_iK_s$ are the stability constants of surface complexes MS_i, as shown below:

$$M^{3+} + S_i \xleftrightarrow{{}_iK_s} MS_i; \quad {}_iK_s = \frac{[MS_i]}{[M^{3+}][S_i]}. \tag{4.5}$$

Therefore, if one assumes that mean shale appropriately normalizes oceanic YREE concentrations for differences in YREE input rates, Eq. (4.1) indicates that the *relative* abundances of YREE in seawater are solely dependent on their solution and surface complexation. The quantity ${}_iK_s$ will be interpreted here as a distribution coefficient, with the ratio $[MS_i]/[S_i]$ calculated as the concentration of sorbed metal per mole of solid substrate since particles may contain more than one type of surface ligand.

Inorganic solution complexation of YREE has been extensively studied and stability constants are known for all solution complexes with major inorganic ligands in seawater. Speciation calculations for YREE in seawater indicate that the MCO_3^+ complex dominates the inorganic solution speciation of the light REE and the $M(CO_3)_2^-$ complex that of the heavy REE, with minor contributions from other complexes, such as MCl^{2+}, MOH^{2+}, and MSO_4^+ (Byrne and Sholkovitz, 1996). Given that the YREE form stable complexes with carbonate and hydroxide, which resemble the dominant functional groups of organic matter, it is presumed that they also form stable complexes with organic ligands. However, little is known about YREE organic complexation in seawater because the identity and concentration of marine organic ligands are largely unknown. Byrne and Li (1995) used linear free-energy relations (LFERs) to assess the general behavior of REE organic solution complexation using 110 different organic compounds, however the majority of the ligands investigated are relatively weak or do not occur in

seawater, and the individual stability constant patterns exhibit substantial variability. Recently, I reported stability constants for complexes of YREE with the siderophore desferrioxamine B (DFOB), and found that DFOB complexes could make up a substantial fraction of total YREE concentrations in seawater at free DFOB concentrations that may exist under realistic conditions (Christenson and Schijf, 2011).

YREE surface complexation and the properties of marine particulate matter are less well understood, but have been gaining more attention in the last decade. Quinn et al. (2004) investigated the effects of YREE sorption on freshly precipitated hydroxides of Fe, Al, Ga, and In. Recently, Marshall and Schijf (*Chemical Geology*, in prep.) studied YREE sorption on hydrated Mn(IV) oxide particles, as well as on Fe(III) hydroxides (Schijf and Marshall, 2011), as a function of pH at near-seawater ionic strength (I = 0.5 M). Relatively few studies have measured YREE interactions with natural organic matter. Zoll and Schijf (2012) investigated YREE sorption on a marine macroalga, *Ulva lactuca*, at different ionic strengths as a function of pH.

With the current lack of data, it is difficult to fully understand the processes controlling seawater YREE patterns. Two indirect methods have been previously used to model YREE solution and surface complexation behavior. In the first approach, relative YREE sorption behavior was estimated from LFERs with the YREE hydroxide stability constant (e.g., Erel and Morgan, 1991). The second approach is to predict relative surface complexation behavior from Eq. (4.1) discussed above. Using the best inorganic solution complexation constants available at that time and the average stability constants of 15 REE–carboxylate complexes, Byrne and Kim (1990) predicted relative oceanic abundances if YREE scavenging were predominantly influenced by organic surfaces with

monocarboxylate functional groups and found their model patterns to be in good agreement with observed shale-normalized REE abundance patterns in seawater.

In this work, a modification of the Byrne and Kim (1990) approach was used to model YREE surface complexation in seawater. This model differs from that of Byrne and Kim (1990) in two ways: (i) organic solution complexation was included in these model calculations, and (ii) instead of deriving relative oceanic YREE abundances, the relative behavior of YREE sorption on marine particles in seawater is estimated (the M_S /[M] term). First, inorganic solution complexation was modeled for the whole YREE series using the most recent constants available in the literature. Stability constants for YREE–DFOB complexes measured at seawater ionic strength (Christenson and Schijf, 2011) were then added to the model to reflect solution complexation with a strong "model" organic ligand. Using Eq. (4.1) and known YREE concentrations in seawater, their relative surface complexation behavior was obtained. These results were then compared with recently measured ${}_iK_s$ patterns for several inorganic substrates (hydrated Mn(IV) and Fe(III) oxide particles, as well as biogenic silicate and carbonate), in addition to an organic substrate (the marine macroalga *Ulva lactuca).* A comparison is also made between this more detailed model of YREE speciation in seawater and the earlier model of YREE complexation with marine dissolved organic matter (e.g., Byrne and Kim, 1990) on which it is based.

4.3. MINEQL modeling

Model speciation calculations were performed with the computer code MINEQL2.0 (Westall et al., 1976). A standard seawater speciation model (S = 35, pH fixed at 8.2) that includes all major anions and cations was first created as previously discussed in Chapter

2. Because MINEQL extrapolates all equilibrium constants using the Davies Equation, which is unreliable at ionic strengths above 0.5 M, the database THRM.DAT was updated with constants appropriate for seawater (I = 0.7 M), which were then retained by setting the model ionic strength to I = 0 (Schijf et al., 1995). Each individual YREE was subsequently added to the model at a fixed concentration of 1 pM. The most recent stability constants measured at I = 0.7 M for all relevant YREE dissolved inorganic ligands were obtained from the literature (Table 4.1).

Table 4.1. Stability constants for YREE complexes with the major anions in seawater taken from the literature: hydroxide (Klungness and Byrne, 2000), carbonate and bicarbonate (Liu and Byrne, 1998; Luo and Byrne, 2004), sulfate (Schijf and Byrne, 2004), and chloride (Luo and Byrne, 2001).

M^{3+}	$\log \beta_1^*$	$\log_{CO_3} \beta_1$	$\log_{CO_3} \beta_2$	$\log_{HCO_3} \beta_1$	$\log_{SO_4} \beta_1$	$\log_{Cl} \beta_1$
Y	–8.11	5.75	10.11	1.27	1.83	–0.399
La	–9.12	5.17	8.78	1.29	1.94	–0.399
Ce	–8.65	5.53	9.24	1.26	1.94	–0.399
Pr	–8.62	5.71	9.56	1.20	1.95	–0.399
Nd	–8.49	5.76	9.65	1.23	1.93	–0.399
Pm	—	—	—	—	—	—
Sm	–8.15	5.81	10.01	1.29	1.96	–0.399
Eu	–8.06	5.85	10.11	1.42	1.97	–0.399
Gd	–8.14	5.72	9.96	1.31	1.94	–0.399
Tb	–7.95	5.76	10.26	1.41	1.92	–0.399
Dy	–7.89	5.86	10.39	1.45	1.90	–0.399
Ho	–7.87	5.84	10.48	1.41	1.87	–0.399
Er	–7.82	5.87	10.60	1.44	1.84	–0.399
Tm	–7.70	5.96	10.75	1.47	1.81	–0.399
Yb	–7.55	6.08	10.78	1.48	1.79	–0.399
Lu	–7.57	6.03	10.85	1.44	1.77	–0.399

These include hydroxide (Klungness and Byrne, 2000), carbonate and bicarbonate (Liu

and Byrne, 1998; Luo and Byrne, 2004), sulfate (Schijf and Byrne, 2004), and chloride (Luo and Byrne, 2001). Fluoride was not included in the model as its contribution to YREE speciation in seawater is negligible.

The solution speciation model was run twice at two different concentrations of *free* DFOB. From previous work, it was determined that ~4% of total Lu consists of the hexadentate $LuHDFOB^+$ complex in seawater speciation models with the *free* DFOB concentration fixed at 10^{-14} M. When the *free* DFOB concentration is raised to 10^{-13} M, the contribution of the $LuHDFOB^+$ complex increases to ~28% (Christenson and Schijf, 2011). The present model calculations were performed using the same two scenarios.

Table 4.2. Stability constants of the bidentate (log β_1), tetradentate (log β_2), and hexadentate (log β_3) DFOB complexes with the trivalent YREE (except Ce and Pm), determined from FITEQL4.0 regressions of 5 titrations per individual metal in 0.7 M $NaClO_4$ (Christenson and Schijf, 2011).

M^{3+}	log β_1	log β_2	log β_3
Y	6.16	10.51	13.98
La	4.88	7.7	10.09
Ce	—	—	—
Pr	5.45	8.96	11.96
Nd	5.54	9.24	12.33
Pm	—	—	—
Sm	5.93	10.09	13.38
Eu	6.07	10.32	13.67
Gd	6.04	10.31	13.67
Tb	6.24	10.67	14.15
Dy	6.35	10.83	14.40
Ho	6.32	10.89	14.53
Er	6.38	10.99	14.66
Tm	6.44	11.13	14.90
Yb	6.53	11.27	15.17
Lu	6.48	11.25	15.19

Acid dissociation constants of DFOB measured in $NaClO_4$ (pK_{a1}= 8.54, pK_{a2} = 9.06, pK_{a3} = 9.70, pK_{a4} = 10.89) and stability constants of the YREE–DFOB complexes were taken from Table 4.2 (see Christenson and Schijf (2011) for more details pertaining to the determination of YREE–DFOB stability constants). Stability constants for the Ce(III)–DFOB complex could not be determined because complexation with DFOB induces Ce(III) oxidation, therefore Ce was excluded from the MINEQL modeling in this study. Additionally, Ce oxidation in seawater leads to enhanced scavenging, so even if stability constants for the Ce(III)–DFOB complex could have been determined, my speciation model would not have produced the correct pattern.

Since MINEQL will only allow for the addition of five elements or components that are not already included in the database, three separate models were made which contained five REE each. In order to assure the consistency of these three models, La was included in each one and the results produced were identical. For every model output, a free metal concentration was returned by MINEQL for each REE ([M]), which was used to calculate a solution complexation term with $[M]_T$ = 1 pM. Assuming that PAAS reflects relative differences in the global input rates of individual YREE, Eq. (4.1) can be taken to represent shale-normalized (PAAS) YREE concentrations in seawater:

$$\log\left(\frac{[\mathrm{YREE}]_{\mathrm{sw}}}{\mathrm{PAAS}}\right) = \left[\log\left(M_T/[M]\right)\right] - \left[\log\left(M_S/[M]\right)\right]. \qquad (4.6)$$

This equation can then be rearranged to the following:

$$\left[\log\left(M_S/[M]\right)\right] = \left[\log\left(M_T/[M]\right)\right] - \log\left(\frac{[\mathrm{YREE}]_{\mathrm{sw}}}{\mathrm{PAAS}}\right), \qquad (4.7)$$

which yields the surface complexation term (M_S/[M]) from known solution complexation behavior and PAAS-normalized (McLennan, 1989) YREE concentrations in seawater (Zhang and Nozaki, 1996).

4.4. Results and discussion

4.4.1. YREE solution complexation

Figure 4.3 presents the calculated solution complexation term (M_T/[M]) for standard seawater at pH 8.2 with the free DFOB concentration fixed at 10^{-13} or 10^{-14} M.

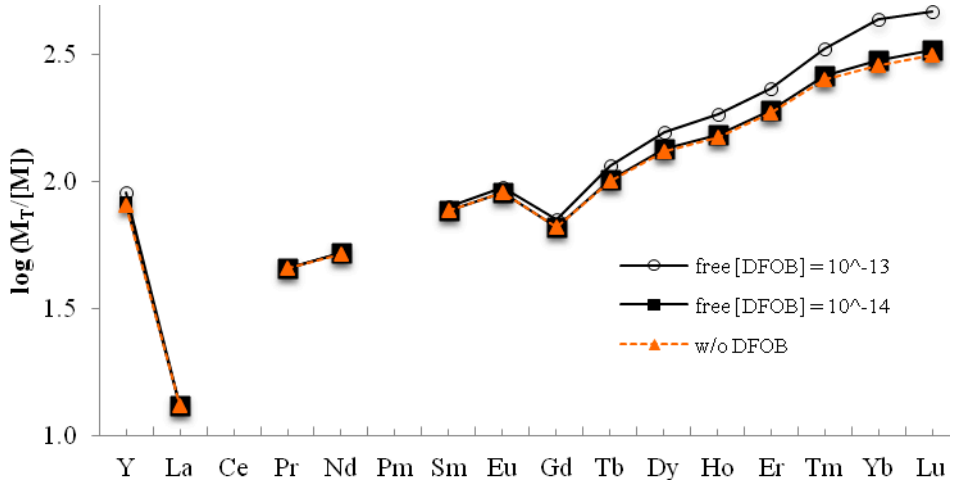

Figure 4.3. Calculated solution complexation term at pH 8.2 with the free DFOB concentration fixed at 10^{-13} M (open circles) and 10^{-14} M (closed squares). Also shown (orange triangles) is the calculated solution complexation for YREEs with DFOB excluded from the speciation model.

The calculated solution complexation for YREE without DFOB (*i.e.*, including only inorganic speciation), which is dominated by carbonate complexation, is also shown (orange triangles). The slope of M_T/[M] across the series is positive, with a local minimum at Gd. Values for Y fall between Gd and Tb in the MREE (middle rare earth elements), which encompass the elements Sm–Dy. For REE heavier than Gd, two subtle

'tetrads', or 'patterns-of-four' (Monecke et al., 2002), are observed centered at Tb–Dy and Tm–Yb. The increase of (M_T/[M]) observed throughout the REE series is largely attributable to the combination of both increasing carbonate complexation and increasing DFOB complexation from La to Lu. The model calculations performed using the scenario where *free* [DFOB] is fixed at 10^{-14} M show similar trends as the calculations under conditions where *free* [DFOB] is fixed at 10^{-13} M. The difference between the two calculated M_T/[M] terms is negligible for the LREE, but becomes more prominent for the HREE. With increasing DFOB concentration, solution complexation increases more strongly for the HREE. It is evident that the change of the YREE pattern by the addition of DFOB into the speciation model is relatively minor since it is similar to the pattern for carbonate, the dominant inorganic ligand. However, these model calculations were performed using a single organic ligand. In reality, YREE in seawater are most likely complexed with a variety of strong organic ligands, which may have dissimilar stability constant patterns, whereby their effect on YREE speciation should be cumulative.

4.4.2. Modeled YREE surface complexation patterns in seawater

Average YREE surface complexation characteristics (i.e., log ${}_iK_s$ pattern) of marine particles were derived from Eq. (4.7). Figure 4.4 depicts shale-normalized (McLennan, 1989) YREE concentrations at two different depths (one surface seawater and one deep seawater) in the western South Pacific (Zhang and Nozaki, 1996). Relative values of ${}_iK_s$ were calculated by subtracting the shale-normalized seawater YREE concentrations (Figure 4.4) from the modeled M_T/[M] values (Figure 4.3).

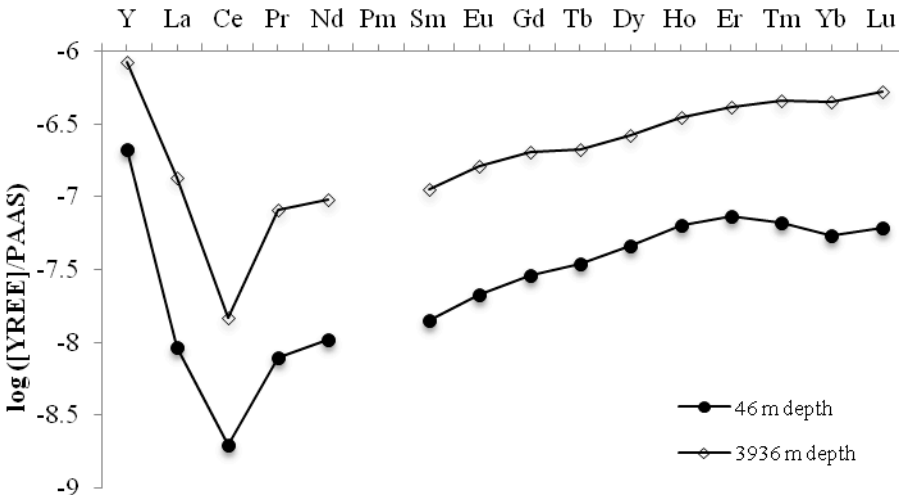

Figure 4.4. YREE concentrations measured directly in seawater at two different depths (Zhang and Nozaki, 1996), normalized to Post-Archaean Australian Shale (PAAS) (McLennan, 1989).

Figure 4.5. shows the modeled ${}_iK_s$ behavior with free DFOB concentrations fixed at 10^{-13} M (~0–30% YREE–DFOB complexation, depending on the element) for two different depths, in addition to the modeled behavior with DFOB fixed at 10^{-14} M (~0–5% YREE–DFOB complexation, depending on the element) for the surface depth only. All patterns, calculated for two solution complexation scenarios (free DFOB fixed at 10^{-13} M and 10^{-14} M) at two depths (46 and 3936 m), are very similar except for minor differences in slope. Due to the low degree of DFOB complexation for the LREE, the largest deviation between the two different *free* DFOB concentrations is seen in the HREE, where complexation with DFOB increases. Although the ionic radius of Y is similar to that of Ho, the behavior of Y is not always consistent with that of Ho. Instead, Y may display more ionic (LREE-like) or covalent (HREE-like) character, depending on the nature of the ligand it is complexed with. In these modeled YREE surface complexation patterns, Y exhibits weaker sorption than the REE and is therefore behaving more like an LREE.

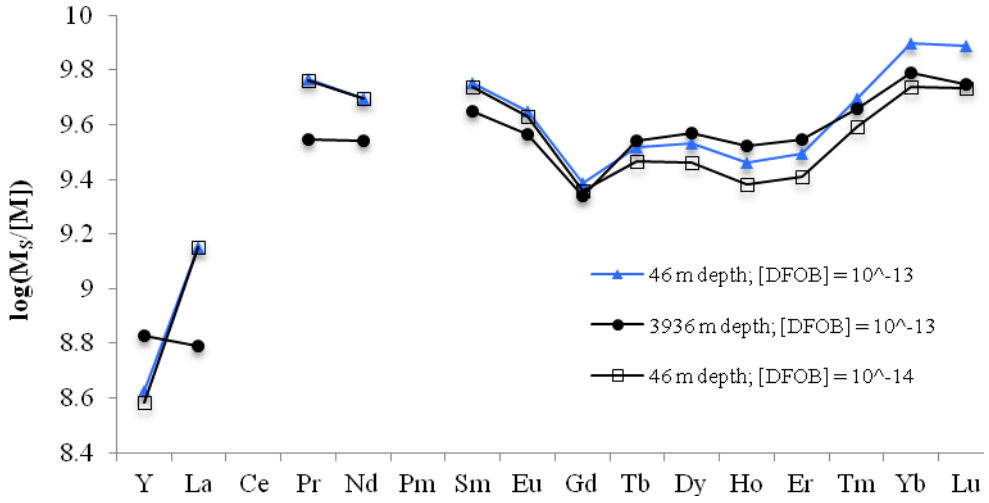

Figure 4.5. Modeled YREE surface complexation (M_S/[M]) with free [DFOB] fixed at 10^{-13} M for 46 m and 3936 m depth, and with free [DFOB] fixed at 10^{-14} M for 46 m depth, calculated by subtracting the curves in Figure 4.4 from the curves in Figure 4.3. Modeled surface complexation patterns were vertically shifted to coincide at Gd, for visual comparison.

If the pattern for YREE complexation with DFOB is representative of that for YREE complexation with dissolved organic ligands in seawater, then the relative surface complexation behavior should be similar to the patterns depicted in Figure 4.5.

4.4.3. Comparison between model results and measured values

The ${}_iK_s$ behavior predicted from this work is compared with recent YREE sorption data for one organic surface (*Ulva lactuca*) and four inorganic surfaces (hydrated Mn(IV) and Fe(III) oxides, as well as biogenic silicate and carbonate) (Figure 4.6). Since the modeled surface complexation patterns for each depth and concentration of free DFOB are very similar, only the results derived at depth 46 m with free [DFOB] fixed at 10^{-13} M are plotted here for simplicity.

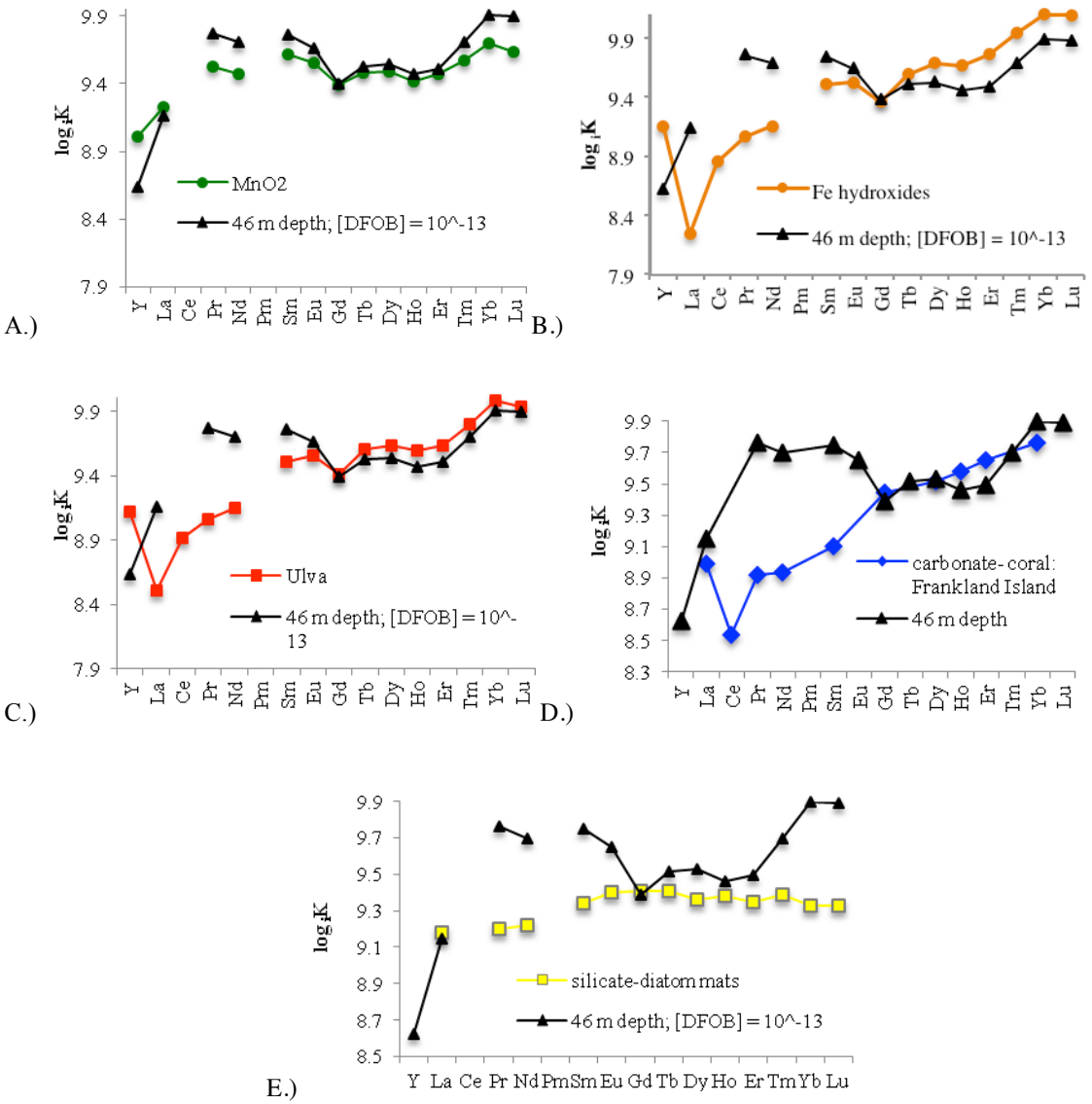

Figure 4.6. The predicted $_iK_s$ behavior at 46 m depth from this work (with free [DFOB] fixed at 10^{-13} M) plotted with recent YREE sorption data for (A) hydrated Mn(IV) oxides, (B) Fe(III) hydroxides, (C) an organic surface, *Ulva lactuca*, (D) coral carbonate, and (E) biogenic silicate. YREE sorption data with hydrated Mn oxides was measured at pH 6.98 in 0.5 M NaCl (Marshall and Schijf, *Chemical Geology*, in prep). YREE sorption data with Fe hydroxides was measured at pH 8.38 in 0.5 M NaCl (Schijf and Marshall, 2011). YREE sorption data with *Ulva* was measured at pH 8.2 in 0.5 M NaCl (Zoll and Schijf, 2012). Distribution patterns of REE in coral carbonate samples are from Frankland Island, off the Great Barrier Reef in Australia (Wyndham et al., 2004). Distribution patterns of REE in laminated diatom mats are from the upper unit (0–286 cm) of core WPD-03 (Xiong et al., 2012). Measured sorption patterns were vertically shifted to coincide at Gd for comparisons with the modeled pattern.

When compared for the whole YREE series, the best visual match of the modeled surface complexation pattern is obtained with the recently measured data for YREE sorption on hydrated Mn(IV) oxides, as it appears to depict the general behavior of both LREE and HREE. This strong resemblance between the modeled and measured surface complexation data indicates that YREE sorption characteristics of marine particles are remarkably similar to those of hydrated Mn oxides. When split into two groups (HREE vs. LREE), the HREE appear to match the measured *Ulva* and Fe hydroxide sorption data, in addition to the hydrated Mn oxide data. The modeled surface complexation pattern for the LREE on the other hand, shows different behavior and does not closely match the *Ulva* and Fe hydroxide sorption data.

It is evident from these plots that some of the published sorption patterns for the five particle surfaces shown here are different from the others. In particular, the patterns for both silicate and carbonate deviate greatly from the other measured sorption patterns, as well as the from surface complexation behavior derived in this work. In contrast to recent publications (Akagi et al., 2011; Akagi, 2013), this suggests that YREE patterns in seawater are not significantly influenced by sorption on silicate or carbonate particles.

If YREE in seawater are predominantly sorbed on organic particles, the behavior of dissolved organic ligands may provide an approximation for YREE surface complexation with organic particles. For this reason, Byrne and Kim (1990) modeled the REE sorption behavior that might be observed for organic particles dominated by carboxylic acid functional groups by using the average stability constant for REE complexation with 15 simple monocarboxylic acids (black line in Figure 4.7). The behavior of these 15

compounds is highly variable and the average does not appear to fully capture the range of surface complexation behaviors that exist throughout the YREE series.

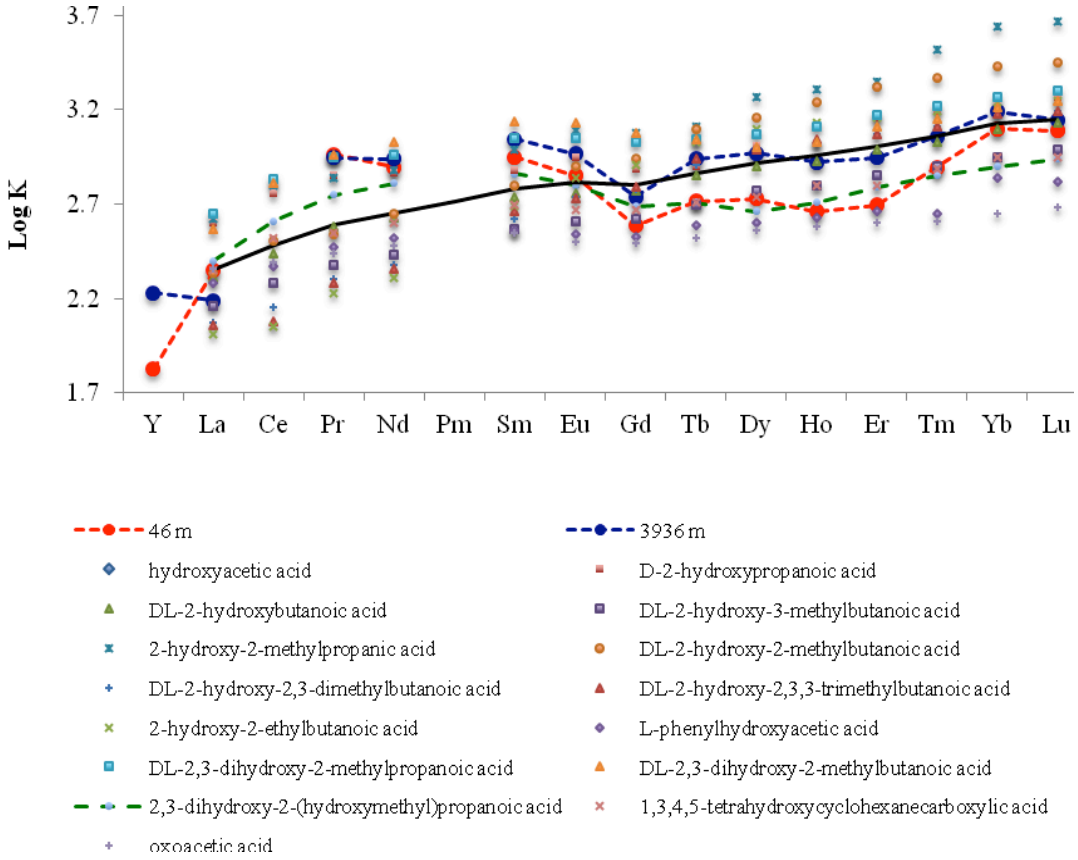

Figure 4.7. Modeled YREE surface complexation (M_S/[M]) with the free [DFOB] concentration fixed at 10^{-13} M at 46 m depth (red dashed line) and 3936 m depth (blue dashed line), compared to the average stability constant for REE complexation with 15 simple monocarboxylic acids (black line) (Byrne and Kim, 1990).

Compared with the modeled surface complexation in this work, which exhibits several "tetrads" (red and blue dashed lines in Figure 4.7), the modeled behavior of Byrne and Kim (1990) appears fairly flat and linear, with a slight Gd anomaly. This incongruent behavior with regard to YREE complexation even for small selection of chemically similar organic ligands reveals that without detailed investigations of the specific surface

complexation properties of marine organic matter, a comprehensive description of YREE scavenging in seawater will not be feasible.

Of the 15 monocarboxylic acids examined by Byrne and Kim (1990), it does appear that 2,3-dihydroxy-2-(hydroxymethyl)propanoic acid (highlighted with the green dashed line) does a better job of capturing the pattern derived in this work than the average. This particular compound contains several additional hydroxyl functional groups, which suggests that sorption on organic particles in seawater involves surface ligands that are more intricate than the simplest monocarboxylic acids. However, at this time it remains unknown which carboxylic acids, if any, dominate YREE surface complexation in seawater, even ignoring the fact that we lack vital information about the fundamental nature of marine organic particles.

Section 4.5. Conclusions and implications

When it comes to YREE sorption in seawater there are still a lot of unknowns, including the identity and concentration of marine particles, as well as the different types of surface ligands. Direct measurements of ${}_iK_s$ with a variety of particle surfaces are scarce and will differ dramatically depending on the location studied, as different places and conditions in the ocean will produce different results, making it difficult to draw general conclusions about YREE sorption behavior in seawater. There have been a variety of laboratory YREE sorption experiments, however most of these studies thus far have been conducted under conditions that are only approximately applicable to seawater and do not capture the heterogeneity of real marine particles. Consequently, efforts have been made in the past two decades to set up thermodynamic models that are suitable for

predicting complexation and sorption in natural waters (e.g. Byrne and Kim, 1990; Erel and Stolper, 1993).

Models of oceanic trace metal scavenging postulate that trace metal distributions are governed by the competition between metal complexation with solution and surface ligands. Using a simplified equation derived from a residence time model, the relative surface complexation behavior of YREE was predicted based on the most recent constants available for inorganic ligands in seawater, as well as stability constants for YREE–DFOB complexes, which were added to the model to represent solution complexation with a strong organic ligand.

These results suggest that YREE surface complexation in seawater may be dominated by sorption onto hydrated Mn oxides. These are ubiquitous in marine sediments and in the water column (Johnson et al., 1996), and are strong natural oxidants of redox-sensitive elements, such as Ce (Marshall and Schijf, *Chemical Geology*, in prep), which causes anomalous behavior of Ce compared to the other REE and may have implications for both the fate and reactivity of Ce in seawater. The modeled surface complexation patterns for the HREE are also very similar to recently measured sorption patterns for Fe hydroxides and a typical marine organic substrate. It is likely that relative YREE surface complexation behavior is controlled by a combination of these three particles (hydrated Mn oxides, Fe hydroxides, and organic matter), however more laboratory experiments exploring possible combinations and interactions of particle surfaces (e.g. Mn oxides with *Ulva*) are necessary to fully understand YREE sorption in seawater. These results also suggest that YREE surface complexation behavior is not significantly influenced by sorption onto biogenic silicate or carbonate in seawater, which

is not surprising since silicate (diatoms) and carbonate (foraminifera) contain very low REE concentrations (Palmer, 1985; Dubinin, 2004; Xiong et al., 2012), and both have been found to poorly correlate with REE concentrations in marine environments. However, in order to completely rule out silicate and carbonate as major YREE scavengers in seawater, more detailed and controlled laboratory studies need to be conducted examining YREE sorption on pure silicate and carbonate at relevant concentrations and ionic strength. These model data indicate that the LREE and HREE display different behaviors, and it appears that LREE surface complexation is influenced by some other particle surface not examined here. It is possible that relative LREE surface complexation is controlled by authigenic clays, which are an important component of marine particles (Beaucaire et al., 2012), and have been shown to scavenge REE in aquatic environments due to their high surface area and negative charge (Tertre et al., 2006; Tertre et al., 2008). At this time, experimental results regarding the surface chemistry of clay minerals are conflicting, most likely due to contrasting methods and substrates used, and more work is needed on this subject in order to determine if YREE are significantly influenced by sorption onto authigenic clays particles.

Chapter 5: Conclusion

5.1. Closing remarks

Complexation with organic ligands of unknown nature and origin dominates the chemical speciation of many trace metals in seawater. Because metal-binding compounds regulate the bioavailability of trace metals and impact primary productivity and plankton community structure, it is important to expand our understanding of the role of these ligands in ocean biogeochemistry. My research provides new insights into the role of trace metal complexation in seawater, by examining organic complexation of metals with a model siderophore and by describing the potential effects of siderophores on metal speciation in seawater. While the results are specific to trace metal complexation with DFOB, my conclusions likely apply to other metal cations and to similar types of organic ligand.

My first research objective was to determine if unidentified organic ligands that strongly complex with Zn, Cd and Pb in seawater might be siderophores. The Zn–DFOB and Pb–DFOB stability constants I presented in Chapter 2 are similar to conditional stability constants that have been measured in seawater for Pb- and Zn-specific classes of organic ligands, which suggests that the unidentified organic ligands that form strong complexes with these metals in seawater may be siderophore-like molecules. Conversely, the Cd–DFOB stability constants are substantially lower than conditional stability constants for Cd-specific organic ligands measured in seawater, suggesting that Cd speciation is dominated by a different type of organic ligand. I also concluded that both

Zn and Cd form hexadentate complexes with DFOB, whereas the Pb–DFOB complex is tetradentate.

My second research objective was to determine if siderophores could provide a mechanism for Hg uptake and subsequent methylation within the oceanic water column. Although stability constants could not be derived from non-linear regressions, I concluded in Chapter 3 that Hg forms stable complexes with DFOB and may therefore promote the acquisition of Hg by methylating microorganisms in the marine environment. I also concluded that, contrary to Hg, MeHg does not form a complex with DFOB, refuting my hypothesis that siderophores aid the release of MeHg from the cell and increase the bioavailability of this more toxic form to other marine organisms.

My final research objective was to use my own stability constants for YREE–DFOB complexes (Christenson and Schijf, 2011), in combination with the best published stability constants for YREE inorganic complexes, to examine the identity of YREE-scavenging particles in seawater. The model results suggest that YREE removal from seawater may be dominated by sorption onto hydrated Mn oxides, as well as Fe hydroxides and organic matter, yet is not significantly influenced by sorption onto biogenic silicate or carbonate in seawater. While this approach is useful, it is limited in the sense that it cannot identify a specific type of substrate from the modeled surface complexation pattern if YREE sorption on that substrate has not been independently studied through controlled laboratory experiments. Nevertheless, these modeled YREE surface complexation patterns provide important constraints on the contributions of various surfaces to source-normalized YREE distributions in seawater.

5.2. Future work

5.2.1. Hg–DFOB

Although stability constants could not be derived from the non-linear regressions of the Hg and MeHg titrations, it does appear that the ligand competition experiment I presented in Chapter 3 is feasible for Hg. As previously mentioned, it is likely that Hg does not form the full hexadentate complex, as was also found for Pb, which may explain why the regressions are not converging. In the future, this possibility will be tested by reanalyzing the Hg data with a tetradentate complexation model (β_1 and β_2 only) assuming that only the first two complexes are formed. The titration data for MeHg suggest that only a bidentate complex of low stability is formed, therefore these will be refit with a 1-step, bidentate complexation model with just one adjustable parameter (β_1).

5.5.2. Oxidation of M–DFOB complexes

As stated in Chapter 4, Ce is the only REE that can be oxidized to the +IV oxidation state in natural waters, resulting in increased reactivity and anomalous distributions compared to the other REE. Yoshida et al. (2004a) suggest that the Ce anomaly observed in their work is due to the oxidation of Ce(III)–DFOB complex to the more stable Ce(IV)–DFOB complex, and that naturally occurring organic ligands contribute to Ce anomalies observed in the marine environment. Our initial titrations and spectrophotometric tests conducted with Ce(III) and DFOB do suggest that oxidation is occurring, and that it can be suppressed with a reducing agent, hydroxylamine. Although Yoshida et al. (2004a) concluded that the stability of Ce(IV)–DFOB is much higher than that of Ce(III)–DFOB, they never present any stability constants. It is therefore important

to determine the stability constant for DFOB complexes with both Ce(III) and Ce(IV), allowing them to be used in more realistic YREE speciation calculations.

There are several others metals that would be of particular interest to study with regard to DFOB complexation and subsequent oxidation. Hernlem et al. (1996) has measured DFOB complexation with Sn(II), however they report a β_4 value in their fit indicating that Sn coordinates with the terminal amine group. This suggests that the titration data of Hernlem et al. (1996) actually represent the Sn(IV)–DFOB complex, formed by oxidation of Sn(II). Complexation of chromium (Cr) and platinum (Pt) with DFOB would also be interesting to study, as they can similarly be oxidized from the +III state to the +VI state, and from the +II to the +IV state, respectively. Palladium(II), which cannot be oxidized, and platinum(II) have square-planar coordination, like Hg(II).

5.2.3. YREE sorption experiments in the presence of DFOB

As discussed in Chapter 4, it is likely that relative YREE surface complexation behavior in seawater is controlled by a mixture of organic and inorganic particles. More detailed laboratory experiments exploring various combinations and interactions of pure particle surfaces are necessary to fully understand YREE sorption in seawater. Future work could include YREE sorption experiments in the presence of DFOB with inorganic surfaces (hydrated Fe or Mn oxides), as well as with an organic surface (*Ulva lactuca*). Various experiments can be performed with hydrated surfaces in the presence of YREE and DFOB in order to study interactions among sorption of the metal and the ligand, and possibly the metal–ligand complex. These results can be directly compared with the results of YREE sorption experiments in the absence of DFOB in order to decipher the

sorption mechanism between YREE–DFOB complexes and particle surfaces. Such information will increase our scientific understanding of metal cycling, geochemistry, and interactions with solution and surface ligands in seawater.

Bibliography

Akagi, T. (2013) Rare earth element (REE)-silicic acid complexes in seawater to explain the incorporation of REEs in opal and the "leftover" REEs in surface water: New interpretation of dissolved REE distribution profiles. *Geochim. Cosmochim. Acta* **113**, 174-192.

Akagi, T., Fu, F. F., Hongo, Y. and Takahashi, K. (2011) Composition of rare earth elements in settling particles collected in the highly productive North Pacific Ocean and Bering Sea: Implications for siliceous-matter dissolution kinetics and formation of two REE-enriched phases. *Geochim. Cosmochim. Acta* **75**, 4857-4876.

Albrecht-Gary, A. M. and Crumbliss, A. L. (1998) Coordination chemistry of siderophores: Thermodynamics and kinetics of iron chelation and release. *Metal Ions in Biological Systems, Vol 35* **35**, 239-327.

Amirbahman, A., Reid, A. L., Haines, T. A., Kahl, J. S. and Arnold, C. (2002) Association of methylmercury with dissolved humic acids. *Environ. Sci. Technol.* **36**, 690-695.

Anderegg, G., l'Eplattenier, F. and Schwarzenbach, G. (1963a) Hydroxamatkomplexe II. Die Anwendung der pH-Methode. *Helv. Chim. Acta* **46**, 1400-1408.

Anderegg, G., l'Eplattenier, F. and Schwarzenbach, G. (1963b) Hydroxamatkomplexe III. Eisen(III)-Austausch zwischen Sideraminen und Komplexonen. Diskussion der Bildungskonstanten der Hydroxamatkomplexe. *Helv. Chim. Acta* **46**, 1409-1422.

Anderson, D. M. and Morel, F. M. M. (1978) Copper sensitivity of *Gonyaulax lamarensis*. *Limnol. Oceanogr.* **23**, 283-295.

Aplin, A. C. (1984) Rare earth element geochemistry of Central Pacific ferromanganese encrustations. *Earth Planet. Sci. Lett.* **71**, 13-22.

Beaucaire, C., Tertre, E., Ferrage, E., Grenut, B., Pronier, S. and Made, B. (2012) A thermodynamic model for the prediction of pore water composition of clayey rock at 25 and 80 degrees C - Comparison with results from hydrothermal alteration experiments. *Chem. Geol.* **334**, 62-76.

Benoit, J. M., Gilmour, C. C., Mason, R. P. and Heyes, A. (1999) Sulfide controls on mercury speciation and bioavailability to methylating bacteria in sediment pore waters. *Environ. Sci. Technol.* **33**, 951-957.

Benoit, J. M., Mason, R. P., Gilmour, C. C. and Aiken, G. R. (2001) Constants for mercury binding by dissolved organic matter isolates from the Florida Everglades. *Geochim. Cosmochim. Acta* **65**, 4445-4451.

Bernhardt, P. V. (2007) Coordination chemistry and biology of chelators for the treatment of iron overload disorders. *Dalton Trans.*, 3214-3220.

Bi, Y. Q., Hesterberg, D. L. and Duckworth, O. W. (2010) Siderophore-promoted dissolution of cobalt from hydroxide minerals. *Geochim. Cosmochim. Acta* **74**, 2915-2925.

Biedermann, G. and Ciavatta, L. (1962) Studies on the hydrolysis of metal ions. Part 41. The hydrolysis of the cadmium ion, Cd^{2+}. *Acta Chem. Scand.* **16**, 2221-2239.

Biller, D. V. and Bruland, K. W. (2012) Analysis of Mn, Fe, Co, Ni, Cu, Zn, Cd, and Pb in seawater using the Nobias-chelate PA1 resin and magnetic sector inductively coupled plasma mass spectrometry (ICP-MS). *Mar. Chem.* **130**, 12-20.

Boukhalfa, H. and Crumbliss, A. L. (2002) Chemical aspects of siderophore mediated iron transport. *Biometals* **15**, 325-339.

Boyd, P. W., Jickells, T., Law, C. S., Blain, S., Boyle, E. A., Buesseler, K. O., Coale, K. H., Cullen, J. J., de Baar, H. J. W., Follows, M., Harvey, M., Lancelot, C., Levasseur, M., Owens, N. P. J., Pollard, R., Rivkin, R. B., Sarmiento, J., Schoemann, V., Smetacek, V., Takeda, S., Tsuda, A., Turner, S. and Watson, A. J. (2007) Mesoscale iron enrichment experiments 1993-2005: Synthesis and future directions. *Science* **315**, 612-617.

Boyle, E. A., Sclater, F. R. and Edmond, J. M. (1976) Marine geochemistry of cadmium. *Nature* **263**, 42-44.

Brand, L. E., Sunda, W. G. and Guillard, R. R. L. (1983) Limitation of marine phytoplankton reproductive rates by zinc, manganese, and iron. *Limnol. Oceanogr.* **28**, 1182-1198.

Brand, L. E., Sunda, W. G. and Guillard, R. R. L. (1986) Reduction of marine phytoplankton reproduction rates by copper and cadmium. *J. Exp. Mar. Biol. Ecol.* **96**, 225-250.

Bruland, K. W. (1980) Oceanographic distributions of cadmium, zinc, nickel, and copper in the North Pacific. *Earth Planet. Sci. Lett.* **47**, 176-198.

Bruland, K. W. (1983a) Trace elements in sea water. In *Chemical Oceanography 8*. Academic Press, London, pp. 157-220.

Bruland, K. W. (1983b) Trace elements in sea-water. In *Chemical Oceanography*, *Vol. 8*, J.P. Riley and R. Chester (Eds.). Academic Press, London, pp. 157-220.

Bruland, K. W. (1989) Complexation of zinc by natural organic ligands in the central North Pacific. *Limnol. Oceanogr.* **34**, 269-285.

Bruland, K. W. (1992) Complexation of cadmium by natural organic ligands in the central North Pacific *Limnol. Oceanogr.* **37**, 1008-1017.

Bruland, K. W., Donat, J. R. and Hutchins, D. A. (1991) Interactive inlfuences of bioactive trace-metals on biological production in oceanic waters. *Limnol. Oceanogr.* **36**, 1555-1577.

Bruland, K. W., Orians, K. J. and Cowen, J. P. (1994) Reactive trace metals in the stratified central North Pacific. *Geochim. Cosmochim. Acta* **58**, 3171-3182.

Butler, A. and Theisen, R. M. (2010) Iron(III)-siderophore coordination chemistry: Reactivity of marine siderophores. *Coord. Chem. Rev.* **254**, 288-296.

Byrne, R. H. (1981) Inorganic lead complexation in natural seawater determined by UV spectroscopy. *Nature* **290**, 487-489.

Byrne, R. H. and Kim, K.-H. (1990) Rare earth element scavenging in seawater. *Geochim. Cosmochim. Acta* **54**, 2645-2656.

Byrne, R. H., Kump, L. R. and Cantrell, K. J. (1988) The influence of temperature and pH on trace-metal speciation in seawater. *Mar. Chem.* **25**, 163-181.

Byrne, R. H. and Li, B. Q. (1995) Comparative complexation behavior of the rare earths. *Geochim. Cosmochim. Acta* **59**, 4575-4589.

Byrne, R. H. and Sholkovitz, E. R. (1996) Marine chemistry and geochemistry of the lanthanides. In *Handbook on the Physics and Chemistry of Rare Earths*, *23*, K.A.G. Jr. and L. Eyring (Eds.). Elsevier, Amsterdam, pp. 497–593.

Capodaglio, G., Coale, K. H. and Bruland, K. W. (1990) Lead speciation in surface waters of the eastern North Pacific. *Mar. Chem.* **29**, 221-233.

Christenson, E. A. and Schijf, J. (2011) Stability of YREE complexes with the trihydroxamate siderophore desferrioxamine B at seawater ionic strength. *Geochim. Cosmochim. Acta* **75**, 7047-7062.

Clarkson, T. W. and Magos, L. (2006) The toxicology of mercury and its chemical compounds. *Crit. Rev. Toxicol.* **36**, 609-662.

Coale, K. H. and Bruland, K. W. (1988) Copper complexation in the Northeast Pacific. *Limnol. Oceanogr.* **33**, 1084-1101.

Coale, K. H., Johnson, K. S., Fitzwater, S. E., Gordon, R. M., Tanner, S., Chavez, F. P., Ferioli, L., Sakamoto, C., Rogers, P., Millero, F., Steinberg, P., Nightingale, P., Cooper, D., Cochlan, W. P., Landry, M. R., Constantinou, J., Rollwagen, G., Trasvina, A. and Kudela, R. (1996) A massive phytoplankton bloom induced by an ecosystem-scale iron fertilization experiment in the equatorial Pacific Ocean. *Nature* **383**, 495-501.

Cocozza, C., Tsao, C. C. G., Cheah, S. F., Kraemer, S. M., Raymond, K. N., Miano, T. M. and Sposito, G. (2002) Temperature dependence of goethite dissolution promoted by trihydroxamate siderophores. *Geochim. Cosmochim. Acta* **66**, 431-438.

Crawford, D. W., Lipsen, M. S., Purdie, D. A., Lohan, M. C., Statham, P. J., Whitney, F. A., Putland, J. N., Johnson, W. K., Sutherland, N., Peterson, T. D., Harrison, P. J. and Wong, C. S. (2003) Influence of zinc and iron enrichments on phytoplankton growth in the northeastern subarctic Pacific. *Limnol. Oceanogr.* **48**, 1583-1600.

Croot, P. L., Moffett, J. W. and Brand, L. E. (2000) Production of extracellular Cu complexing ligands by eucaryotic phytoplankton in response to Cu stress. *Limnol. Oceanogr.* **45**, 619-627.

Dhungana, S., White, P. S. and Crumbliss, A. L. (2001) Crystal structure of ferrioxamine B: a comparative analysis and implications for molecular recognition. *J. Biol. Inorg. Chem.* **6**, 810-818.

Dubinin, A. V. (2004) Geochemistry of rare earth elements in the ocean. *Lithol. Miner. Resour.* **39**, 289-307.

Duckworth, O. W., Bargar, J. R., Jarzecki, A. A., Oyerinde, O., Spiro, T. G. and Sposito, G. (2009a) The exceptionally stable cobalt(III)-desferrioxamine B complex. *Mar. Chem.* **113**, 114-122.

Duckworth, O. W., Bargar, J. R. and Sposito, G. (2009b) Quantitative Structure-Activity Relationships for Aqueous Metal-Siderophore Complexes. *Environ. Sci. Technol.* **43**, 343-349.

Dupont, C. L., Nelson, R. K., Bashir, S., Moffett, J. W. and Ahner, B. A. (2004) Novel copper-binding and nitrogen-rich thiols produced and exuded by *Emiliania huxleyi*. *Limnol. Oceanogr.* **49**, 1754-1762.

Dymond, J. and Lyle, M. (1985) Flux comparisons between sediments and sediment traps in the eastern tropical Pacific: Implications for atmospheric CO2 variations during the Pleistocene. *Limnol. Oceanogr.* **30**, 699-712.

Easley, R. A. and Byrne, R. H. (2011) The ionic strength dependence of lead (II) carbonate complexation in perchlorate media. *Geochim. Cosmochim. Acta* **75**, 5638-5647.

Elderfield, H. and Greaves, M. J. (1982) The rare earth elements in seawater. *Nature* **296**, 214-219.

Ellwood, M. J. (2004) Zinc and cadmium speciation in subantarctic waters east of New Zealand. *Mar. Chem.* **87**, 37-58.

Ellwood, M. J. and van den Berg, C. M. G. (2001) Determination of organic complexation of cobalt in seawater by cathodic stripping voltammetry. *Mar. Chem.* **75**, 33-47.

Erel, Y. and Morgan, J. J. (1991) The effect of surface reactions on the relative abundances of trace metals in deep-ocean water. *Geochim. Cosmochim. Acta* **55**, 1807-1813.

Erel, Y. and Stolper, E. M. (1993) Modeling of rare-earth element partitioning between particles and solution in aquatic environments. *Geochim. Cosmochim. Acta* **57**, 513-518.

Evers, A., Hancock, R. D., Martell, A. E. and Motekaitis, R. J. (1989) Metal-ion recognition in ligands with negatively charged oxygen donor groups - Complexation of Fe(III), Ga(III), In(III), Al(III), and othe highly charged metal-ions. *Inorg. Chem.* **28**, 2189-2195.

Falkowski, P. G. (1997) Evolution of the nitrogen cycle and its influence on the biological sequestration of CO_2 in the ocean. *Nature* **387**, 272-275.

Farkas, E., Csoka, H., Micera, G. and Dessi, A. (1997) Copper(II), nickel(II), zinc(II), and molybdenum(VI) complexes of desferrioxamine B in aqueous solution. *J. Inorg. Biochem.* **65**, 281-286.

Fleming, E. J., Mack, E. E., Green, P. G. and Nelson, D. C. (2006) Mercury methylation from unexpected sources: Molybdate-inhibited freshwater sediments and an iron-reducing bacterium. *Appl. Environ. Microbiol.* **72**, 457-464.

Florence, T. M. and Stauber, J. L. (1986) Toxicity of copper complexes to the marine diatom *Nitzschia closterium*. *Aquat. Toxicol.* **8**, 11-26.

Gledhill, M., McCormack, P., Ussher, S., Achterberg, E. P., Mantoura, R. F. C. and Worsfold, P. J. (2004) Production of siderophore type chelates by mixed bacterioplankton populations in nutrient enriched seawater incubations. *Mar. Chem.* **88**, 75-83.

Gledhill, M. and van den Berg, C. M. G. (1994) Determination of complexation of iron(III) with natural organic complexing ligands in seawater using cathodic stripping voltammetry. *Mar. Chem.* **47**, 41-54.

Gould, B. L. and Langerman, N. (1982) A thermodynamic description of the binding of iron to ferrioxamine B in aqueous solutions. *Arch. Biochem. Biophys.* **215**, 148-156.

Haitzer, M., Aiken, G. R. and Ryan, J. N. (2003) Binding of mercury(II) to aquatic humic substances: Influence of pH and source of humic substances. *Environ. Sci. Technol.* **37**, 2436-2441.

Haygood, M. G., Holt, P. D. and Butler, A. (1993) Aerobactin production by a planktonic marine vibrio sp. *Limnol. Oceanogr.* **38**, 1091-1097.

Henderson, G. M., Anderson, R. F., Adkins, J., Andersson, P., Boyle, E. A., Cutter, G., de Baar, H., Eisenhauer, A., Frank, M., Francois, R., Orians, K., Gamo, T., German, C., Jenkins, W., Moffett, J., Jeandel, C., Jickells, T., Krishnaswami, S., Mackey, D., Measures, C. I., Moore, J. K., Oschlies, A., Pollard, R., van der Loeff, M. R. D., Schlitzer, R., Sharma, M., von Damm, K., Zhang, J., Masque, P. and Grp, S. W. (2007) GEOTRACES - An international study of the global marine biogeochemical cycles of trace elements and their isotopes. *Chem Erde-Geochem.* **67**, 85-131.

Herbelin, A. L. and Westall, J. C. (1999) *FITEQL. A Computer Program for Determination of Chemical Equilibrium Constants from Experimental Data. Version 4.0.* In: O.S.U. Department of Chemistry (Editor), Corvallis, OR.

Hernlem, B. J., Vane, L. M. and Sayles, G. D. (1996) Stability constants for complexes of the siderophore desferrioxamine B with selected heavy metal cations. *Inorg. Chim. Acta* **244**, 179-184.

Hernlem, B. J., Vane, L. M. and Sayles, G. D. (1999) The application of siderophores for metal recovery and waste remediation: Examination of correlations for prediction of metal affinities. *Water Res.* **33**, 951-960.

Heyes, A., Mason, R. P., Kim, E. H. and Sunderland, E. (2006) Mercury methylation in estuaries: Insights from using measuring rates using stable mercury isotopes. *Mar. Chem.* **102**, 134-147.

Hider, R. C. and Kong, X. L. (2010) Chemistry and biology of siderophores. *Nat. Prod. Rep.* **27**, 637-657.

Janz, G. J., Oliver, B. G., Lakshmin.Gr and Mayer, G. E. (1970) Electrical conductance, diffusion, viscosity, and density of sodium nitrate, sodium perchlorate, and sodium thiocyanate in concentrated aqueous solutions. *J. Phys. Chem.* **74**, 1285-1289.

Johnson, K. S., Coale, K. H., Berelson, W. M. and Gordon, R. M. (1996) On the formation of the manganese maximum in the oxygen minimum. *Geochim. Cosmochim. Acta* **60**, 1291-1299.

King, J. K., Kostka, J. E., Frischer, M. E., Saunders, F. M. and Jahnke, R. A. (2001) A quantitative relationship that remonstrates mercury methylation rates in marine sediments are based on the community composition and activity of sulfate-reducing bacteria. *Environ. Sci. Technol.* **35**, 2491-2496.

Klungness, G. D. and Byrne, R. H. (2000) Comparative hydrolysis behavior of the rare earths and yttrium: the influence of temperature and ionic strength. *Polyhedron* **19**, 99-107.

Koch, B. P., Ludwichowski, K. U., Kattner, G., Dittmar, T. and Witt, M. (2008) Advanced characterization of marine dissolved organic matter by combining reversed-phase liquid chromatography and FT-ICR-MS. *Mar. Chem.* **111**, 233-241.

Kozelka, P. B. and Bruland, K. W. (1998) Chemical speciation of dissolved Cu, Zn, Cd, Pb in Narragansett Bay, Rhode Island. *Mar. Chem.* **60**, 267-282.

Laglera, L. M. and van den Berg, C. M. G. (2003) Copper complexation by thiol compounds in estuarine waters. *Mar. Chem.* **82**, 71-89.

Lamborg, C. H., Fitzgerald, W. F., Skoog, A. and Visscher, P. T. (2004) The abundance and source of mercury-binding organic ligands in Long Island Sound. *Mar. Chem.* **90**, 151-163.

Laurier, F. J. G., Mason, R. P., Gill, G. A. and Whalin, L. (2004) Mercury distributions in the North Pacific Ocean - 20 years of observations. *Mar. Chem.* **90**, 3-19.

Lee, J. G., Roberts, S. B. and Morel, F. M. M. (1995) Cadmium - A nutrient for the marine diatom *Thalassiosira weissflogii*. *Limnol. Oceanogr.* **40**, 1056-1063.

Lewis, B. L., Holt, P. D., Taylor, S. W., Wilhelm, S. W., Trick, C. G., Butler, A. and Luther, G. W. (1995) Voltammetric estimation of iron(III) thermodynamic

stability constants for catecholate siderophores isolated from marine bacteria and cyanobacteria. *Mar. Chem.* **50**, 179-188.

Liermann, L. J., Kalinowski, B. E., Brantley, S. L. and Ferry, J. G. (2000) Role of bacterial siderophores in dissolution of hornblende. *Geochim. Cosmochim. Acta* **64**, 587-602.

Liu, X. W. and Byrne, R. H. (1998) Comprehensive investigation of yttrium and rare earth element complexation by carbonate ions using ICP mass spectrometry. *J. Solut. Chem.* **27**, 803-815.

Louis, Y., Garnier, C., Lenoble, V., Omanovic, D., Mounier, S. and Pizeta, I. (2009) Characterisation and modelling of marine dissolved organic matter interactions with major and trace cations. *Mar. Environ. Res.* **67**, 100-107.

Luo, Y. R. and Byrne, R. H. (2001) Yttrium and rare earth element complexation by chloride ions at 25 degrees C. *J. Solut. Chem.* **30**, 837-845.

Luo, Y. R. and Byrne, R. H. (2004) Carbonate complexation of yttrium and the rare earth elements in natural waters. *Geochim. Cosmochim. Acta* **68**, 691-699.

Luther, G. W. and Wu, J. F. (1997) What controls dissolved iron concentrations in the world ocean? - a comment. *Mar. Chem.* **57**, 173-179.

Malcolm, E. G., Schaefer, J. K., Ekstrom, E. B., Tuit, C. B., Jayakumar, A., Park, H., Ward, B. B. and Morel, F. M. M. (2010) Mercury methylation in oxygen deficient zones of the oceans: No evidence for the predominance of anaerobes. *Mar. Chem.* **122**, 11-19.

Maldonado, M. T., Strzepek, R. F., Sander, S. and Boyd, P. W. (2005) Acquisition of iron bound to strong organic complexes, with different Fe binding groups and photochemical reactivities, by plankton communities in Fe-limited subantarctic waters. *Glob. Biogeochem. Cycle* **19**.

Manceau, A., Boisset, M. C., Sarret, G., Hazemann, R. L., Mench, M., Cambier, P. and Prost, R. (1996) Direct determination of lead speciation in contaminated soils by EXAFS spectroscopy. *Environ. Sci. Technol.* **30**, 1540-1552.

Manceau, A. and Matynia, A. (2010) The nature of Cu bonding to natural organic matter. *Geochim. Cosmochim. Acta* **74**, 2556-2580.

Martell, A. E., Smith, R. M. and Motekaitis, R. J. (2004) *NIST Critically Selected Stability Constants of Metal Complexes.*, *NIST Standard Reference Database 46*, Texas A&M University.

Martin, D. F. (1967) Coordination Chemistry of the Oceans. *Advances in Chemistry Series*, 255-269.

Martin, J. H. (1990) Glacial-interglacial CO_2 change: the iron hypothesis. *Paleoceanography* **5**, 1-13.

Martin, J. H., Coale, K. H., Johnson, K. S., Fitzwater, S. E., Gordon, R. M., Tanner, S. J., Hunter, C. N., Elrod, V. A., Nowicki, J. L., Coley, T. L., Barber, R. T., Lindley, S., Watson, A. J., Vanscoy, K., Law, C. S., Liddicoat, M. I., Ling, R., Stanton, T., Stockel, J., Collins, C., Anderson, A., Bidigare, R., Ondrusek, M., Latasa, M., Millero, F. J., Lee, K., Yao, W., Zhang, J. Z., Friederich, G., Sakamoto, C., Chavez, F., Buck, K., Kolber, Z., Greene, R., Falkowski, P., Chisholm, S. W., Hoge, F., Swift, R., Yungel, J., Turner, S., Nightingale, P., Hatton, A., Liss, P. and Tindale, N. W. (1994) Testing the iron hypothesis in ecosystems of the equatorial Pacific-Ocean. *Nature* **371**, 123-129.

Martinez, J. S., Carter-Franklin, J. N., Mann, E. L., Martin, J. D., Haygood, M. G. and Butler, A. (2003) Structure and membrane affinity of a suite of amphiphilic siderophores produced by a marine bacterium. *Proc. Natl. Acad. Sci. U. S. A.* **100**, 3754-3759.

Martinez, J. S., Haygood, M. G. and Butler, A. (2001) Identification of a natural desferrioxamine siderophore produced by a marine bacterium. *Limnol. Oceanogr.* **46**, 420-424.

Martinez, J. S., Zhang, G. P., Holt, P. D., Jung, H. T., Carrano, C. J., Haygood, M. G. and Butler, A. (2000) Self-assembling amphiphilic siderophores from marine bacteria. *Science* **287**, 1245-1247.

Mason, R. P. and Fitzgerald, W. F. (1993) The distribution and biogeochemical cycling of mercury in the equatorial Pacific Ocean. *Deep-Sea Research Part I Oceanographic Research Papers* **40**, 1898-1924.

Mason, R. P., Laporte, J. M. and Andres, S. (2000) Factors controlling the bioaccumulation of mercury, methylmercury, arsenic, selenium, and cadmium by freshwater invertebrates and fish. *Archives of Environmental Contamination and Toxicology* **38**, 283-297.

Mason, R. P., Reinfelder, J. R. and Morel, F. M. M. (1996) Uptake, toxicity, and trophic transfer of mercury in a coastal diatom. *Environ. Sci. Technol.* **30**, 1835-1845.

Mawji, E., Gledhill, M., Milton, J. A., Tarran, G. A., Ussher, S., Thompson, A., Wolff, G. A., Worsfold, P. J. and Achterberg, E. P. (2008) Hydroxamate Siderophores: Occurrence and Importance in the Atlantic Ocean. *Environ. Sci. Technol.* **42**, 8675-8680.

Mawji, E., Gledhill, M., Milton, J. A., Zubkov, M. V., Thompson, A., Wolff, G. A. and Achterberg, E. P. (2011) Production of siderophore type chelates in Atlantic Ocean waters enriched with different carbon and nitrogen sources. *Mar. Chem.* **124**, 90-99.

McCormack, P., Worsfold, P. J. and Gledhill, M. (2003) Separation and detection of siderophores produced by marine bacterioplankton using high-performance liquid chromatography with electrospray ionization mass spectrometry. *Anal. Chem.* **75**, 2647-2652.

McKnight, D. M. and Morel, F. M. M. (1979) Release of weak and strong copper-complexing agents by algae. *Limnol. Oceanogr.* **24**, 823-837.

McLennan, S. M. (1989) Rare earth elements in sedimentary rocks: Influence of provenance and sedimentary processes. *Rev. Miner.* **21**, 169-200.

Millero, F. J., Woosley, R., Ditrolio, B. and Waters, J. (2009) Effect of Ocean Acidification on the Speciation of Metals in Seawater. *Oceanography* **22**, 72-85.

Moffett, J. W. and Brand, L. E. (1996) Production of strong, extracellular Cu chelators by marine cyanobacteria in response to Cu stress. *Limnol. Oceanogr.* **41**, 388-395.

Moffett, J. W. and Dupont, C. (2007) Cu complexation by organic ligands in the sub-arctic NW Pacific and Bering Sea. *Deep-Sea Res. Part I-Oceanogr. Res. Pap.* **54**, 586-595.

Moffett, J. W., Zika, R. G. and Brand, L. E. (1990) Distribution and potential sources and sinks of copper chelators in the Sargasso Sea. *Deep-Sea Research Part a-Oceanographic Research Papers* **37**, 27-36.

Monecke, T., Kempf, U., Monecke, J., Sala, M. and Wolf, D. (2002) Tetrad effect in rare earth element distribution patterns: A method of quantification with application to rock and mineral samples from granite-related rare metal deposits. *Geochim. Cosmochim. Acta* **66**, 1185-1196.

Morel, F. and Morgan, J. (1972) A Numerical Method for Computing Equilibria in Aqueous Chemical Systems. *Environ. Sci. Technol.* **6**, 58-67.

Morel, F. M. M., Kraepiel, A. M. L. and Amyot, M. (1998) The chemical cycle and bioaccumulation of mercury. *Annu. Rev. Ecol. Syst.* **29**, 543-566.

Morel, F. M. M., Reinfelder, J. R., Roberts, S. B., Chamberlain, C. P., Lee, J. G. and Yee, D. (1994) Zinc and carbon co-limitation of marine phytoplankton. *Nature* **369**, 740-742.

Neilands, J. B. (1981) Iron-absorption and transport in microorganisms. *Annu. Rev. Nutr.* **1**, 27-46.

Neilands, J. B. (1995) Siderophores - Structure and function of microbial iron transport compounds. *J. Biol. Chem.* **270**, 26723-26726.

Ozaki, T., Suzuki, Y., Nankawa, T., Yoshida, T., Ohnuki, T., Kimura, T. and Francis, A. J. (2006) Interactions of rare earth elements with bacteria and organic ligands. *J. Alloy. Compd.* **408**, 1334-1338.

Palmer, M. R. (1985) Rare Earth Elements in Foraminifera Tests. *Earth Planet. Sci. Lett.* **73**, 285-298.

Piepgras, D. J. and Jacobsen, S. B. (1992) The behavior of rare earth elements in seawater: Precise determination of variations in the North Pacific water column. *Geochim. Cosmochim. Acta* **56**, 1851-1862.

Pitman, I. H. and Morris, I. J. (1979) Covalent Additions of Glutathione, Cysteine, Homocysteine, Cystearnine and Thioglycolic Acid to Quinazoline Cation. *Aust. J. Chem.* **32**, 1567-1573.

Plocke, D. J., Levinthal, C. and Vallee, B. L. (1962) Alkaline phosphatase of *Escherichia col*i - Zinc metalloenzyme. *Biochemistry* **1**, 373-378.

Price, N. M. and Morel, F. M. M. (1990) Cadmium and cobalt substitution for zinc in a marine diatom. *Nature* **344**, 658-660.

Quinn, K. A., Byrne, R. H. and Schijf, J. (2004) Comparative scavenging of yttrium and the rare earth elements in seawater: Competitive influences of solution and surface chemistry. *Aquat. Geochem.* **10**, 59-80.

Raven, J. A., Evans, M. C. W. and Korb, R. E. (1999) The role of trace metals in photosynthetic electron transport in O_2-evolving organisms. *Photosynth. Res.* **60**, 111-149.

Rue, E. L. and Bruland, K. W. (1995) Complexation of Iron(III) by natural organic-ligands in the central north Pacific as determined by a new competitive ligand equilibration adsorptive cathodic stripping voltammetric method. *Mar. Chem.* **50**, 117-138.

Rue, E. L. and Bruland, K. W. (1997) The role of organic complexation on ambient iron chemistry in the equatorial Pacific Ocean and the response of a mesoscale iron addition experiment. *Limnol. Oceanogr.* **42**, 901-910.

Santana-Casiano, J. M., Gonzalez-Davila, M., Perez-Peña, J. and Millero, F. J. (1995) Pb^{2+} interactions with the marine phytoplankton *Dunaliella tertiolecta Mar. Chem.* **48**, 115-129.

Schaefer, J. K. and Morel, F. M. M. (2009) High methylation rates of mercury bound to cysteine by *Geobacter sulfurreducens*. *Nat. Geosci.* **2**, 123-126.

Schaule, B. K. and Patterson, C. C. (1981) Lead concentrations in the Northeast Pacific - Evidence for global anthropogenic perturbations. *Earth Planet. Sci. Lett.* **54**, 97-116.

Schijf, J. and Byrne, R. H. (2004) Determination of $_{SO4}\beta_1$ for yttrium and the rare earth elements at $I = 0.66$ m and $t = 25^{\circ}C$ - Implications for YREE solution speciation in sulfate-rich waters. *Geochim. Cosmochim. Acta* **68**, 2825-2837.

Schijf, J., de Baar, H. J. W. and Millero, F. J. (1995) Vertical distributions and speciation of dissolved rare earth elements in the anoxic brines of Bannock Basin, eastern Mediterranean Sea. *Geochim. Cosmochim. Acta* **59**, 3285-3299.

Schijf, J. and Ebling, A. M. (2010) Investigation of the Ionic Strength Dependence of *Ulva lactuca* Acid Functional Group pK(a)s by Manual Alkalimetric Titrations. *Environ. Sci. Technol.* **44**, 1644-1649.

Schijf, J. and Marshall, K. S. (2011) YREE sorption on hydrous ferric oxide in 0.5 M NaCl solutions: A model extension. *Mar. Chem.* **123**, 32-43.

Schorsch, G. (1964) Etude de l'hydrolyse de l'ion Zn2+ a 250 C en milieu KCl et NaCl 2M. *Bull. Soc. Chim. Fr.*, 1449-1455.

Schwarzenbach, G. and Schwarzenbach, K. (1963) Hydroxamatkomplexe 1. Die Stabilität der Eisen(III)-Komplexe einfacher Hydroxamsäuren und des Ferrioxamins B. *Helv. Chim. Acta* **46**, 1390-1400.

Selin, N. E. (2009) Global Biogeochemical Cycling of Mercury: A Review. In *Annual Review of Environment and Resources*, *34*. Annual Review of Environment and Resources. Annual Reviews, Palo Alto, pp. 43-63.

Shannon, R. D. (1976) Revised effective ionic radii and systematic studies of interatomic distances in halides and chalcogenides. *Acta Crystallogr. Sect. A* **32**, 751-767.

Sigman, D. M. and Boyle, E. A. (2000) Glacial/interglacial variations in atmospheric carbon dioxide. *Nature* **407**, 859-869.

Simanova, A. A., Persson, P. and Loring, J. S. (2010) Evidence for ligand hydrolysis and Fe(III) reduction in the dissolution of goethite by desferrioxamine-B. *Geochim. Cosmochim. Acta* **74**, 6706-6720.

Sohrin, Y. and Bruland, K. W. (2011) Global status of trace elements in the ocean. *Trac-Trends Anal. Chem.* **30**, 1291-1307.

Stanley, J. K. and Byrne, R. H. (1990) Inorganic complexation of zinc(II) in seawater. *Geochim. Cosmochim. Acta* **54**, 753-760.

Stricks, W., Kolthoff, I. M. and Heyndrickx, A. (1954) Formation and Properties of Various Mercuric Mercapto Thioglycolates Formed in Reactions between Mercuric Mercury and Thioglycolic Acid. *J. Am. Chem. Soc.* **76**, 1515-1519.

Sunda, W. G. (2012) Feedback interactions between trace metal nutrients and phytoplankton in the ocean. *Frontiers in Microbiology* **3**.

Sunda, W. G. and Guillard, R. R. L. (1976) The relationship between cupric ion activity and the toxicity of copper to phytoplankton. *J. Mar. Res.* **34**, 511-529.

Sunda, W. G. and Huntsman, S. A. (1995) Cobalt and zinc interreplacement in marine phytoplankton: Biological and geochemical implications. *Limnol. Oceanogr.* **40**, 1404-1417.

Sunderland, E. M., Krabbenhoft, D. P., Moreau, J. W., Strode, S. A. and Landing, W. M. (2009) Mercury sources, distribution, and bioavailability in the North Pacific Ocean: Insights from data and models. *Glob. Biogeochem. Cycle* **23**.

Tertre, E., Berger, G., Simoni, E., Castet, S., Giffaut, E., Loubet, M. and Catalette, H. (2006) Europium retention onto clay minerals from 25 to 150 degrees C: Experimental measurements, spectroscopic features and sorption modelling. *Geochim. Cosmochim. Acta* **70**, 4563-4578.

Tertre, E., Hofmann, A. and Berger, G. (2008) Rare earth element sorption by basaltic rock: Experimental data and modeling results using the "Generalised Composite approach". *Geochim. Cosmochim. Acta* **72**, 1043-1056.

Turner, D. R., Whitfield, M. and Dickson, A. G. (1981) The equilibrium speciation of dissolved components in freshwater and seawater at 25° C and 1 atm pressure. *Geochim. Cosmochim. Acta* **45**, 855-881.

Turonek, M. L., Hefter, G. T. and May, P. M. (1998) The ionic product of water in highly concentrated sodium perchlorate solutions. *Talanta* **45**, 931-934.

Ullrich, S. M., Tanton, T. W. and Abdrashitova, S. A. (2001) Mercury in the aquatic environment: A review of factors affecting methylation. *Crit. Rev. Environ. Sci. Technol.* **31**, 241-293.

van den Berg, C. M. G. and Dharmvanij, S. (1984) Organic complexation of zinc in estuarine interstitial and surface water samples. *Limnol. Oceanogr.* **29**, 1025-1036.

Vraspir, J. M. and Butler, A. (2009) Chemistry of Marine Ligands and Siderophores. In *Annual Review of Marine Science*, *1*. Annual Review of Marine Science. Annual Reviews, Palo Alto, pp. 43-63.

Westall, J. C., Zachary, J. L. and Morel, F. M. M. (1976) MINEQL- General algorithm for computation of chemical equilibrium in aqueous systems. *Abstr. Pap. Am. Chem. Soc.* **172**, 8-8.

Whitfield, M. and Turner, D. R. (1987) The role of particles in regulating the composition of sea-water. In *Aquatic Surface Chemistry*, W. Stumm (Ed.). Wiley, New York, pp. 457-493.

Winkelmann, G. (2002) Microbial siderophore-mediated transport. *Biochem. Soc. Trans.* **30**, 691-696.

Winston, A. and Kirchner, D. (1978) Hydroxamic acid polymers. Effect of structure on the selective chelation of iron in water. *Macromolecules* **11**, 597-603.

Witter, A. E., Hutchins, D. A., Butler, A. and Luther, G. W. (2000) Determination of conditional stability constants and kinetic constants for strong model Fe-binding ligands in seawater. *Mar. Chem.* **69**, 1-17.

Witter, A. E. and Luther, G. W. (1998) Variation in Fe-organic complexation with depth in the Northwestern Atlantic Ocean as determined using a kinetic approach. *Mar. Chem.* **62**, 241-258.

Wyndham, T., McCulloch, M., Fallon, S. and Alibert, C. (2004) High-resolution coral records of rare earth elements in coastal seawater: Biogeochemical cycling and a new environmental proxy. *Geochim. Cosmochim. Acta* **68**, 2067-2080.

Xiong, Z. F., Li, T. G., Algeo, T., Chang, F. M., Yin, X. B. and Xu, Z. K. (2012) Rare earth element geochemistry of laminated diatom mats from tropical West Pacific: Evidence for more reducing bottomwaters and higher primary productivity during the Last Glacial Maximum. *Chem. Geol.* **296**, 103-118.

Xu, Y., Feng, L., Jeffrey, P. D., Shi, Y. G. and Morel, F. M. M. (2008) Structure and metal exchange in the cadmium carbonic anhydrase of marine diatoms. *Nature* **452**, 56-61.

Yoshida, T., Ozaki, T., Ohnuki, T. and Francis, A. J. (2004a) Adsorption of rare earth elements by gamma-Al(2)O(3) and *Pseudomonas fluorescens* cells in the presence of desferrioxamine B: implication of siderophores for the Ce anomaly. *Chem. Geol.* **212**, 239-246.

Yoshida, T., Ozaki, T., Ohnuki, T. and Francis, A. J. (2004b) Interactions of trivalent and tetravalent heavy metal-siderophore complexes with *Pseudomonas fluorescens*. *Radiochim. Acta* **92**, 749-753.

Zhang, J. and Nozaki, Y. (1996) Rare earth elements and yttrium in seawater: ICP-MS determinations in the East Caroline, Coral Sea, and South Fiji basins of the western South Pacific Ocean. *Geochim. Cosmochim. Acta* **60**, 4631-4644.

Zoll, A. M. and Schijf, J. (2012) A surface complexation model of YREE sorption on *Ulva lactuca* in 0.05-5.0 M NaCl solutions. *Geochim. Cosmochim. Acta* **97**, 183-199.